FLUID INCLUSION AND STABLE ISOTOPE STUDIES

OF HYDROTHERMAL VEIN DEPOSITS,

SCHWARZWALD, GERMANY.

DISSERTATION

zur Erlangung des Grades eines Doktors der Naturwissenschaften

der Geowissenschaftlichen Fakultät

der Eberhard-Karls-Universität Tübingen

vorgelegt von

BALDORJ BAATARTSOGT

aus Bayan Önjuul, Mongolei.

2006

Tag der mündlichen Prüfung: 27. Januar 2006

Dekan: Prof. Ph.D. Klaus-Georg Nickel

1. Berichterstatter: Prof. Dr. Gregor Markl

2. Berichterstatter: Prof. Dr. Dr.h.c Muharrem Satir

TABLE OF CONTENT

ACKNOWLEDGEMENTS

ABSTRACT

In the Schwarzwald area, southwest Germany, more than 400 hydrothermal veins hosting different gangue and ore mineral assemblages cross-cut the crystalline basement rocks. An integrated fluid inclusion and stable isotope study has been carried out on hydrothermal veins (Pb-Zn-Cu-bearing fluorite-barite-quartz veins, Co-Ni-Ag-Bi-U-bearing and barren barite-fluorite-quartz veins) from the Schwarzwald district. More than 400 individual samples from 110 Variscan and post-Variscan deposits covering a large area of 120 by 40 km were studied by microthermometry, Raman spectroscopy, stable isotope analysis of minerals and fluid inclusions.

Natural waters of various origins exhibit systematic differences in their deuterium (D) and ^{18}O contents. The most straightforward method for the determination of paleofluid signatures is the direct extraction of fluid inclusion water from hydrothermal minerals. Inclusion fluids in fluorite are particularly useful, because their host is presumable or normally devoid of oxygen and hydrogen, thus precluding post-entrapment isotope exchanges. The δD values for water extracted from fluorites at 400°C range widely between -60 and +82 ‰, whereas at 650°C the values range from -78 to +40 ‰. The systematic differences between δD values obtained from the same samples at both extraction temperatures indicate that most likely two isotopically distinct reservoirs contribute to the extracted water. To clarify the nature of these reservoirs, FTIR (Fourier transformation infrared) analyses were performed on the fluid inclusions and host fluorite. The FTIR spectra of fluid inclusions show that two dominant peaks at absorbance values of about 3400 cm^{-1} and 5200 cm^{-1} are present, which conform to structurally bound and molecular water, respectively. In contrast, the FTIR spectra of fluid inclusion free areas in the host fluorites show only a peak at 3400 cm^{-1}. These results demonstrate that significant amounts of structurally bound water must be present in most of the studied hydrothermal fluorites. Based on the isotopic and spectroscopic data, we believe that water released at extraction temperatures greater than 500-600 °C is dominantly originating from interstitial OH^- defect sites in the fluorite structure. This structurally bound water appears to be isotopically depleted compared to the original fluid inclusion water, resulting in a significant shift of the δD values. This calls for extreme caution in setting up appropriate analytical procedures for the determination of δD values and has important implications for the interpretation of paleofluid signatures.

Most Variscan fluids are of the H_2O-NaCl-(KCl) type, have low salinities (0-10 wt.% eqv. NaCl) and comparatively high homogenization temperatures (150-350 °C). In some of these samples, an additional gas-rich CO_2-CH_4-H_2O fluid inclusion type is present. Oxygen isotope data for quartz from the Variscan veins range from +2.8 to +12.2 ‰, indicating $\delta^{18}O_{H2O}$ values of the hydrothermal fluids of –12.5 to +4.4 ‰. The δD values of water extracted from fluid inclusions in Variscan quartz samples vary between –49 and +4 ‰. The geological framework as well as fluid inclusion and stable isotope characteristics of the Variscan veins suggest an origin of the mineralizing fluids from regional metamorphic devolatilization processes.

The salinities of fluid inclusions in post-Variscan primary fluorite, calcite, barite and quartz are in the range of 22–25 wt.% eqv. NaCl, and the eutectic temperatures range between –57 and –45 °C, indicating the presence of H_2O-NaCl-$CaCl_2$ fluids. Homogenization temperatures vary from 110 to 180 °C. A low-salinity fluid (0 to 15 wt.% eqv. NaCl) was observed in some late-stage fluorite, calcite and quartz samples, which were trapped at similar temperatures. Raman microprobe analyses show that detectable concentrations of volatiles such as CH_4 or CO_2 are present in the Variscan fluid, whereas only CO_2 was detected in post-Variscan fluids. Almost all $\delta^{18}O$ measurements of quartz from the fluorite-bearing post-Variscan veins range between +11.1 and +19.5 ‰, indicating $\delta^{18}O_{H2O}$ values between –11.0 and +4.4 ‰ (Matsuhisa *et al.* 1979). This is perfectly consistent with $\delta^{18}O_{H2O}$ values of fluid inclusion water directly extracted from fluorites (–11.6 to +1.1 ‰). The δD values of fluid inclusion water in post-Variscan calcites (extracted from primary and late calcite samples) are in a narrow range between –26 and –15 ‰, while fluid inclusion water from quartz and fluorite samples varies between –63 and +9 ‰ and between -29 and -1 ‰, respectively. The $\delta^{13}C$ and $\delta^{18}O$ values of fluid inclusion gas (CO_2) range between –21.4 and –6.7 ‰ and from –16.3 to –7.1 ‰, respectively. Calculations for fluorite-barite-quartz veins combining oxygen isotope equilibria with microthermometric data result in quartz precipitation temperatures of 130–180 °C at pressures between 0.3 to 0.5 kbar. The $\delta^{18}O_{H2O}$ and δD data, particularly the observed wide range in hydrogen isotopic compositions, indicate that the hydrothermal mineralizations formed through large-scale mixing of a basement-derived saline NaCl-$CaCl_2$ brine with meteoric water.

Hence, many of the post-Variscan fluorite-barite-quartz veins are considered to have precipitated through mixing of a deep saline brine with meteoric, low salinity waters. This hypothesis was tested using carbon, sulfur, and oxygen isotope data of sulfides, sulfates and

calcite, coupled with fluid inclusion studies. Primary hydrothermal calcites from the deposits show a positive correlation of their $\delta^{13}C$ (V-PDB) and $\delta^{18}O$ (V-SMOW) values, which range from –12 to –3 ‰ and from +12 to +18.5 ‰, respectively. Carbon and oxygen isotope compositions of paragenetically young, remobilized calcite types are shifted towards higher values and range from –12 to –1 ‰ and from +20 to +25 ‰, respectively. We developed an improved calculation procedure for modeling the covariation of carbon and oxygen isotopes in calcite resulting from mixing of two fluids with different isotopic compositions and total carbon concentrations. In our model, the carbon speciations in the two model fluid end-members and the fluid mixtures are calculated using a speciation and reaction path code. The carbon and oxygen isotope covariation of primary Schwarzwald calcites can effectively be modeled by a mixing trend of a deep saline brine and a low salinity water of meteoric origin. Sulfur isotope data of barites from 22 hydrothermal fluorite-barite-quartz veins vary from +9 to +18 ‰ (CDT), sulfide ore minerals show $\delta^{34}S$ values between –14.4 and +2.9. Calculated sulfide-sulfate equilibrium temperatures are in the range between 300 and 350°C. These temperatures differ significantly from the formation temperatures of 150 to 200°C of most of the deposits as estimated from fluid inclusions, and are interpreted as preserved paleotemperatures of the deep aquifer. This assumption has been carefully checked against possible contamination of an equilibrated sulfide-sulfate system from the deep aquifer with sulfate from surface-derived sources, considering also the kinetics of the sulfide-sulfate isotope exchange. A combination of the sulphur isotopic results with microthermometric data of fluid inclusion and constraints on the temperature of the meteoric water was used to calculate mixing ratios of the two fluid end-members. The results indicate that mass fractions of the deep saline brine in the mixed fluid were between 0.5 and 0.75. Considering all geologic, geochemical and isotopic information, we propose that the majority of the post-Variscan hydrothermal veins in the Schwarzwald area were precipitated by district-scale mixing of homogeneous deep saline brine with meteoric waters.

Our comprehensive study of a large number of deposits provides evidence for two fundamentally different fluid systems in the crystalline basement. The younger (post-Variscan) system shows remarkable persistent geochemical and isotopic features over a prolonged period of more than 100 Ma and in an area exceeding 120 by 40 km.

ZUSAMMENFASSUNG

Im kristallinen Grundgebirge des Schwarzwalds (Südwestdeutschland) treten mehr als 400 hydrothermale Gänge mit unterschiedlichen Erz- und Gangartparagenesen auf. Im Rahmen der vorliegenden Arbeit wurden umfassende Fluideinschluss- und stabile Isotopenuntersuchungen an den verschiedenen hydrothermalen Gangtypen (Pb-Zn-Cu-führende Fluorit-Baryt-Quarz-Gänge, Co-Ni-Ag-Bi-U-führende und unvererzte Baryt-Fluorit-Quarz-Gänge) durchgeführt. Insgesamt wurden mehr als 400 Proben von 110 varistischen und postvaristischen Gängen untersucht, die in einem 120 mal 40 km grossen Gebiet auftreten. Die Proben wurden mittels Mikrothermometrie, Raman-Spektroskopie und stabiler Isotopenanalytik von Einzelmineralen und Fluideinschlüssen untersucht.

Natürliche hydrothermale Fluide und Mineralwässer zeigen systematische Variationen hinsichtlich ihrer Wasserstoff- und Sauerstoff-Isotopenzusammensetzung. Die aussagekräftigste Methode zur Bestimmung von Paläofluid-Isotopensignaturen ist die direkte Extraktion von Wasser aus Fluideinschlüssen in hydrothermal gebildeten Mineralen. Fluideinschlüsse in Fluorit sind hierzu besonders geeignet, da Fluorit keinen Sauerstoff und Wasserstoff enthält und daher kein späterer Isotopenaustausch mit den eingeschlossenen Fluiden erfolgen kann. Die δD-Werte von H_2O, das aus Fluorit bei 400 °C extrahiert wurde, liegen in einem weiten Bereich zwischen -60 und $+82$ ‰, während bei 650 °C aus denselben Proben extrahiertes H_2O δD-Werte zwischen -78 und $+40$ ‰ aufweist.

Der systematische Unterschied zwischen den δD-Werten bei den beiden Extraktionstemperaturen deutet darauf hin, dass sehr wahrscheinlich zwei isotopisch unterschiedliche Reservoire im hydrothermalen Fluorit vorhanden sind. Hierbei wird H_2O aus dem zweiten Reservoir erst bei höheren Temperaturen vermehrt freigesetzt. Um diese beiden Reservoire genauer zu charakterisieren, wurden repräsentative Proben mittels FTIR-Spektroskopie (Fourier Transform Infra Red) untersucht. Hierbei wurden Spektren von Fluorit und Fluideinschlüssen aufgenommen. Die FTIR-Spektren von Fluideinschlüssen zeigen zwei dominante Banden bei Absorptionswerten von 3400 cm^{-1} und 5200 cm^{-1}, die auf die O-H-Streckschwingung und die Rotationsschwingung des Wassermoleküls zurückzuführen sind. Im Unterschied dazu zeigen FTIR-Spektren von fluideinschlussfreien Bereichen des Fluorit nur die Streckschwingungsbande bei 3400 cm^{-1}. Dies belegt, dass signifikante Mengen an strukturgebundenem H_2O in den hydrothermalen Fluoriten vorliegen.

Wenn man die spektroskopischen und Isotopen-Daten zusammenfasst, so erscheint es plausibel, dass bei Extraktionstemperaturen oberhalb von 500-600 °C überwiegend strukturgebundenes H_2O freigesetzt wird. Dieses ist vermutlich als OH^- in Gitterdefekten im Fluorit eingebaut. Das strukturgebundene H_2O ist gegenüber dem aus Fluideinschlüssen stammenden H_2O isotopisch negativer, was zu einer signifikanten Verschiebung der Gesamt-Isotopensignatur führen kann. Solche Effekte müssen bei der Auswahl und Etablierung geeigneter analytischer Methoden für die H_2O-Extraktion aus Fluideinschlüssen berücksichtigt werden, um verfälschte Ergebnisse zu vermeiden. Weiterhin ergibt sich daraus, dass bei der Interpretation anomal niedriger δD-Werte grosse Vorsicht geboten ist.

Die mikrothermometrischen Untersuchungen der varistischen und postvaristischen Mineralisationen zeigen signifikante Unterschiede hinsichtlich der dominanten Fluid-Zusammensetzungen. Die meisten varistischen Fluideinschlüsse gehören zum H_2O-NaCl-(KCl)-Typ und zeichnen sich durch generell niedrige Salinitäten (0-10 Gew.-% NaCl-Äquivalent) und verhältnismässig hohe Homogenisierungstemperaturen (150-350 °C) aus. In einigen varistischen Proben ist zusätzlich ein sehr gasreicher CO_2-CH_4-H_2O-Einschlusstyp nachweisbar. Die Sauerstoffisotopendaten von Quarz der varistischen Gänge liegen zwischen +2.8 und +12.2 ‰, woraus sich $\delta^{18}O_{H2O}$-Werte der hydrothermalen Fluide von –12.5 bis +4.4 ‰ berechnen lassen. Die δD-Werte von H_2O, das aus Fluideinschlüssen extrahiert wurde, liegen zwischen –49 und +4 ‰. Unter Berücksichtigung der tektono-metamorphen Entwicklung legt die Synthese aller Daten eine Beziehung zwischen varistischer Mineralisation und regional-metamorphen Devolatilisierungs-Prozessen nahe.

Die postvaristischen Fluide haben deutlich andere mikrothermometrische und isotopische Signaturen. Alle Fluideinschlüsse in primärem Fluorit, Calcit, Baryt und Quarz gehören zum H_2O-NaCl-$CaCl_2$-Typ und die Salinitäten sind generell deutlich höher (22-25 Gew.-% NaCl-Äquivalent). Die Homogenisierungstemperaturen sind viel niedriger und liegen zwischen 110 und 180 °C. In einigen Proben von Fluorit, Calcit und Quarz, die zu einer späteren Generation gehören, ist noch ein niedrigsalinares (0-15 Gew.-% NaCl-Äquivalent) Fluid vorhanden. Die Homogenisierungs-temperaturen dieses Fluidtyps liegen in einem ähnlichen Bereich wie diejenigen des hochsalinaren Typs. Ramansonden-Messungen zeigen, dass in den postvaristischen Fluiden nur geringe Mengen an CO_2 (in der Gasphase) vorhanden sind.

Praktisch alle $\delta^{18}O$-Werte von Quarz der fluoritführenden postvaristischen Gänge liegen in einem relativ engen Bereich zwischen +11.1 und +19.5 ‰. Aus diesen Daten lassen

sich mittels der durchschnittlichen Homogenisierungstemperaturen der betreffenden Proben $\delta^{18}O_{H2O}$-Werte der hydrothermalen Fluide von -11.0 bis $+4.4$ ‰ berechnen. Diese Werte stimmen sehr gut mit den $\delta^{18}O$-Werten von direkt aus Fluoriten extrahiertem Fluideinschluss-H_2O überein, die zwischen -11.6 und $+1.1$ ‰ liegen. Die δD-Werte von H_2O aus Fluideinschlüssen in Calcit sind sehr homogen (-26 bis -15 ‰), während die δD-Werte von H_2O aus Quarz (-63 bis $+9$ ‰) und Fluorit (-29 bis -1 ‰) deutlich variabler sind. Aus Fluoriten konnte zusätzlich CO_2 extrahiert werden, dessen $\delta^{13}C$-Werte zwischen -21.4 und -6.7 ‰ liegen. Durch Kombination der mikrothermometrischen Daten mit O-Isotopengleichgewichten lassen sich Bildungsbedingungen der Gänge von 130-180 °C und 0.3-0.5 kbar berechnen. Die $\delta^{18}O_{H2O}$- und insbesondere die variablen δD-Werte belegen, dass die postvaristischen hydrothermalen Mineralisationen auf grossräumige Fluidmischungsprozesse zurückgehen. Die beiden Endglieder der Mischungsprozesse waren aus dem Grundgebirge stammende hochsalinare Fluide und aus oberflächennahen Bereichen zugeströmte niedrigsalinare meteorische Wässer.

Dieses konzeptionelle Modell wurde durch zusätzliche systematische C-, O- und S-Isotopenuntersuchungen an Sulfiden, Sulfaten und Carbonaten überprüft und durch integrierte Modellrechnungen quantifiziert. Primäre Calcite aus allen hydrothermalen Gängen zeigen eine signifikante positive Korrelation zwischen den $\delta^{13}C_{VPDB}$- und $\delta^{18}O_{VSMOW}$-Werten, die jeweils von -13 bis -3 ‰ und von $+12$ bis $+18.5$ ‰ variieren. Die C- und O-Isotopenzusammensetzungen von remobilisierten Calcitgenerationen sind deutlich zu positiveren Werten verschoben. Die $\delta^{13}C$- und $\delta^{18}O$-Werte dieser Calcite liegen im Bereich von -12 bis -1 ‰ und von $+20$ bis $+25$ ‰. Um die Kovariation der C- und O-Isotopendaten zu modellieren, wurde ein verbessertes numerisches Fluidmischungsmodell entwickelt. In diesem Modell wird die C-Speziation in den beiden Fluid-Endgliedern und den resultierenden Fluidmischungen mittels eines komplexen Speziations- und Reaktionspfad-Computercodes berechnet. Basierend auf diesen Modell-Daten wird dann die isotopische Massenbilanz unter Berücksichtigung von Konzentrationseffekten durch unterschiedliche Fluidzusammensetzungen (C-Konzentrationen, Salinität) gelöst. Die Berechnungen zeigen, dass die Kovariation der $\delta^{13}C$- und $\delta^{18}O$-Werte hydrothermaler Calcite des Schwarzwalds effektiv durch Mischung eines relativ hochtemperierten hochsalinen Fluids und kühlem meteorischen Wasser modelliert werden kann.

Die S-Isotopendaten sind mit dem Fluidmischungsmodell konsistent und erlauben eine Abschätzung der Paläotemperaturen der hochsalinen Tiefenfluide. Die $\delta^{34}S_{VCDT}$-Werte von 22 Bariten aus verschiedenen hydrothermalen Fluorit-Baryt-Quarz-Gängen variieren zwischen +9 und +18 ‰, während die $\delta^{34}S$-Werte verschiedener Sulfidminerale (Galenit, Chalkopyrite, Pyrit) zwischen –14.4 und +2.9 ‰ liegen. Die für koexistierende Sulfat-Sulfidpaare berechneten Gleichgewichts-Temperaturen liegen in einem sehr engen Bereich von etwa 300-350 ℃. Dieser Temperaturbereich unterscheidet sich deutlich von den Bildungstemperaturen der Gänge, die bei 150-200 ℃ liegen. Unter Berücksichtigung der Kinetik der Sulfat-Sulfid-Reaktion können die S-Isotopentemperaturen daher zuverlässig als Paläotemperaturen der Fluide interpretiert werden, die die Einstellung des Isotopengleichgewichts im Tiefenaquifer reflektieren. Dieses Modell wurde quantitativ auf seine Robustheit gegen mögliche Kontamination eines equilibrierten Sulfat-Sulfid-System durch zusätzliche Sulfatzufuhr während Fluidmischung getestet.

Eine Kombination der Fluideinschlussdaten mit den S-, C- und O-Isotopendaten ermöglicht eine Abschätzung der Mischungsverhältnisse zwischen dem hochtemperierten hochsalinen Fluid und dem kühlem meteorischen Wasser. Die Ergebnisse der Berechnungen zeigen, dass der Massenanteil des hochsalinaren Fluids im Bereich von 0.5 bis 0.75 liegt. Unter Berücksichtigung aller geologischen, geochemischen und isotopischen Daten ergibt sich ein konsistentes genetisches Modell für die Entsehung der postvaristischen hydrothermalen Gänge im Schwarzwald. Dieses Modell geht davon aus, dass praktisch alle metallführenden Fluorit-Baryt-Quarz-Gänge durch grossräumige variable Mischung von homogenen hochsalinaren Tiefenfluiden mit kühlen meteorischen Wässern gebildet wurden. Zusätzlich zeigt die vorliegende umfassende Studie, dass im Schwarzwald zwei sehr unterschiedliche Fluidsysteme aktiv waren, die beide ihren Ursprung im kristallinen Grundgebirge haben. Das jüngere, postvaristische Fluidsystem zeigt dabei sehr konstante geochemische und isotopische Zusammensetzungen über ein grosses Gebiet und einen sehr langen gelogischen Zeitraum von mindestens 100 Ma. Zahlreiche im Schwarzwald und in der Nähe des Rheingrabens aktive Thermalquellen legen nahe, dass ähnliche Fluidprozesse wie in den postvaristischen Mineralisationen konserviert immer noch aktiv sind.

1. INTRODUCTION

Triassic-Jurassic hydrothermal activity and mineralization throughout central and southern Europe were first identified by Mitchell and Halliday (1976). Typically, these mineralizations are characterized by base metals (mostly Pb-Zn) with minor amounts of Ag, and are hosted in quartz - carbonate - fluorite - barite veins. It has been noted that these base-metal veins occur preferentially along the margins of Mesozoic basins, particularly in the vicinity of older granites (Mitchell and Halliday 1976; Halliday and Mitchell 1984). The fluids are typically $CaCl_2$-NaCl-rich brines of moderate to high salinity with homogenization temperatures in the range of 70-200°C. Features indicative of repeated mixing with cooler meteoric waters, e.g. alternating growth zones within gangue minerals hosting high- and low-salinity fluid inclusions, are very abundant (Lüders and Franzke 1993). Pronounced examples of this widespread mineralization style are found in the French Massif Central (Munoz *et al*. 1994; 2005), the Paris basin (Charef and Sheppard 1988; Clauer *et al*. 1995), southwest Cornwall (Gleeson *et al*. 2000), Ireland (Wilkinson *et al*. 1995; 1999), Spain (Canals and Cardellach 1993) and many areas in Germany (Behr *et al*. 1987; Behr and Gerler 1987; Franzke *et al*. 1996; Meyer *et al*. 2000; Werner and Dennert 2004; Schwinn *et al*. in press).

The Schwarzwald is one of the old mining regions in Germany and well known for Pb-Zn-Cu-Ag mineralizations that occur in hydrothermal fluorite – barite – calcite - quartz veins in Variscan crystalline basement. The mining potential of the Schwarzwald was estimated as 0.2-0.3 Mt of Pb+Zn (Walther 1981); the fluorite+barite resources are on the order of about 10 Mt (Huck and Walther 1984). Based on fluid inclusion characteristics, the hydrothermal veins and fissure mineralizations in the Paleozoic basement and Permian-Mesozoic cover rocks of Germany can be grouped into two main classes (Behr and Gerler 1987): (1) mineralizations which are geologically and structurally related to the Variscan metamorphism and deformation or to Paleozoic granitic intrusions which mostly contain inclusion solutions with eutectic temperatures not below -24 °C, ($T_{m\ ice}$=-6-0 °C and T_h=140-350 °C) and (2) mineralizations related to post-Variscan tectonic processes, such as the rifting of the northern Atlantic ocean in the Jurassic-Cretaceous or in the Oberrhein region in the Tertiary. The Variscan veins contain predominantly fluid inclusions of the H_2O-NaCl-KCl type, which have generally low salinities and variable homogenization temperatures between 140 and 350 °C (Behr and Gerler 1987; Hein 1993; Muchez *et al*. 1998; 2000; Wagner and Cook 2000). In contrast, post-Variscan vein mineralizations with barite, fluorite and Pb-Zn ores in Harz, Rheinisches Schiefergebirge, Schwarzwald and Oberpfalz, Germany, contain fluid inclusions of the H_2O-NaCl-$CaCl_2$ type, which have high salinities (21-26 wt.%) and

homogenization temperatures in a much narrower range of 150-200 °C (Behr and Gerler 1987). These post-Variscan fluids were most likely derived from formation waters that migrated out of Permo-Triassic sedimentary basins into the Variscan basement. Fluid-rock interaction at temperatures of 300-350°C resulted in leaching of metals from the granites and gneisses; subsequent ascent of these metal-bearing brines along fault zones and mixing with meteoric sulphate and/or bicarbonate waters led to hydrothermal vein mineralization (Behr & Gerler 1987; Schwinn *et al*. in press).

Prolonged hydrothermal activity in the Schwarzwald area resulted in both multistage vein-type mineralization and large-scale alteration of the basement rocks. Most of the crystalline rocks show various degrees of hydrothermal alteration, with chloritization of biotite and sericitization and albitization of feldspars being the most notable alteration reactions. Entirely fresh metamorphic or igneous rocks are virtually absent in the Schwarzwald area. Microthermometric studies of fluid inclusions in quartz from hydrothermally altered granites in the southern Schwarzwald revealed homogenisation temperatures between 200 and 400 °C for the alteration and salinities up to 9 wt.% NaCl-equivalent (eqv.), thereby indicating infiltration of meteoric waters (Simon and Hoefs 1986; Hofmann and Eikenberg 1991). Based on δD and δ^{18}O analysis of altered granites and calculations using models for closed-system and open-system fluid-rock interaction (Taylor 1977; 1979), Hoefs and Emmermann (1983) estimated that the primary oxygen isotope composition of the fluids causing the alteration of the basement was around –9 ‰, which conforms to the typical value for recent surface waters.

This PhD research focused on the following three distinct topics:

- Water is the dominant constituent of ore-forming fluids, so information on its source is fundamental to understand the hydrothermal transport and deposition of metals. Natural waters of various origins exhibit systematic differences in their deuterium (D) and ^{18}O contents. Stable isotope ratios of oxygen (δ^{18}O) and hydrogen (δD) are therefore extremely important geochemical tracers to determine the origin of aqueous fluids in geological environments (Sheppard 1986). The acquisition of δD signatures from fluid inclusions, samples of geological fluids mechanically trapped during crystallization provides an invaluable insight into the isotopic composition of ancient fluids. The best way to directly determine the δD value of hydrothermal water is to measure the of hydrogen isotope composition of H_2O directly from fluid inclusions. However, due to their microscopic dimensions (typically <30 µm) direct determination of the δD signature of individual

13

inclusions is extremely difficult, since only small quantities can be extracted. Inclusion fluids in fluorite are particularly useful, because their host is devoid of oxygen or hydrogen, thus precluding post-entrapment isotope exchanges.

Water from fluid inclusions can be extracted by mechanical decrepitation, either where minerals are crushed in vacuum (Roedder 1958; Horita and Matsuo 1986), or, more typically, by thermal decrepitation which means heating a sample in an extraction line (Kishima and Sakai 1980; Friedman 1953; Craig 1961). The interpretation of δD signatures obtained from anhydrous minerals commonly assumes that the measured hydrogen uniquely comes from decrepitated fluid inclusions and the resulting δD signature is attributed solely to this reservoir. Hydrogen-bearing species released by mineral decrepitation are assumed to be similar in composition to those of the medium from which the crystal grew (Ihinger and Zink 2000). However, previous studies have postulated that non-fluid inclusion hydrogen reservoir may contribute significantly to the δD signature of quartz (Ishiyama *et al*. 1999; Knauth and Eipstein 1975; Simon 1997; 2001). Ishiyama *et al*. (1999) suggested that hydrogen released by decrepitation at temperatures between 300 and 500 °C yield accurate isotopic compositions of the precipitating fluid. However, stepped heating experiments above 500 °C yielded increasingly anomalous δD signatures (Ishiyama *et al*. 1999). This was confirmed by the observations made by Faure (2003) on fluid inclusions from quartz and calcite from a geothermal system. The majority of studies reporting low δD values from quartz employed extraction temperatures greater than 1000 °C (Sheets *et al*. 1996; O'Reilly *et al*. 1997; Gleeson *et al*. 1999; Barker *et al*. 2000).

As part of this thesis, the influence of structurally bound O-H species in hydrothermal fluorites on the anomalous δD value of fluid inclusion water thermally extracted from hydrothermal fluorites at different temperatures was investigated. The results of a combined stable isotope and infrared spectroscopic investigation of hydrothermal vein fluorites are reported here.

- The characteristics of hydrothermal fluids responsible for the large-scale alteration can be clearly distinguished from the $CaCl_2$-NaCl type brines with very high salinities (>23 wt.% NaCl eqv.) and homogenization temperatures <180 °C typical of the vein mineralizations (Lüders and Franzke 1993). Lüders (1994) concluded that the formation of post-Variscan hydrothermal vein minerals in the Freiamt-Sexau and the Badenweiler areas (western Schwarzwald) can be related to interactions and mixing of an ascending saline brine with

descending formation waters derived from the Mesozoic and Tertiary cover. Schwinn *et al.* (in press) calculated mixing ratios between 0.5 and 0.75 (brine/meteoric fluid) for a variety of veins. Hydrothermal processes at the boundary between the Jurassic and the Cretaceous have also been described outside the Schwarzwald based on isotopic dating. For instance, the Montroc fluorite deposit (southern Massif Central, France), the Paris basin and the Thüringischer Wald are related to the regional tectonic events that result from the opening of the north Atlantic ocean (Clauer *et al.* 1995; Franzke *et al.* 1996; Munoz *et al.* 2005). The migration of basinal Ca-Na-Cl brines from sedimentary basins into the basement has been illustrated in Cornwall (Gleeson *et al.* 2000) and Ireland (Wilkinson *et al.* 1999). The recent thermal and mineral waters in the Schwarzwald area show striking similarities to the paleo-hydrothermal systems that were responsible for the formation of the Pb-Zn-Cu ore deposits. Based on a regional study of the hydrochemistry of groundwaters in the crystalline basement of the Schwarzwald, two principal water types can be distinguished (Stober and Bucher 1999):

(1) Saline thermal waters from a number of prominent spas originate in about 3-4 km deep reservoirs. Their composition can be reasonably explained by mixing of surface-derived freshwater with saltwater, with several additional solute components derived from water-rock interaction.

(2) The second type is represented by mineral waters with comparatively low chlorinity and high concentrations of Ca, bicarbonate and dissolved CO_2. Both the low temperature (20-60 °C) and the low chlorinity indicate that their circulation path does not reach a depth greater than a few hundred meters and that mineral waters do not mix with saline deep water.

This research presents a comprehensive study of the fluid inclusion characteristics of the Variscan and post-Variscan hydrothermal veins, which is combined with oxygen isotopic data of vein quartz and hydrogen, oxygen and carbon isotope analyses of inclusion fluids from a large number of hydrothermal veins covering the entire Schwarzwald district. Based on these data and on calculations of isotopic fractionation trends, the fluid compositions and the physico-chemical conditions of ore formation are established. By integrating the available information on potential fluid sources and the geological framework, a consistent model of hydrothermal mineralization in the Schwarzwald district is developed.

- Fluid mixing is a widely recognized process in upper crustal hydrothermal systems (Jamtveit and Hervig 1994; Komninou and Yardley 1997; Gleeson *et al.* 2000; 2003; Douglas *et al.* 2003; Upton *et al.* 2003). Mixing of fluids with different chemical composition and/or

oxidation state commonly results in super saturation of ore and gangue minerals and occurs under conditions far from equilibrium with the host rocks (Bethke 1996). Consequently, fluid mixing is considered a significant precipitation mechanism involved in the formation of hydrothermal ore deposits. Many examples of Mississipi Valley-type deposits are believed to have been produced by the mixing of at least two fluids (Anderson 1975; Ohmoto and Rye 1979; Barrett and Anderson 1982) or a metal-bearing formation water with H_2S gas (Haynes and Kesler 1987; Jones and Kesler 1992). Mixing between basement brines and meteoric waters accounts for the formation of many vein-type Pb-Zn mineralizations, for example within the European Variscides (Lüders and Möller 1992; Lüders and Ebneth 1993; Zheng and Hoefs 1993a, b; Lüders 1994; Ritter 1995; Werner *et al*. 2000; 2002).

Stable isotope investigations of sulfur and carbon are important tools for deciphering the processes involved in the formation of hydrothermal mineralizations and can provide critical information about (1) the temperature of formation, (2) the physico-chemical conditions of the mineralization processes, and (3) the origin of the elements in solution (e.g., Rye and Ohmoto 1974; Ohmoto and Rye 1979; Hoefs 1987; Rye 1993; Ohmoto and Goldhaber 1997; Huston 1999; Heinrich *et al*. 2000; Simmons *et al*. 2000; Blakeman *et al*. 2002). In particular, the sulfide-sulfate redox reaction and the kinetics of the related isotopic fractionation may indicate fluid mixing from non-equilibrium assemblages of sulfide- and sulfate minerals (Ohmoto and Rye 1979). Calcites precipitated by mixing processes show carbon and oxygen isotope covariation trends controlled by the mixing ratio, the temperature and pH of the mixed fluids, and the isotopic compositions of the two or more fluid end-members (Zheng and Hoefs 1993c).

Fluid mixing ratios by a combination of stable isotope and fluid inclusion investigations were quantified. A model for the calculation of calcite precipitation trends, which considers the isotopic composition of the fluid end-members as well as the thermodynamically calculated carbon speciation in the mixed fluid, is proposed. Geochemical data of many individual deposits from an area of 120 by 40 km point to large-scale hydrothermal convection and a consistent model of hydrothermal mineralization via district-scale fluid mixing are developed.

2. GEOLOGICAL AND METALLOGENIC FRAMEWORK

2.1. GEOLOGICAL BACKGROUND

The Schwarzwald is one of the old mining regions of Germany. The oldest document proving mining activities dates from 1028 (Metz 1975; Schneiderhöhn 1958). The Schwarzwald crystalline basement complex belongs to the Moldanubian zone of the Central-European Variscan orogen. It covers an area of approximately 120 by 40 km area in SW Germany. The Variscan orogen is the product of late Palaeozoic continental collision between Gondwana and Laurasia. Volcanism and plutonism occurred from Devonian to Permian times, but mainly during the Carboniferous. The Variscan crystalline basement consists of ortho- and paragneisses, quite common with anatectic textures. Locally, the gneisses contain lenses of more or less retrogressed peridotites, pyroxenites, eclogites, and amphibolites (Kalt *et al*. 2000). The gneisses and migmatites were intruded by Variscan granitoids around 335-315 Ma (Kalt *et al*. 2000). The granites comprise both biotite and two mica S-type varieties. To the north and east, the basement is overlain by Mesozoic sediments, to the west the basement is cut by the Tertiary Rheingraben structure. In the area of the Schwarzwald, numerous SSW-NNE and E-W trending shear zones of Variscan origin are widespread phenomena. In the southern Schwarzwald, the SSE verging Todtnau fault (Badenweiler-Lenzkirch Zone) forms the boundary between the Central Gneiss Complex and the Southern Gneiss Complex. The polyphase Variscan tectono-metamorphic evolution in the central and southern Schwarzwald is distinguished by a sharp change in the tectonical regime. Collisional shortening and crustal stacking give way to crustal extension and thinning in the earliest Upper Carboniferous (Echtler and Chauvet 1992). The timing of the extension tectonics is well constrained by the age of the undeformed Albtal granite (Rb/Sr: 326 ±2 Ma, Schuler and Steiger 1978) and the Malsburg granite (U/Pb: 328 ±6 Ma, Todt 1976). The oldest fault controlled mineralizations are scheelite (Werner *et al*. 1990). Related to this major transition in structural evolution is the development of several crustal-scale ductile-brittle shear zones, which generally trend SSW-NNE and E-W. Activation and further development of these shear zones was accompanied by the formation of structurally-controlled quartz veins, which are locally mineralized with Au- and Sb-bearing sulphide assemblages (Werner *et al*. 1990).

The crystalline basement rocks were exhumed during the formation of the Tertiary Rheingraben structure (Kalt *et al*. 2000; Werner and Franzke 2001). The Schwarzwald area represents an erosional window through the post-Variscan cover to the Central European continental crystalline basement. Figure 1 shows the general geology of the basement and its

major cover units of the post-Variscan sedimentary cover. The local uplift of the Rheingraben shoulders started in the Oligocene and the general regional updoming of the Schwarzwald area has lasted since the Miocene to present times (Thury *et al.* 1994). The strong uplift exposed the Schwarzwald to erosion and led to the removement of most of the Mesozoic sedimentary cover units. The youngest marine sediments in the Rhein valley date back to the middle Oligocene (Schreiner 1991).

Von Gehlen (1989) concluded that Post-Variscan tectonic movements and the related formation of fracture zones and hydrothermal vein mineralization must have occurred almost continuously from the Upper Permian to the Upper Jurassic. The mineral veins were formed by strike-slip faulting along fractures active already during Variscan times. The interaction between these faults, E-W/NW-SE trending shear zones of Jurassic-Cretaceous age, and the reactivation of pre-existing metamorphic foliation resulted in complicated fault and mineral-vein patterns. The distribution of mineralized faults with predominantly sinistral strike-slip in the immediate vicinity of the Rheingraben and dextral strike-slip fault zones ca. 4-7 km east of the Rheingraben margin indicates a major change in the principal tectonic stress directions from NE-SW (early Miocene) to NW-SE and NNW-SSE (late Miocene) (Werner and Franzke 2001). The Sm-Nd dating of fluorite from the Montroc fluorite deposit (southern Massif Central, France), which is comparable to the Schwarzwald deposits gives an age of 111 ±13 Ma, which suggests the Albian/Aptian transition as the most likely period for large-scale fluid circulation during a regional extensional tectonic event related to the opening of the North Atlantic ocean (Munoz *et al.* 2005). The K-Ar dating and $\delta^{18}O$ analyses of sericite from the Offenburg trough indicate that sericitization occurred about 145 Ma ago (Jurassic) and the hydrothermal fluids had temperatures of 150-210 °C (Brockamp *et al.* 2003). The hydrothermal activity was found to have occurred about 145 Ma ago during the breakup of Pangaea, documenting an important step in the geological development of the European continent (Zuther and Brockamp 1988).

Groundwater composition in the crystalline basement of the Schwarzwald is quite variable. There are at least three types of different groundwater: Cl-rich thermal water, CO_2-rich mineral water and weakly mineralized surface-related water. Two chemically very distinct types of groundwater were distinguished: (1) CO_2-rich mineral waters and (2) Cl-rich thermal waters (Stober and Bucher 1999a). Thermal water generally has a higher degree of mineralization than the CO_2 –rich mineral water. Thermal water springs are typically found in granite; mineral water springs are predominantly located in gneiss. Most of the CO_2–rich waters contain Ca as the most abundant cation and are then of the Ca-Na-HCO_3 type. Total

dissolved solids (TDS) are weakly correlated with sampling depth at Peterstal and Griesbach but inversely correlated with depth at Teinach. This is strong evidence for local, shallow-level source of solutes. In the mineral waters, the total dissolved solids (TDS) reach values of 3000-4000 mg kg^{-1} and they contain much dissolved CO_2 (>2000 mg kg^{-1}). Because of the high free CO_2 content of these waters, pH is low throughout, often below six (Bucher and Stober 2000). The mole fraction X_{Na} (=Na/(Na+Ca)) in all the mineral waters varies between 0.39 and 0.70. The silica content of the waters is in equilibrium with quartz at temperatures of around 50-60 °C which suggests that the waters typically reside in the depth of 2-3 km. Dissolved silica in the chloride waters is much lower than in the mineral waters. The pH in this group is significantly higher than of the mineral waters. The average of 7.1, however, is low compared to waters that originate predominantly from silicate hydrolysis and water rock reactions (Bucher and Stober 1999). NaCl dominates all Cl-rich waters. The amount of TDS of the groundwater in the gneisses and granites of the Schwarzwald systematically increases with depth, and the water type changes from low-TDS Ca-Na-HCO$_3$ water near surface to Na-Ca-SO$_4$-HCO$_3$ and finally high-TDS Na-Cl water at depth (Stober 1995).
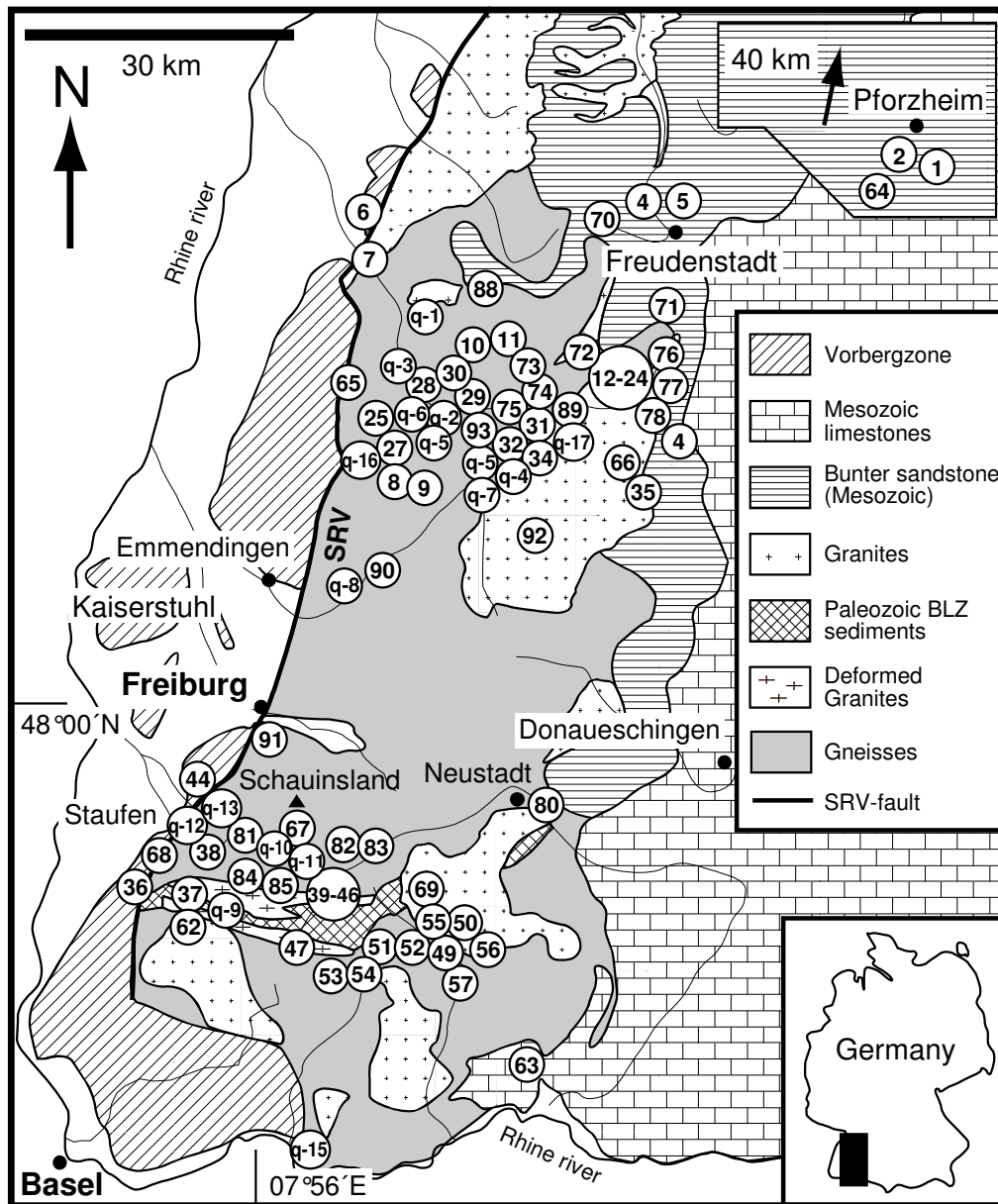
Figure 1. Simplified geological map of the Schwarzwald showing the location of the Variscan and post-Variscan hydrothermal vein deposits (after Walther *et al.* 1986). Numbers correspond to Table 1 and 2.

Table 1. Names of deposits and hydrothermal assemblages of Variscan quartz-veins.

No.	Deposit	Assemblage	No.	Deposit	Assemblage
q-1	Rossgrabeneck	Quartz-Tourmaline-W	q-10	Birkenberg, near St. Ulrich	Quartz-Ag-Pb-Zn-Fe
q-2	Baberast	Quartz-Ag-Sb	q-11	Gründenwald St. Ulrich	Quartz-Sb-Ag
q-3	Artenberg Q	Quartz-Sb-Pb	q-12	Schweizergrund Sulzburg	Quartz-Sb
q-4	Ludwig im Adlersbach	Quartz-Sb	q-13	Holderpfad Sulzburg	Quartz-Sb-Ag
q-5	Erletzberg, near Hausach	Quartz-Fe	q-14	Kleiner Langenbach Belchen	Quartz-Fe-(Cu)-(Pb)-Bi-Au
q-6	Ursula Welschensteinach	Quartz-Sb	q-15	Egghalde Gang A Bad Säckingen	Quartz (Fluorite)-W
q-7	Bärenbach	Quartz-Fe	q-16	Segen Gottes Q Schnellingen	Quartz-Sb-Au
q-8	Hornbühl 32 Suggental	Quartz-Sb-Ag	q-17	Barbara Oberentersbach	Quartz-Sb-Ag
q-9	Münstergrund Münstertal	Quartz-Sb-Ag			

Table 2. Names of deposits and hydrothermal assemblages of post-Variscan fluorite-bearing veins.

No.	Deposit	Assemblage	No.	Deposit	Assemblage
1	Käfersteige, near Pforzheim	Fluorite-Barite Cu-Bi	47	Herrmann, near Görwihl	Quartz-Fluorite Pb
2	Heiligenwald, near Pforzheim	Fluorite	48	Riedlingen, near Kandern	Fluorite
3	Friedenweiler, near Eisenbach	Fluorite Cu-Bi	49	Urberg	Quartz-Fluorite-Barite-Calcite Pb-Zn-Cu
4	Dorothea, near Freudenstadt	Barite Cu-Bi-Ag	50	Bildsteinfelsen, Urberg	Quartz-Fluorite-Barite-Calcite Pb-Zn-Cu-Ag
5	Wittenweiler, near Freudenstadt	Fluorite-Barite	51	Gottesehre, Urberg	Quartz-Fluorite-Barite-Calcite Pb-Zn-Cu-Ag-As-Co-Ni
6	Zunsweier, near Offenburg	Fluorite	52	Neuglück, Urberg	Quartz-Fluorite Pb
7	Ohlsbach, near Offenburg	Fluorite-Apatite-(Barite)	53	Schwarzwaldsegen, Urberg	Quartz-Fluorite Pb
8	Hesselbach, near Oberkirch	Fluorite Cu-(Bi)	54	Neue Hoffnung, Urberg	Quartz-Fluorite Pb
9	Ödsbach, near Oberkirch	Fluorite Cu-(Bi)	55	Ruprechtgang, Urberg	Quartz-Fluorite Pb
10	Clara, near Wolfach	Barite-Fluorite Cu-Ag-Pb-As-Sb	56	Brenden	Quartz-Fluorite Pb-(Cu)
11	Friedrich-Christian	Fluorite-Barite-Quartz-Calcite Pb-Cu-Ag-Bi	57	Igelschlatt, Schlüchttal	Quartz-Fluorite Pb-Cu-(Zn)
12	Sophia, Wittichen	Barite-Fluorite Co-Ni-Ag-Bi-U	58	Hausen, Wiesental	Fluorite
13	Johann, Wittichen	Barite-Fluorite Bi-Cu	59	Wehratal	Fluorite
14	Neuglück, Wittichen	Barite-Fluorite Co-Ni-Ag-Bi-U	60	Tierlen, near Witzau	Fluorite-Barite-Quartz Pb-Zn
15	Bleilersgrund, Wittichen	Fluorite	61	Nöggenschwiel	Fluorite
16	Ilse i. Kaltbrunn, near Wittichen	Fluorite Cu-Bi	62	Sulzburg	Quartz (Amethyst)

17	Burgfelsen, Ilse, near Wittichen	Fluorite		63	Mühlsteinbruch, near Waldshut	Quartz-(Barite)-(Fluorite)
18	König David, Gallenbach	Fluorite-Barite Cu-Bi-Co		64	Neubulach	Quartz-Barite-Calcite Cu-Bi-As
19	Hilfe Gottes, near Schiltach	Quartz Co-Bi-U		65	Michael im Weiler	Barite Pb-Zn-U-As
20	Herzog Friedrich, Reinerzau	Fluorite-Barite Co-Ag-U		66	Geigeshalde	Barite Bi-U
21	Daniel Gallenbach, Wittichen	Fluorite-Barite Cu-Bi		67	Schauinsland	Quartz-Barite-Calcite Pb-Zn
22	Neubergmännisch Glück, Wittichen	Fluorite Cu-Bi		68	Kobaltgrube	Barite-Quartz-(Fluorite) Co-(Ni)-Ag-Pb-Cu-(Zn)
23	Schlechthalde, near Wittichen	Fluorite		69	Menzenschwand	Barite-Fluorite-Quartz U-(Pb)-(Cu)
24	Southern Reinerzau valley	Fluorite Cu-Bi		70	Daniel Dehs, Bad Rippoldsau	Quartz Cu-Ag-Bi
25	Drey, Schnellingen	Barite-Fluorite		71	Johann Baptist, near Rippoldsau	Quartz Cu
26	Barbara, Schnellingen	Barite-Fluorite Pb-Zn		72	Anton im Heubach, Schiltach, Kinzig	Barite-Fluorite Co-Ni-Ag-Bi-U
27	Segen Gottes, Schnellingen	Barite-Fluorite Pb-Zn-Ag		73	Bernhard, Hauserbach	Siderite-Calcite-Barite Pb-Zn-Fe
28	Artenberg quarry, Steinach	Quartz-Calcite-Fluorite Cu-As		74	Maria Theresia Hauserbach	Dolomite-Calcite-Barite Pb
29	Erzengel Gabriel, near Hausach	Fluorite-Barite Pb		75	Katharina,Trillen-grund, near Schiltach	Barite-Calcite Cu-Bi
30	Laßgrund, near Hausach	Fluorite-Barite Pb		76	Rötenbach quarry, near Alpirsbach	Calcite-Dolomite Co-Bi-Ag
31	Wenzel, near Wolfach	Barite-Calcite Ag-Sb-(Ni)		77	Christiana, Wittichen	Barite (Co)
32	Fortuna Gelbach, near Wolfach	Fluorite-Barite Pb-Ag		78	Simson, Wittichen	Barite-Fluorite Co-Ni-Ag-Bi-U
33	Ludwigs Trost, Kuschbach	Fluorite-Barite Fe-(Pb)-(Ag)		79	St. Josef am Silberberg, Wittichen	Barite-Fluorite Co-Ni-Ag-Bi-U
34	Hohberg, near Wolfach	Fluorite-Barite Fe		80	Hammereisenbach, E Titisee-Neustadt	Barite Fe-Mn
35	Tennenbronn, near Schramberg	Fluorite		81	Giftgrube,Kaltwasser Münstertal	Dolomite-Calcite Pb-As
36	Badenweiler	Quartz-Barite-Fluorite Pb-(Zn)-(Cu)		82	Fahl, near Todtnau	Fluorite-Barite-Quartz Pb
37	Sulzburg	Fluorite		83	Gschwend, near Todtnau	Fluorite-Barite Pb
38	Bad Sulzburg	Quartz-Fluorite		84	Herrenwald, Münstertal	Fluorite-Barite Pb-Zn
39	Schlossberg-W, Rammelsbach	Quartz-Fluorite-Barite Pb-Cu		85	Anton, Wieden	Fluorite-Barite Pb-Zn-Ag
40	Teufelsgrund, Münstertal	Quartz-Fluorite-Calcite-Barite Pb-Ag-Zn		86	Silbergründle Seebach	Quartz Pb
41	Tannenboden, Wieden	Fluorite-Barite-Quartz Pb-(Zn)-(Cu)-(As)-(Ag)		87	Königswart Murgtal	Quartz-Barite Cu-Bi
42	Baumhalde, Todtnau	Quartz-Fluorite Pb-Zn-Cu-(Ag)		88	Silberbrünnle Gengenbach	Quartz Cu-Bi-As-(Pb)-(Ag)
43	Brandenberg	Quartz-Fluorite-(Calcite) Pb-(Ag)-(Zn)-(Cu)		89	Lorenz Wolfach	Quartz Cu
44	Schönenberg, Schönau	Fluorite-Barite-Quartz Pb-Cu		90	Tunnel near Waldkirch	Calcite-Dolomite
45	Aitern-Süd, Schönau	Fluorite-Barite-Quartz Pb-Zn-Cu		91	Merzhausen near Freiburg	Calcite-Pyrite
46	Schönau	Fluorite-Quartz Pb		92	Tunnel near Hornberg	Calcite-Siderite-Fluorite
				93	Hechtsberg quarry	Calcite

2.2. METALLOGENESIS AND HYDROTHERMAL VEINS

The Schwarzwald district hosts more than 400 individual hydrothermal veins, which cut the Variscan crystalline basement and the overlying Bunter sandstone quartzites (Fig. 1). The veins have been classified into (1) quartz veins, which are most probably of Variscan origin, and (2) post-Variscan metal-bearing fluorite-barite-quartz veins. The post-Variscan veins follow either pre-existing Variscan fracture zones or structures, which are subparallel to the Rheingraben (Werner and Franzke 2001). Based on their mineralogy, several sub-types of hydrothermal mineralization can be distinguished, which are, for example, Sb-Ag-bearing quartz veins (most likely Variscan, occurring throughout the entire district), Co-Ni-Ag-Bi-U-bearing barite-fluorite-veins (post-Variscan, in the Wittichen area), Fe-Mn-bearing quartz-barite-veins (Jurassic, in the Eisenbach area) and the post-Variscan to Tertiary Pb-(Zn)-(Ag)-bearing quartz-fluorite-assemblages in the southern and central Schwarzwald (Metz *et al.* 1957; Bliedtner and Martin 1988). Most of these veins do not host minerals suitable for radiometric dating. From the previous studies, however three mineralization events could be distinguished based on U-Pb and U-Xe, Xe-Xe dating of hydrothermal pitchblende, on U-He dating of hematite, and on K-Ar dating of K-bearing Mn minerals: one at 280 to 310 Ma during to the end of the Variscan orogeny (Hofmann and Eikenberg 1991; Segev *et al.* 1991; Meshik *et al.* 2000; Wittichen area, Menzenschwand deposit), a second one at 110 to 150 Ma (Segev *et al.* 1991; Wernicke and Lippolt 1993; 1997; Hohberg and Eisenbach area), and a third one at 50-30 Ma related to the formation of the Rheingraben structure (Hofmann and Eikenberg 1991; Menzenschwand deposit). Fluid inclusion (Lüders 1994; Hofmann and Eikenberg 1991; Werner *et al.* 1990; von Gehlen 1989; Behr *et al.* 1987) and tectonic studies (Möller *et al.* 1990a,b; Werner *et al.* 1990; Franzke 1992) combined with the few available radiometric data allow to divide the vein mineralizations in the Schwarzwald area into Variscan quartz veins with or without pitchblende related to low-salinity waters with last melting temperatures of around 0 °C and post-Variscan, mainly fluorite ± barite ± quartz bearing veins related to highly saline brines with last melting temperatures from -20 to -30 °C. From the tectonic point of view, most of the veins are subparallel to the Oberrheingraben structure or they follow fractures, which have been active since late-Variscan time (Werner and Franzke 2001). Within the veins, brecciation of the hydrothermal material, preserved imprints of the dissolved euhedral fluorite crystals, and the common replacement of euhedral barite by quartz prove multiple hydrothermal events (Metz *et al.* 1957; Bliedtner and Martin 1988). Alteration effects have been dated by K-Ar and Ar-Ar studies of sericitized feldspars

from the basement and the overlying Triassic Buntsandstein sandstone at 110-150 Ma (Zuther and Brockamp 1988; Lippolt and Kirsch 1994; Meyer *et al*. 2000).

2.3. PREVIOUS STUDIES

Although a limited number of fluid inclusion analyses of individual post-Variscan deposits has been performed, a systematic and comprehensive study that would link trends on the deposit scale with large-scale processes has not yet been provided. Furthermore, no previous study has integrated the fluid inclusions records with systematic investigations of the stable isotope systematics of the Variscan and post-Variscan veins. The result of the previous studies indicate that the aqueous hydrothermal fluids in the post-Variscan veins are characterized by relatively high salinities (23-26 wt.% eqv. NaCl) and homogenization temperatures below 250 °C (Behr *et al*. 1987; von Gehlen 1989; Werner *et al*. 1990; Hofmann and Eikenberg 1991; Lüders 1994; Ritter 1995; *this study*). Within single deposits, most commonly only one principal fluid type with a comparatively homogeneous range in salinity is present. Some deposits structurally related to the Tertiary Rhein Graben show a somewhat different fluid record. The salinities of aqueous fluid inclusions are highly variable between 1.7 and 25.6 wt. % eqv. NaCl and indicate mixing of low saline water with the deep-sourced saline brine (German *et al*. 1994; Lippolt and Werner 1994; Lüders 1994; Weber 1997; Werner *et al*. 2000; 2002). Most importantly, crush-leach analysis of the Cl/Br ratios of fluid inclusions from more than 30 Schwarzwald deposits shows that formation of the hydrothermal ore deposits is clearly related to mixing of low-salinity meteoric waters with a deep saline brine of more than 30 wt.% equivalent NaCl (Markl *et al*. in prep.).

The available stable isotope data are generally very limited in coverage. Previous carbon and oxygen isotope investigations showed $\delta^{13}C$ (V-PDB) and $\delta^{18}O$ (V-SMOW) values from –12 to +2.9 ‰ and from +12 to +18.5 ‰ for primary calcites (Hofmann 1989; Lüders 1994). Sulfur isotope studies indicate that most deposits display a consistent sulfate-sulfide isotope fractionation, which is interpreted as a preserved fractionation that was established in the deep aquifer (Schwinn *et al*. in press). The calculated paleo-temperatures of 300-350 °C are consistent with paleogeothermal models and phase equilibria constraints on alteration assemblages that are observed in hydrothermally overprinted granites. Oxygen isotope studies of only two hydrothermal veins showed $\delta^{18}O$ values from +15.5 to +19.4 ‰ and from +15.3 to +20.0 ‰ in the Schauinsland and Menzenschwand deposits, respectively (Weber 1997; Hofmann 1989). Von Gehlen et al. (1962) have reported the results of a relatively limited sulfur isotope study of sulfide and sulfate minerals from 21 Schwarzwald deposits. The study

24

revealed rather consistent δ^{34}S values for sulfide ores (galena: –12.4 to –2.6 ‰; sphalerite: –1.2 to +2.3 ‰) and barite (+8.3 to +16.8 ‰) from different deposits. Few additional sulfur isotope data exists from deposits, which are structurally related to the Tertiary Schwarzwald Randverwerfung fault. Sulfide and sulfate values from the Freiamt-Sexau mining area, Badenweiler (Lüders 1994) and from the Schauinsland deposit (Mittelstädt 1987; Weber 1997) show the same range of δ^{34}S values as reported by von Gehlen (1962). Based on these data, a qualitative fluid mixing model was proposed for the formation of the hydrothermal mineralizations. This model assumes that the aqueous sulfates were derived from sulphate bearing units of the sedimentary cover, whereas reduced sulfur originated from destruction of sulfides in metamorphic rocks of the crystalline basement (Werner *et al.* 2000; Werner *et al.* 2002). Variscan and post-Variscan barite could be distinguished in the Menzenschwand mine (Hofmann 1989), with the Variscan mineralization having distinctly lower δ^{34}S values (+7.2 to +8.0 ‰) than post-Variscan barites (+15.4 to +15.8 ‰). Müller et al. (1966) have analyzed sulfates in the Mesozoic sedimentary cover and the Tertiary sediments of the Rheingraben. The Triassic Muschelkalk and Keuper units show δ^{34}S values of +18.5 to +21.0 ‰ and +14.3 to +18.3 ‰, respectively. Jurassic sediments display δ^{34}S values of +16.0 to +19.0 ‰ and Tertiary units have values between +11.0 and +13.0 ‰.

Carbon and oxygen isotope data were reported from the Freiamt-Sexau mining area and from the Schauinsland deposit (Lüders 1994). Two generations of siderites from Freiamt-Sexau show slight differences in their isotopic composition (generation 1: δ^{13}C of –1.7 to +2.9 ‰ and δ^{18}O of +17.3 to +17.8 ‰; generation 2: δ^{13}C of –3.5 to –3.2 ‰ and δ^{18}O of +14.6 to +15.5 ‰). In contrast, calcites from the Schauinsland mine display distinctly lower δ^{13}C and δ^{18}O values of –9 and +12 ‰, respectively, indicating different carbonate sources in these deposits. The δ^{13}C values of Variscan and post-Variscan calcites from the Menzenschwand mine cover a range between –10 and 0 ‰, whereas post-Variscan samples display significantly lower values than Variscan calcites (Hofmann 1989). Weber (1997) reports a single measurement of strontianite with δ^{13}C of –5.8 ‰ and δ^{18}O of +20.3 ‰ from the Schauinsland mine.

In contrast to most previous fluid inclusion and stable isotope work, the present study provides a systematic and comprehensive dataset of a variety of hydrothermal mineralization styles from entire Schwarzwald district covering almost 300 Ma of formation history. In addition to the isotope data obtained from hydrothermal minerals, direct isotopic measurements of fluid inclusion water provide much better constraints on the sources and

processes involved into the formation of the hydrothermal veins. Through a systematic carbon and sulfur isotope study, we could demonstrate that the δ^{13}C and δ^{18}O covariation of hydrothermal calcites is related to mineral deposition through mixing of two fluid end-members.

3. SAMPLE DESCRIPTION AND PETROGRAPHY

3.1. SAMPLING STRATEGY AND GENERAL SAMPLE DESCRIPTION

The samples analyzed for the present study cover the whole area of the Schwarzwald, hence an area of about 120 by 40 km. So far, around 400 hydrothermal veins from the Schwarzwald basement have been sub-economically mined. In the frame of this PhD project, samples of hydrothermal quartz, fluorite, calcite, sulfides (galena, chalcopyrite, sphalerite, pyrite) and barite from 110 different Variscan and post-Variscan hydrothermal mineralizations have been analyzed. The locations are shown in Figure 1; the names and hydrothermal assemblages of the deposits are listed in Table 1 for Variscan and Table 2 for post-Variscan deposits. The selected deposits host various proportions of fluorite, quartz, calcite and barite as the major vein-filling gangue minerals, which are associated with complex ore assemblages of Pb, Zn, Cu, Fe, Co, Ni, Ag, U, Bi, Sb, As and W. Most of the veins crosscut the gneisses (Fig. 2A) and granites (Fig. 2B) of the Variscan crystalline basement, but the sedimentary Bunter sandstone cover rocks also host some deposits (Fig. 2C).
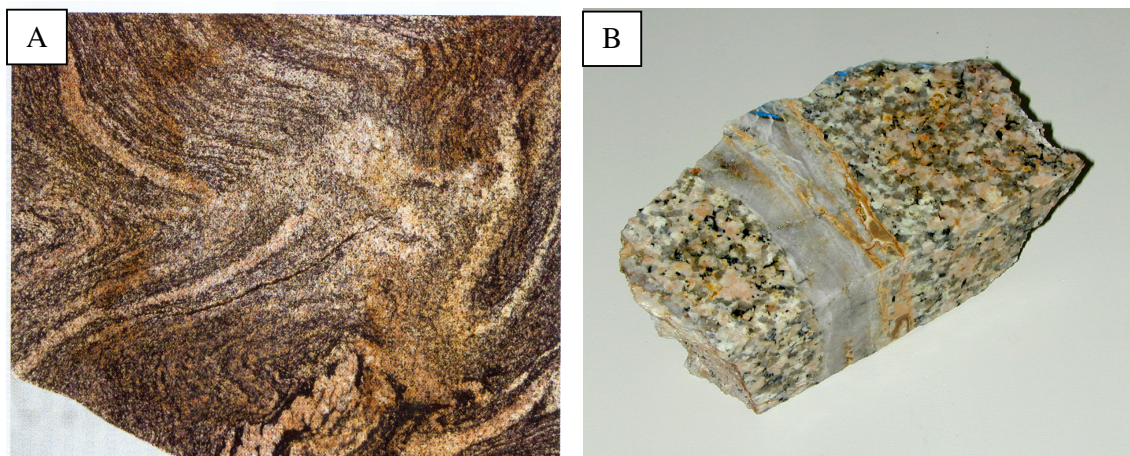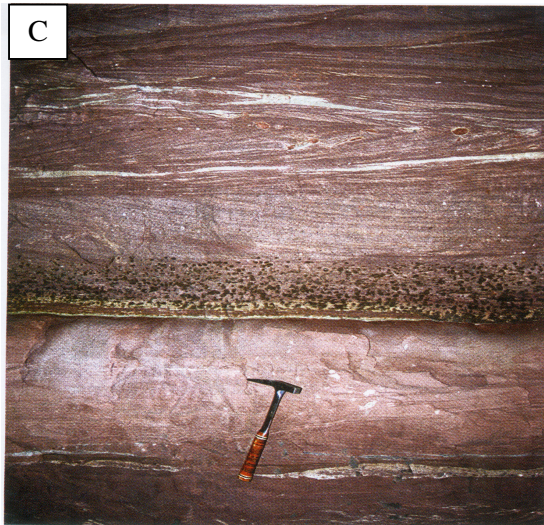
Fig. 2. Photographs of host rocks. **(A).** Deformed, biotite rich paragneiss. Typical rock from Feldberg-Schauinsland massif. **(B).** Granite-hosted quartz veinlet. Location: Igelschlatt deposit.

(C). Typical Bunter sandstone from northern Schwarzwald. Red- and yellow-layered sandstones represent the characteristics of cross-bedding textures. The dark mottling is the weathering of mangan bearing carbonite. Location: Hella-Glück-Stollen at Neubulach

Some typical vein mineralizations are illustrated in Figure 3.

Fig. 3. (A). Hydrothermal vein I: Quartz brecciation in shearzone. An about eight cm thick quartz vein with pyrite and marcasite are the result of tectonic movement during quartz deposition. Bleached and silicified gneiss is broken and is mineralized again. Location Steinbruck Artenberg at Steinach. **(B).** Hydrothermal vein II: Bismuth-chalcopyrite bearing quartz- rose calcite vein is hosted in altered granite. Location: Friedrich-Christian deposit. **(C).** Hydrothermal vein III: An about 10 cm thick white quartz band in gneiss from the Friedrich-Christian deposit. Silver gray galena occurs at the contact between gneiss and quartz and contains silver ore. **(D).** Hydrothermal vein IV: Typical Pb-Zn-Cu-bearing fluorite-barite-quartz vein. Location: Brenden deposit.

Most common and particular characteristics of the minerals from the Schwarzwald deposits are shown in Figure 4.
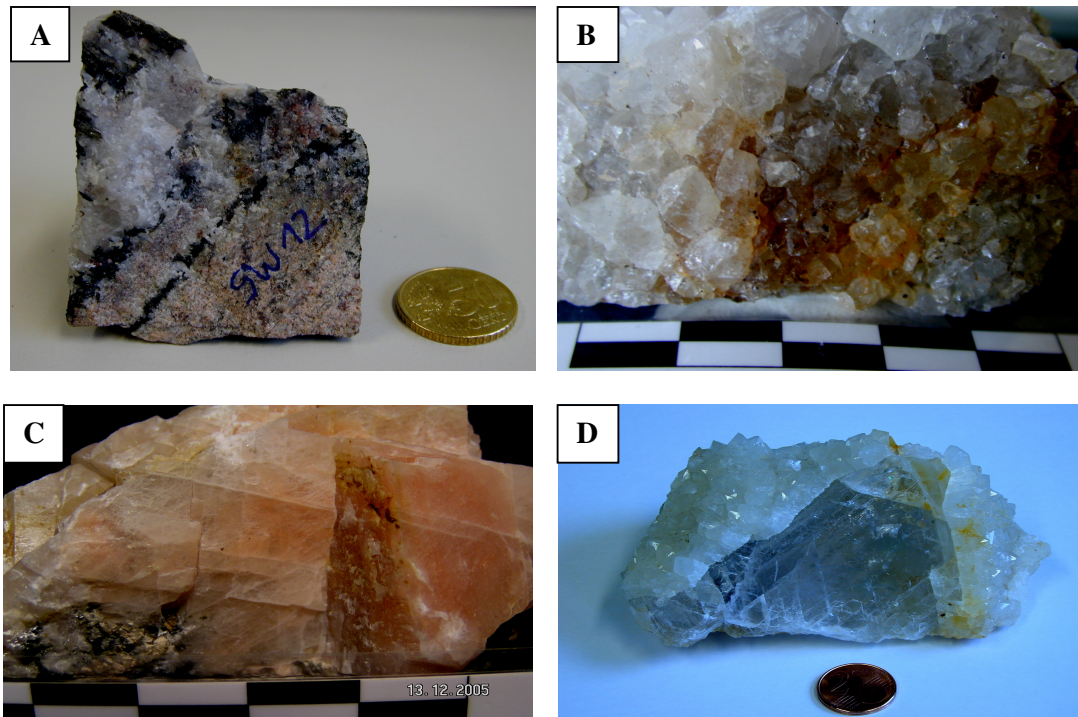
Fig. 4. Hydrothermal vein minerals. **(A).** Vein mineral I: Quartz-tourmaline-wolframite vein in granite. Quite a common mineral in the hydrothermal vein is dense, fine-grained, and gray to white quartz. Location: Rossgrabeneck deposit. **(B).** Vein mineral II: Euhedral quartz with goethite coating. Vuggy, euhedral quartz crystals are common. Location: Segen Gottes deposit. **(C).** Vein mineral III: Dense barite. Another common mineral in the Schwarzwald is barite, which typically occurs in compact masses with hematite fractures. Location: Neuglück Wittichen. **(D).** Vuggy, euhedral quartz crystals overgrow colorless fluorite. Location: Friedrich-Christian deposit.

All samples were carefully compared with previous detailed descriptions (Metz *et al*. 1957; Bliedtner and Martin 1988) to identify different generations of formation within the veins. In order to compare the data from the hydrothermal veins, some Variscan, deformed quartz veins

and lenses in the basement gneisses and post-sedimentary chalcedony in the feldspathic sandstones from the sedimentary cover were sampled as well. Apart from the Clara mine near Wolfach, the deposits of the Schwarzwald were abandoned thenths to hundreds of years ago. Nevetheless, several still accessible mines were sampled in detail during fieldwork and distinguishable generations of minerals within the single deposits could be investigated. The other samples used for investigations were taken from the collection of the Institute of Geosciences in Tübingen and from private collections but were checked carefully against older descriptions of comparative sample material in order to make sure, which mineral generation from which deposit was analyzed.

The information about the stage of mineralization for the deposits of the Northern and Middle Schwarzwald refers to the publication of Bliedtner and Martin (1988), for the deposits of the Southern Schwarzwald to the publication of Metz *et al.* (1957).

3.2. SAMPLES USED FOR FLUID INCLUSION AND RAMAN SPECTROSCOPY

For fluid inclusion study, more than 150 individual samples were selected from 75 localities of different hydrothermal vein-types (Pb-Zn-Cu-bearing fluorite-barite-quartz veins, Co-Ni-Ag-Bi-U-bearing barite-fluorite-quartz veins and Sb-Ag-bearing quartz veins) within the Schwarzwald. Fluorite, calcite, barite and quartz samples were selected from various localities in the Schwarzwald and were prepared as double polished wafers (up to 500 μm thickness) by hand polishing at the Fluid inclusion laboratory at the University Tübingen for fluid inclusion petrography and microthermetry. The names of the deposits with their hydrothermal assemblages and the sampled mineralization stage are given in Table 1 and 2 while Fig. 1 shows the deposit's locations.

3.3. SAMPLES USED FOR OXYGEN ISOTOPE IN QUARTZ

For oxygen isotopes, we analyzed 125 quartz samples from 48 localities in the Schwarzwald. The names, hydrothermal assemblages of the ore deposits and sample descriptions are listed in Table 3 for Variscan and in Table 4 for post-Variscan deposits.

3.4. SAMPLES USED FOR SULFUR AND CARBON ISOTOPES

For sulfur isotopes, we analyzed 116 sulfides (galena, chalcopyrite, sphalerite, pyrite) and barite samples from 23 post-Variscan deposits in the Schwarzwald. Furthermore, more than 80 samples of carbonates from 36 different post-Variscan deposits were analyzed. The locations are shown in Fig. 1, the names and hydrothermal assemblages of the ore deposits are

listed in Table 1. All samples were carefully compared with detailed textural descriptions (Metz *et al.* 1957; Bliedtner and Martin 1988) to identify different mineral generations within the veins and to ensure that only cogenetic sulfide-sulfide and sulfide-sulfate mineral pairs were used for the calculation of isotopic equilibrium temperatures. Primary hydrothermal calcite I usually occurs as coarse-grained, rhombohedral calcite of white or reddish colour. The remobilized calcite generations II and III are skalenohedral crystals of white or yellow colour, most frequently calcite II and III occur as euhedral crystals in vugs. Calcites IV are sub-recent calcite sinters deposited on the walls of the mining place. In addition, samples from the limestone units of the sedimentary cover and from a metamorphic prehnite-pectolite vein of Variscan age were analyzed.

4. ANALYTICAL TECHNIQUES

4.1. MICROTHERMOMETRY

Microthermometric measurements were carried out on doubly polished sections (200-400 μm thickness) using a Leica DMLP microscope equipped with a Linkam THMS-600 programable freezing-heating stage and a digital photo camera and image analysis system. The heating rate close to the phase transitions was 0.2 °C per minute throughout the measurements. The cooling-heating stage was calibrated by replicate measurements of synthetic fluid inclusion standards, i.e. the triple point of pure CO_2 (-56.6 °C), the melting point of pure H_2O (0.0 °C) and the critical homogenization of pure H_2O (374.1 °C). The reproducibility of all measured melting and homogenization temperatures is around 0.1-0.2 °C and 2-3 °C, respectively. Apparent salinities, expressed as weight percent (wt.%) NaCl equivalent, were calculated from the measured final ice melting temperatures of aqueous two-phase fluids following the methods described in Roedder (1984) and Bodnar *et al*. (1994). For the system NaCl-CaCl$_2$-H$_2$O, salinities were termed as weight percent (wt.%) NaCl and (wt.%) CaCl$_2$ equivalents, for which final melting temperatures of ice and hydrohalite are required.

4.2. OXYGEN ISOTOPE ANALYSIS OF QUARTZ

Mineral separates were prepared by careful hand-picking under a binocular microscope, followed by cleaning in deionized water. Oxygen isotope analysis was performed at the Institut für Geowissenschaften, University of Tübingen, using a laser extraction procedure

that essentially follows the techniques described by Sharp (1990) and Rumble and Hoering (1994). Approximately 2 mg of quartz grains were loaded onto a small Pt-sample holder and evacuated. After overnight prefluorination of the sample chamber, the samples were heated with a CO_2 laser at an F_2 pressure of 50 mbar. Excess F_2 was removed from oxygen by reaction with KCl at 150 °C; residual Cl_2 was separated from oxygen using a liquid nitrogen cold trap (-180 °C and -110 °C). The extracted O_2 was collected on a molecular sieve, subsequently expanded and measured on a Finnigan MAT-252 gas source mass spectrometer for the $^{18}O/^{16}O$ isotope ratio. Reproducibility of the analytical results, and mass spectrometer calibration, was monitored through replicate measurements of the international standard NBS-28 ($\delta^{18}O_{V-SMOW}$: +9.6 ‰). The analytical precision (1σ) was around ± 0.2 ‰. All oxygen isotopic data are reported in standard delta notation, relative to V-SMOW.

4.3. STABLE ISOTOPE ANALYSIS OF FLUID INCLUSIONS

4.3.1. δD, $\delta^{13}C$ AND $\delta^{18}O$ ISOTOPE ANALYSIS OF FLUID INCLUSIONS IN QUARTZ, FLUORITE AND CALCITE.

Following microthermometric characterization, exclusively samples containing a single generation of fluid inclusions were selected for δD, $\delta^{18}O$ and $\delta^{13}C$ analyses of inclusion fluids in pure fluorite, quartz or calcite. Approximately 4 g of each sample with a grain size of 3-6 mm were carefully hand-picked and cleaned in deionized water. Extraction of the inclusion fluids was performed in a vacuum extraction line following techniques outlined by Kishima and Sakai (1980), Friedman (1953), Craig (1961) and Jenkin *et al.* (1994). The samples were loaded into vacuum glass tubes and heated at 150 °C overnight. Inclusion fluids were extracted by thermal decrepitation under vacuum at 400 °C for analysis of δD (fluorite, quartz, calcite), and at 650 °C for analysis of $\delta^{13}C$ and $\delta^{18}O$ (only fluorite). The extracted fluids were collected in a liquid nitrogen cold trap; volatiles were not passed over a CuO furnace. The liquid nitrogen cold trap was then replaced by an alcohol and dry-ice slush (–80 °C) to separate molecular water from the condensable gases (Vennemann and O'Neil 1993; Demeny 1995). The water itself was converted to H_2 gas by reaction with 150 mg of Zn (obtained from Indiana University, USA) in vacuum quartz-glass tubes for 15 minutes at about 500 °C, as described by Friedman (1953) and Craig (1961).

For oxygen and carbon isotopes of fluid inclusions from fluorites, the cryogenically purified water (-80 °C) was equilibrated with a measured amount of carbon dioxide gas of

known initial isotopic compositions (δ^{13}C=-30.22‰ V-PDB, δ^{18}O=-1.07‰ V-PDB) for three days in glass tube at 25 °C. After equilibration, the carbon dioxide gas was then separated from the water using cold liquid nitrogen trap. Cryogenically purified CO_2 of inclusion gas from fluorites was directly collected. The δD and δ^{18}O values of released fluid inclusion water and the δ^{13}C and δ^{18}O values of released CO_2-fluid inclusion gas were measured on a Finnigan MAT-252 mass spectrometer with working standards calibrated against international standards (V-SMOW for oxygen and hydrogen, V-PDB for carbon). Results of hydrogen isotope analysis are normalized to internal biotite and kaolinite standards, which have δD value of –64 ±5.0 ‰ and -125 ±5.0 ‰, respectively. This internal biotite and kaolinite standards had previously been calibrated against the international biotite standard NBS-30 (δD: –65 ‰). The extraction procedure for the biotite and kaolinite standards was slightly different from the method described above. Biotite and kaolinite were heated to about 1200 °C and the released volatiles were passed over a CuO furnace to oxidize hydrogen to water. The analytical precision is estimated to be better than 0.3 ‰ for oxygen and carbon, and better than 5 ‰ for hydrogen isotope compositions. Results are reported in standard delta notation, relative to V-SMOW and V-PDB.

4.3.2. THE DEPENDENCE OF HYDROGEN ISOTOPE COMPOSITIONS OF FLUID INCLUSIONS ON THE EXTRACTION METHOD

In order to distinguish between fluid inclusion water and structurally bound water a two step heating technique was developed and applied. We have developed a modified extraction method, where coarse-grained fluorite samples were decrepitated up to 650 °C for two hours. During first hour, the released volatiles up to 400 °C were trapped in a quartz glass tube in a liquid nitrogen trap. Only molecular water and gases were collected in a cool trap with liquid nitrogen (volatiles were not passed over CuO furnace to oxidize gases to H_2O).

We assume all fluid inclusion water can be liberated and decrepitated up to 400 °C and was trapped in the cool trap. The liquid nitrogen trap was replaced by alcohol and dry-ice slush in order to trap only purified molecular water (H_2O) at –80 °C and to liberate gases (CO_2, CH_4) (Vennemann and O'Neil 1993; Demeny 1995). Released gases at -80 °C were then oxidized to H_2O by passing over the hot CuO furnace. This water was again trapped in a quartz glass tube in a cool trap with liquid nitrogen. The cool trap was replaced by alcohol trap (-80 °C) in order to trap only oxidized molecular water while the other liberated gases were pumped away at -80 °C. Then, the same sample was further heated up to 650 °C for another hour. The

expected structurally bound water in cool trap with liquid nitrogen in quartz glass tube. The liquid nitrogen trap was replaced by alcohol and dry-ice slush (-80 °C) and only H_2O can be trapped at -80 °C. Released gases at -80 °C were passed over a hot CuO furnace to be oxidized. This water was collected in a cool trap with liquid nitrogen and was purified by an alcohol trap (-80 °C).

Secondly, we extracted fluid inclusion water from hydrothermal fluorites at 400 °C and 650 °C respectively. In this case, at 400 °C only molecular water and gases were collected (volatiles were not passed over CuO furnace to oxidize gases to H_2O) in a cool trap with liquid nitrogen and was purified by an alcohol trap. The sample material from the same hand specimen was heated up to 650 °C and volatiles (molecular water, gases and additionally expected structurally bound water) were trapped in a cool trap with liquid nitrogen. This volatile was purified by an alcohol trap (-80 °C) and we assume both molecular water from fluid inclusions and structurally bound water were trapped in the alcohol trap.

The extracted water was then reduced to hydrogen by reaction with 150 mg of Zn (Indiana University, USA) at 500 °C for 15 minutes, as described by Friedman (1953), Craig (1961) and Godfrey (1962). Results are normalized to an internal biotite standard, which have a δD value of –64 ±5.0 per mil. This internal biotite standard was previously calibrated against the international biotite standard NBS 30 (δD: -65 ‰). Extraction of hydrogen from the biotite standard was done by the above extraction method, except heating to 1200 °C and volatiles passed over a CuO furnace to oxidize hydrogen to water. The δD values of released fluid inclusion water were measured on a Finnigan MAT-252 gas source mass spectrometer with a working standard calibrated against international standards (SMOW) at the University of Tübingen. The overall analytical precision is around ±5.0 ‰ for hydrogen isotope measurements. Results are reported in standard delta (δ) notation, as per mil, relative to V-SMOW.

4.4. SULFUR AND CARBON ISOTOPES

Mineral separates of hydrothermal sulfides (galena, chalcopyrite, sphalerite, pyrites), sulfates (barite, gypsum) and carbonates (calcite, dolomite) were prepared by careful hand-picking under a binocular microscope, followed by cleaning in doubly-distilled water. Sulfides and sulfates were measured after procedures given in Giesemann *et al*. (1994). The samples were sealed in tin capsules and converted by an EA-analyzer to SO_2 at a reaction temperature of 1050 °C and separated at a column temperature of 100°C. The isotopic composition of SO_2

was measured with a Finnigan Delta+XL mass spectrometer. Maximum sample sizes were 0.25 mg for sphalerite and barite, and 0.16 mg for pyrite.

Carbonate samples were analyzed after the method of Spötl and Vennemann (2003). The isotopic composition of CO_2 was measured with a Finnigan MAT 252 mass spectrometer. The reproducibility of the $CaCO_3$ content of the samples was ± 5 %, the reproducibility of the isotopic ratios was ± 0.1 ‰ for the $\delta^{13}C$ and ± 0.2 ‰ for the $\delta^{18}O$ measurements. Used standards were the NBS 123 (ZnS), IAEA S1 (AgS), IAEA S3 (AgS), and NBS 127 (BaSO$_4$) for sulphur isotopes, and the NBS 19 (CaCO$_3$) for carbon and oxygen isotopes. All sulphur, carbon and oxygen isotope compositions are reported in standard delta notation relative to V-CDT, V-PDB and V-SMOW, respectively.

4.5. INFRARED SPECTROSCOPY

Fourier transformation infrared (FTIR) analyses were carried out on double polished wafers (300-900 μm) that had previously been studied by microthermometry. The thickness of each doubly polished wafer was measured using a micrometer with a precision of ±1 μm. Individual wafers were first inspected under an optical microscope and fluid inclusions and regions free of fluid inclusions were selected for spectrometric analysis. Polarized infrared spectra were obtained in the wavenumber range from 2500 to 5500 cm^{-1} using a Bruker IFS 125 high resolution FTIR spectrometer coupled to a microscope with all reflecting, Cassegranian optics (Bruker IRscope I). Near-infrared measurements were performed using a tungsten light source, a Si coated CaF$_2$ beam splitter and high sensitivity narrow-band MCT (mercury-cadmium-telluride) detector cooled by liquid nitrogen. During the measurements, the optics of the spectrometer were kept under vacuum and the microscope was purged with a continuous stream of purified air in order to avoid absorption bands due to water vapor. An aperture of 10x10 μm was applied to the collected spectra for each sample. After background and linear baseline corrections, all spectra were normalized to 1 cm thickness.

The spot size on the sample was constrained by an adjustable rectangular aperture in the rear focal plane of the objective. Several hundred to several thousand scans were accumulated for one measurement.

4.6. RAMAN SPECTROSCOPY

In order to confirm the microthermometrically determined fluid inclusion volatiles, representative samples were analyzed by Laser Raman spectrometry, with a Dilor LABRAM-

2 Raman microspectrometer at the University of Tübingen, using a 514.5 nm Ar-ion laser source of excitation, according to the method of Burke (2000). Raman spectra from micrometer-sized objects within transparent samples can be obtained by coupling a research grade microscope to a Raman spectrometer. Laser Raman spectroscopy examines the inelastic scattering of monochromatic visible light as it interacts with covalent bonds in molecules such as N_2, hydrocarbons, CO_2, or H_2S. The energy and symmetry of the vibrational characteristics of different species in a sample corresponds with the peaks in Raman spectra (McMillan 1985; 1989; Burke 2000).

5. RESULTS

5.1. VARISCAN VEINS

5.1.1. FLUID INCLUSION DATA AND RAMAN SPECTROSCOPY

Fluid inclusions were studied in quartz samples from Variscan veins. The majority of fluid inclusions appears to be primary, occurring randomly distributed through the quartz as isolated inclusions with irregular and ellipsoidal shape. Clearly secondary inclusions are also present. The size of the inclusions ranges from 5 to 15 µm (Fig. 5). Two major types of fluids have been recognized in most studied Variscan veins:

Type1 (aqueous fluid inclusions). These inclusions consist of two phases (H_2O-rich liquid + vapor), with high degrees of filling, $V_{liquid}/(V_{liquid}+V_{vapor})$ being between 0.8 and 0.9 (Fig. 5A). Aqueous fluid inclusions homogenize exclusively into the liquid phase. This fluid inclusion type can be subdivided into two groups with different salinities.

Low salinity aqueous fluid inclusions. Most fluid inclusions in the Variscan veins show initial melting temperatures of ice between –30 and –20°C, indicating the presence of NaCl-KCl-H_2O fluids. The final melting temperatures of ice range from –6.5 to 0°C (Table 5), corresponding to salinities of 0 to 10.0 wt.% equivalent (eqv.) NaCl. These fluid inclusions homogenize exclusively into the liquid phase at temperatures of 150-350 °C (Fig. 5).

High salinity aqueous fluid inclusions. In several Variscan veins, a second group of aqueous fluid inclusions can be distinguished. These fluid inclusions are exclusively present as secondary inclusions, arranged along trails crosscutting the grain boundaries of the quartz. The inclusions show significantly lower final melting temperatures of ice, ranging from –27.7 to –21.8 °C (Table 5). Calculated salinities are in the range of 23.6 to 27.2 wt.% eqv. NaCl.

Homogenization of the high salinity aqueous fluid inclusions occurred into the liquid phase, with systematically lower homogenization temperatures between 90 and 150°C (Table 5 and Fig. 7). Some of the Variscan veins clearly exhibit a two-stage mineralization history (e.g., Holderpfad), which (by comparison with the fluid characteristics of the post-Variscan veins) is most likely related to a post-Variscan overprint (Fig. 6). In this case, vug-filling quartz crystals and drusy crystals coat early anhedral milky quartz. Primary fluid inclusions in the early anhedral quartz show relatively low salinities, whereas primary inclusions in growth zones within the drusy quartz have significantly higher salinities (20.2-26.2 wt.% eqv. NaCl).

Type 2 (CH_4-CO_2–H_2O fluid inclusions). These fluid inclusions consist of two phases, an aqueous liquid phase and gaseous CO_2-CH_4 phase (Fig. 5B). These CH_4–CO_2–H_2O fluid inclusions occur as isolated or as small clusters throughout the quartz grains and show negative crystal shapes. Melting of the carbonic phase occurs either at the CO_2 triple point of –56.6°C, or within a relatively small interval of depressed melting temperatures between –58.7 and –56.8°C (Table 5). No clathrate melting was observed in any inclusions. CH_4-CO_2-H_2O inclusions show total homogenization into the liquid phase between 200 and 350°C.
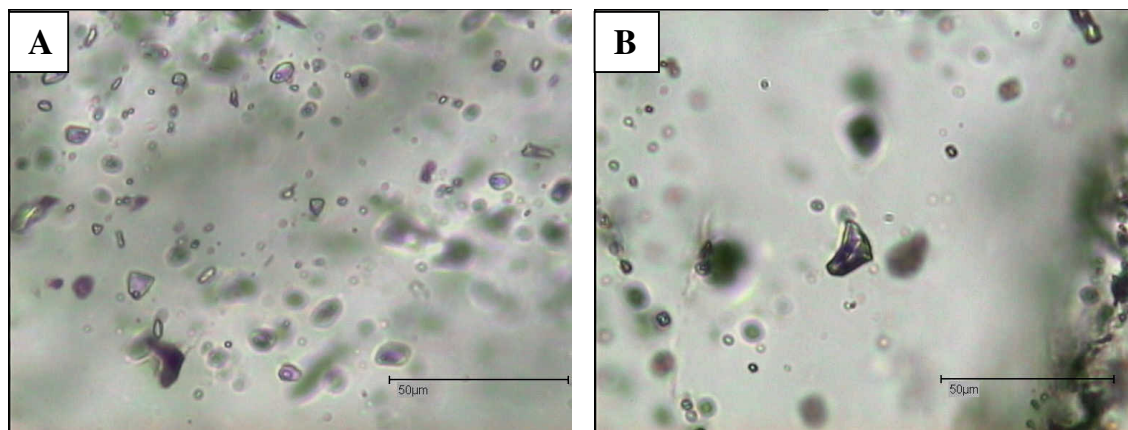
Figure 5. Photomicrographs showing principal fluid inclusion types in quartz of the Variscan hydrothermal deposits, Schwarzwald. **(A)**. Type 1 fluid inclusions. Sample: SW-11, Roßgrabeneck deposit**. (B)**. CH_4-CO_2 rich type 2 fluid inclusion. Sample: SW-10, Kleiner Langenbach deposit.

Table 5. Summary of microthermometric and compositional data of fluid inclusions from the Variscan hydrothermal veins of the Schwarzwald.

No. of deposit	Locality	Sample	Type of inclusion	N	T_m CO_2	$T_m$ice (°C)	T_h (°C)	Salinity NaCl (wt.%)
q-1	Roßgrabeneck	SW-09	Type 1	9		-1.9 to -2.9	180-310	3.2-4.8
q-1	Roßgrabeneck	SW-11	Type 1	19		-1.7 to -2.9	180-260	2.9-4.8
q-2	Fellmatt, SE of Baberast	SW-17	Type 1	8		-1.5 to -2.5	140-250	2.6-4.2
			Type 2	5	-57.4			
q-2	Baberast, Bergmannstrost	SW-22b	Type 1	7		-4.9 to -11.0		7.7-15.0
q-3	Artenberg	SW-14	Type 1	12		-26.3 to -28.5	95-123	26.4-27.7
			Type 1	7		-2.3 to -3.2		3.9-5.3
			Type 2	4	-58.0			
q-4	Ludwig im Adlersbach	GS-161	Type 1	4		-0.5 to -1.5	135-165	0.9-2.6
q-5	Erletzberg, Hausach	SW-06	Type 1	18		-0.5 to -1.0	200-390	0.9-1.7
			Type 1	8		-22.4 to -25.2		24.0-25.7
			Type 2	4	-56.8			
q-7	Bärenbach, Mühlenbach	SW-19a	Type 1	25		-1.5 to -4.0	220-270	2.6-6.4
q-10	St. Ulrich *	GMS-02	Type 1	19		-20.0 to -28.9	56-150	22.4-28.0
q-11	Gründenwald	DSU-57	Type 1	11		-17.1 to -31.5	100-260	20.3-29.6
			Type 2	11		-0.3 to -1.1	165-260	0.5-1.9
q-12	Schweizergrund	GS-179	Type 1			0.0	150	0.0
		GMS-01	Type 1	26		-20.0 to -23.5	110-140	22.4-24.6
			Type 1	7		-2.0		3.4
q-13	Holderpfad *	GS-208	Type 1	47		-17 to -26	80-180	20.2-26.2
q-14	Kleiner Langenbach	SW-02	Type 1	7		-0.5 to -2.9	250-300	0.9-4.8
			Type 2	6	-57.6			
q-14	Kleiner Langenbach	SW-03	Type 1	17		-0.4 to -3.0	210-340	0.7-5.0
q-14	Kleiner Langenbach	SW-10	Type 1	10		-1.3 to -3.7	260-300	2.2-6.0
q-15	Egghalde, Gang A	SW-05	Type 1	19		-2.4 to -2.8	210-270	4.0-4.6
q-17	Katzenstein, Oberentersbach	SW-21	Type 1	20		-0.9 to -3.2	170-245	1.6-5.3
				6		-15.7 to -25.0	85-140	19.2-25.6
	Nillhöfe, Fischerbach	SW-16	Type 1	5		-24.7 to -25.7	55-95	25.4-26
			Type 1	14		-0.7 to -3.4	235-315	1.2-5.6
	Werners Eck, Bollenbach	SW-18	Type 1	7		-10.5 to -24.7	55-90	14.5-25.4
			Type 1	5		-1.8 to -2.2	150-310	3.1-3.7
	Entersbacherhütte, Nillhöfe	SW-20	Type 1	11		-15.4 to -27.1	100-130	19.0-26.9
			Type 1	8		-0.3 to -3.1	145-245	0.5-5.1
			Type 2	5	-58.7			

* Late drusy quartz in Variscan vein.
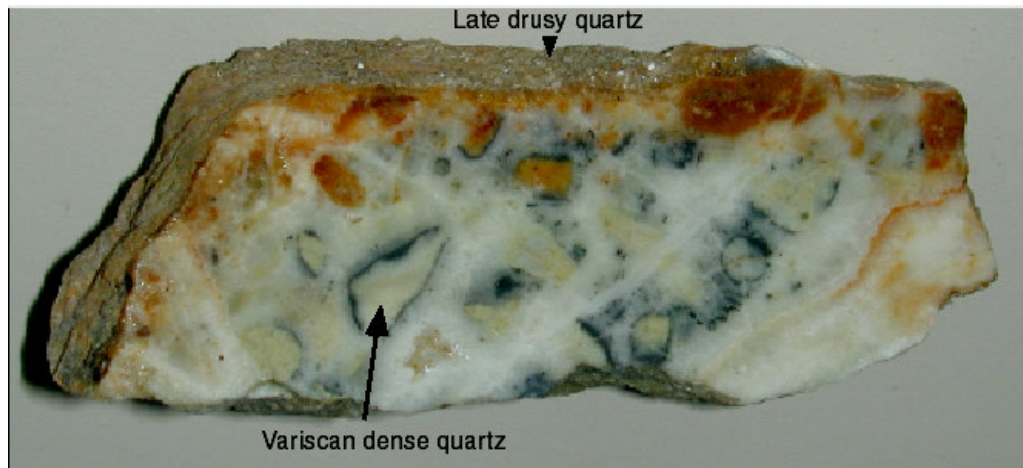
Figure 6. Variscan vein with post-Variscan overprint and late drusy quartz in a Variscan vein. Location: Holderpfad deposit. Sample length is about 12 cm.
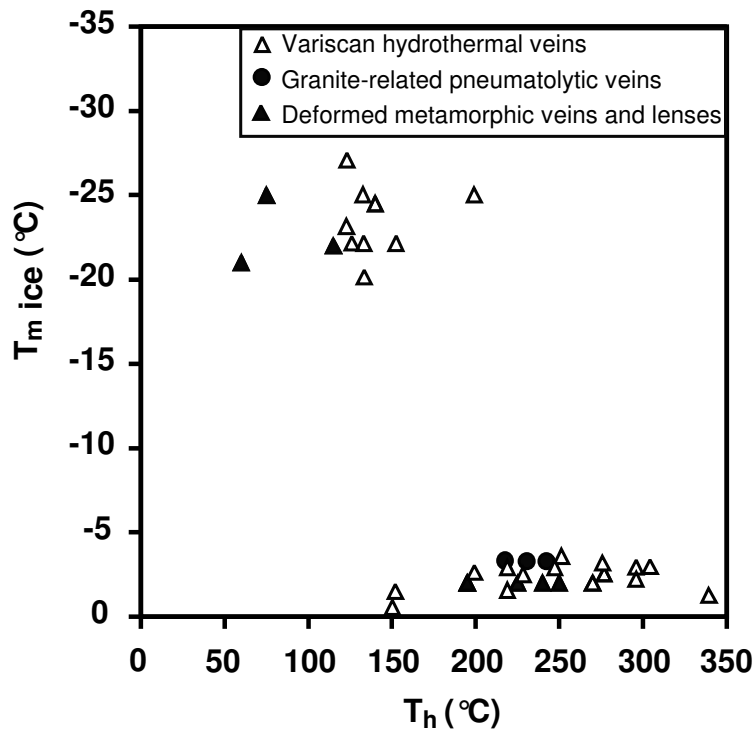
Figure 7. T_m vs. T_h diagram for the measured fluid inclusion in the Variscan quartz veins in the Schwarzwald.

Inclusions of different microthermometric behaviour were analyzed with Raman microprobe. Laser Raman spectroscopy was used to determine the presence of other components in addition to CO_2 and methane in the fluid inclusions. Aqueous and methane inclusions in quartz were examined. Individual inclusions as small as eight μm were successfully analyzed.

Raman spectra from quartz hosted fluid inclusions contain bands of CH_4, CO_2 and minor H_2S, N_2. These analyses show that concentration of volatiles such as CH_4, H_2S or CO_2 ($\pm$ N_2) are present (Fig. 8).
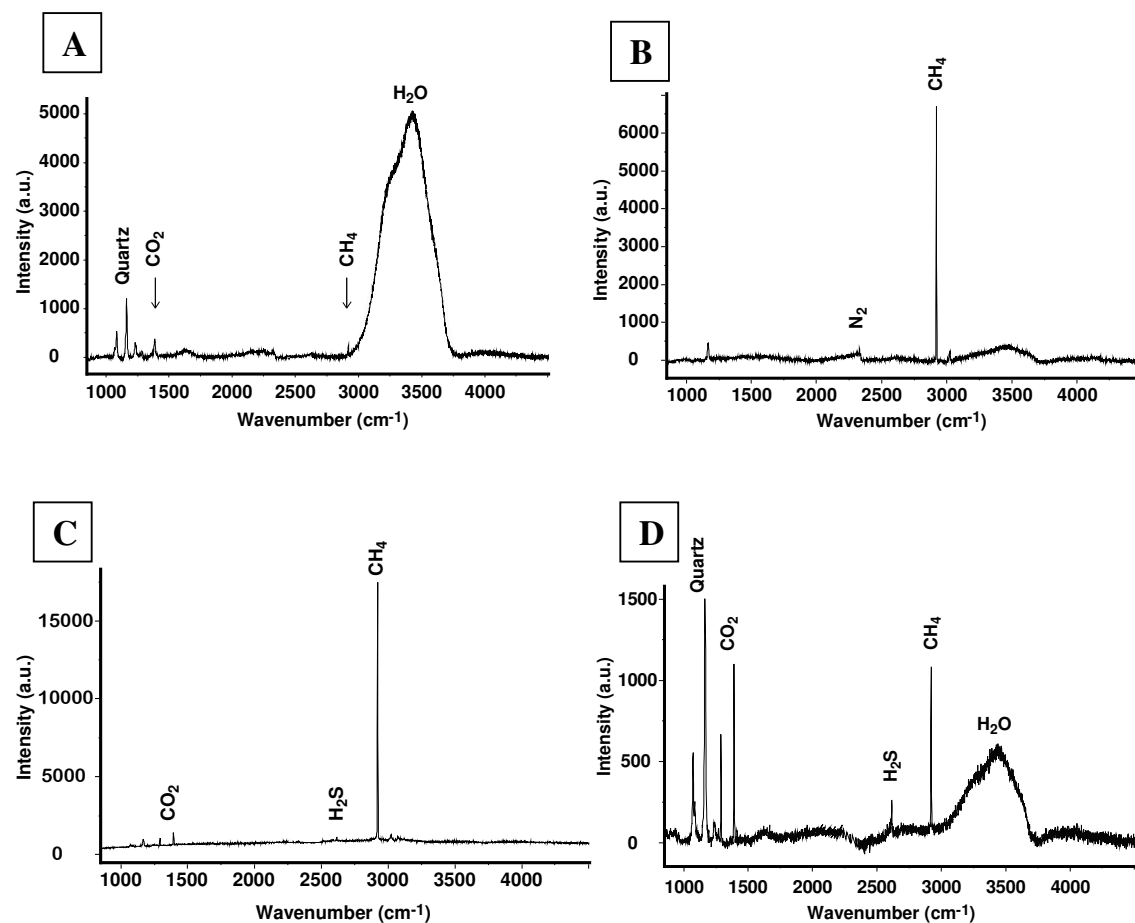
Figure 8. RAMAN spectra of fluid inclusions in quartz. (**A**). Spectrum from an inclusion in quartz sample SW-10 showing the small CO_2 and methane bands at 1388 cm^{-1} and 2917 cm^{-1}, respectively, together with H_2O bands. Peaks at 1084 and 1161 cm-1 represent the quartz host. (**B**). Spectra from inclusion in quartz in sample SW-17 showing the N_2 peak at 2331 cm^{-1} and dominant methane peak at 2917 cm^{-1}. (**C**). Dominant methane peak at 2917 cm^{-1} from inclusions in SW-17 quartz. There are also small CO_2 peaks at 1285 and 1388 cm^{-1}, very small peak at 2611 cm^{-1} represents H_2S. (**D**). SW-10 quartz hosted fluid inclusion's spectra showing dominant CO_2 and methane peaks at 1285, 1388 cm^{-1} and 2917 cm^{-1}, respectively. There are small H_2S peak at 2611 cm^{-1} together with H_2O bands.

5.1.2. OXYGEN ISOTOPE DATA OF VEIN QUARTZ

Oxygen isotope ratios for quartz from Variscan hydrothermal veins range from +2.8 to +12.2 ‰ (Table 3). Combining these $\delta^{18}O$ values with fluid inclusion homogenization temperatures

(representing minimum values of the formation temperatures), the oxygen isotopic composition of the hydrothermal fluids is calculated as between –12.5 and +4.4 ‰ (Table 3).

Table 3. Summary of oxygen isotopic data for analyzed quartz samples and calculated isotopic composition of the fluid from the Variscan hydrothermal veins of the Schwarzwald.

No.	No. of deposit	Deposit	Sample ID	Description	$\delta^{18}O$ (‰)	Th (°C)	$\delta^{18}O_{H2O}$ (‰)
1	q-1	Roßgrabeneck	SW-09	Coarse grained vein quartz	11.9	237	2.4
2	q-1	Roßgrabeneck	SW-11	Coarse grained vein quartz	12.2	220	1.8
3	q-1	Roßgrabeneck	SW-12	Tourmalin bearing coarse grained vein	12.2		
4	q-2	Baberast	SW-22b	Coarse grained vein quartz	4.3		
5	q-2	Baberast	SW-22e	Chalcedony	9.2		
6	q-3	Artenberg	SW-14	Dense, milky quartz	8.4	110	-11.0
7	q-3	Artenberg	XSA-47	Dense, milky quartz	5.8		
8	q-4	Ludwig/Adlersbach*	GS-160	Dense, milky quartz	18.8		
9	q-4	Ludwig/Adlersbach*	GS-161	Dense, milky quartz	15.1		
10	q-4	Ludwig/Adlersbach*	GS-162	Dense, milky quartz	18.4		
11	q-5	Erletzberg, Hausach	SW-06	Euhedral crystals	9.7	325	3.7
12	q-6	Ursula	BTR-11	Blue, dense quartz	5.2		
13	q-7	Bärenbach	SW-19a	Coarse grained vein quartz	12.2	250	3.3
14	q-8	Hornbühl, Waldkirch	SW-08	Dense, milky quartz	12		
15	q-9	Münstergrund**	SW-07	Euhedral crystals	14.6		
16	q-10	St. Ulrich*	GMS-02	Dense, milky quartz	13.7	86	-8.9
17	q-10	St. Ulrich*	DSM-16	Dense, milky quartz	14.7		
18	q-11	Gründenwald	DSU-57		6.5		
19	q-12	Schweizergrund	GS-184	Qtz pseudomorph after barite	7.5		
20	q-12	Schweizergrund	GS-188	Dense, milky quartz	7.9		
21	q-12	Schweizergrund	GMS-01	Euhedral crystals	6.3	122	-11.8
22	q-12	Schweizergrund	GS-179	Dense, milky quartz	2.8	150	-12.5
23	q-13	Holderpfad	GS-210	Dense, milky quartz	8.5		
24	q-13	Holderpfad*	GS-211	Dense, milky quartz	12.2		
25	q-13	Holderpfad	GMS-09	Dense, milky quartz	9.4		
26	q-13	Holderpfad	GS-208	Dense, milky quartz	8.1	102	-12.3
27	q-14	Kleiner Langenbach	SW-02	Coarse grained vein quartz	10.5	280	2.9
28	q-14	Kleiner Langenbach	SW-03	Coarse grained vein quartz	11.4	295	4.4
29	q-14	Kleiner Langenbach	SW-04	Coarse grained vein quartz	11.7		
30	q-14	Kleiner Langenbach	SW-10	Coarse grained vein quartz	11.2	270	3.2
31	q-15	Egghalde, Gang A	SW-05	Coarse grained vein quartz	11.4	233	1.7
32	q-16	Segen Gottes	XSG-22	Dense quartz	9.2		

Note: $\delta^{18}O_{H2O}$ was calculated using the equation of Matsuhisa *et al.* (1979) and temperatures were in most cases deduced from fluid inclusions. In some sample, the T_h was not determined due to too small inclusions.
* Variscan vein with post-Variscan overprint.   ** Late drusy quartz in a Variscan vein.

For these calculations, the quartz-water fractionation equation from Matsuhisa *et al.* (1979) and the most of the measured T_h were used. In some of the Variscan veins, a later post-Variscan overprint has been observed, manifested by euhedral drusy quartz crystals grown onto the dense Variscan quartz (Münstergrund, Holderpfad, Ludwigsbach, St. Ulrich). These

later post-Variscan quartz generations have consistently higher $\delta^{18}O$ values in the range between +14.6 and +18.8 ‰, which markedly contrast with the Variscan vein quartz analyzed from the same deposits.

5.1.3. HYDROGEN ISOTOPE DATA OF FLUID INCLUSIONS

Water yields and the δD values of inclusion fluids from eight hydrothermal quartz samples are shown in Table 6 and Figure 9. The δD values for water extracted from fluid inclusions in quartz samples generally have a variable range between –49 and +4 ‰.

Table 6. Summary of stable isotope data of Variscan hydrothermal fluids in the Schwarzwald.

Locality	No. of deposit	Sample ID	Mineral	H_2O content (%)	H_2O	
					$\delta^{18}O_{H2O}$	δD
					(‰ VSMOW)	
Bärenbach	q-7	SW-19a	Quartz	0.02	3.3	3.9
Egghalde, Gang A	q-15	SW-05	Quartz	0.13	1.7	-49
Kleiner Langenbach	q-14	SW-03	Quartz	0.03	4.4	-31.3
Kleiner Langenbach	q-14	SW-10	Quartz	0.05	3.2	-15
Kleiner Langenbach	q-14	SW-02	Quartz	0.04	2.9	-10
Roßgrabeneck	q-1	SW-09	Quartz	0.03	2.4	-6.6
Roßgrabeneck	q-1	SW-11	Quartz	0.12	1.8	-45.3
Schweizergrund	q-12	GS-179	Quartz	0.08	-12.5	-31.7

Note: $\delta^{18}O_{H2O}$ for quartz were calculated using the equation of Matsuhisa *et al.* (1979). δD measured from extracted fluid inclusions.

In a plot of δD vs. $\delta^{18}O$ (Fig. 9) in which $\delta^{18}O$ was calculated from quartz as reported above, almost all quartz samples are located within or just adjacent to the metamorphic water field or between it and SMOW.
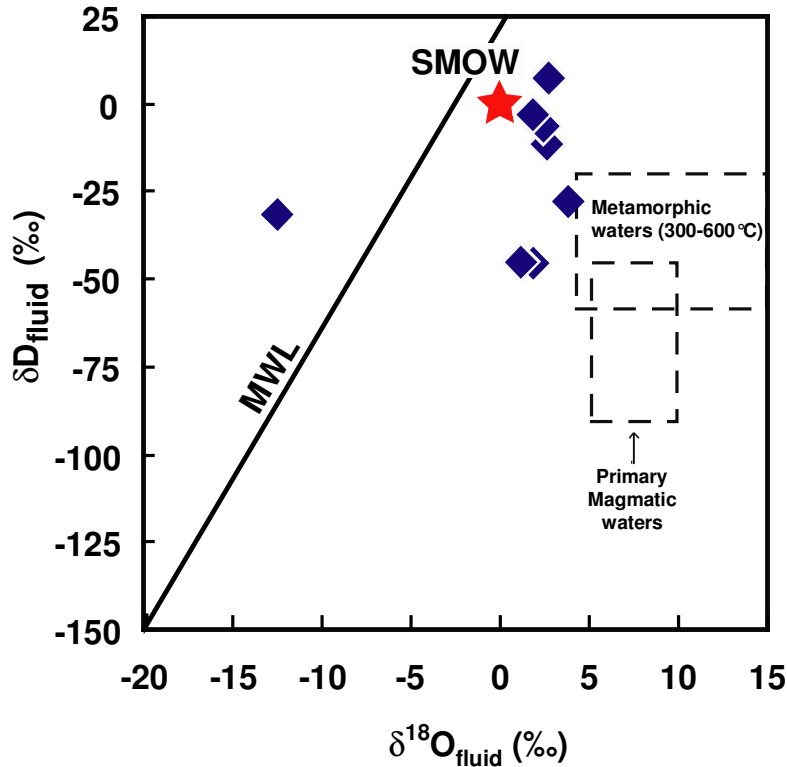
Figure 9. Fluid δD and δ^{18}O characteristics of Variscan hydrothermal veins, along with the fields of estimated isotopic compositions for primary magmatic and metamorphic fluids (Sheppard 1986). $\delta^{18}O_{H2O}$ for quartz was calculated using the equation of Matsuhisa *et al*. (1979). MWL-Meteoric Water Line.

5.2. POST-VARISCAN VEINS

5.2.1. FLUID INCLUSION DATA AND RAMAN SPECTROSCOPY

Fluid inclusion petrography

Fluid inclusions were studied in quartz, fluorite, calcite and barite crystals representing different mineral generations. The size of the inclusions generally ranges from 5 to 40 μm, with most inclusions being about 10-20 μm in size; fluid inclusions in quartz are generally smaller, about 5-10 μm. The majority of the fluid inclusions appears to be secondary and occurs randomly distributed throughout the quartz, fluorite, calcite and barite crystals. The inclusions in fluorite are mostly present as clusters (Fig. 10A), as isolated inclusions (Fig. 10B), and oriented along microfractures (Fig. 10C). The inclusions are up to 40 μm in size and show mainly round, elongate, and, less commonly, irregular shapes. Many of the fluid inclusions in barite and calcite appear to be decrepitated. Shape and occurrence of inclusions in barite and calcite are similar to the inclusions in fluorite. Fluid inclusions in quartz

frequently show irregular shapes. According to their textural distribution and phase relationships at room temperature, three distinct types of inclusions have been distinguished, which are described below in order of decreasing abundance:

Type 1 (high salinity two-phase aqueous fluid inclusions). These inclusions consist of two phases (H_2O-rich liquid + vapour), with typical degrees of fill, $V_{liquid}/(V_{liquid}+V_{vapour})$ between 0.9 and 0.95. Few fluid inclusions of this type contain a single daughter crystal, most likely halite. Approximately 90 percent of all individual samples contain type 1 inclusions. There are also some fluid inclusions that consist of two phases (vapour + H_2O-liquid), with significantly lower degrees of fill, $V_{liquid}/(V_{liquid}+V_{vapour})$ generally below 0.7 (Fig. 10B).

Type 2 (low salinity two-phase aqueous fluid inclusions). Aqueous inclusions of low to moderate salinity are found in quartz and some late-stage fluorite samples. These inclusions consist of two phases (H_2O + vapour), with degrees of fill around 0.9.

Type 3 (monophase fluid inclusion). This type only contains one homogeneous aqueous fluid phase and is generally associated with type 1 inclusions (Fig. 10D).
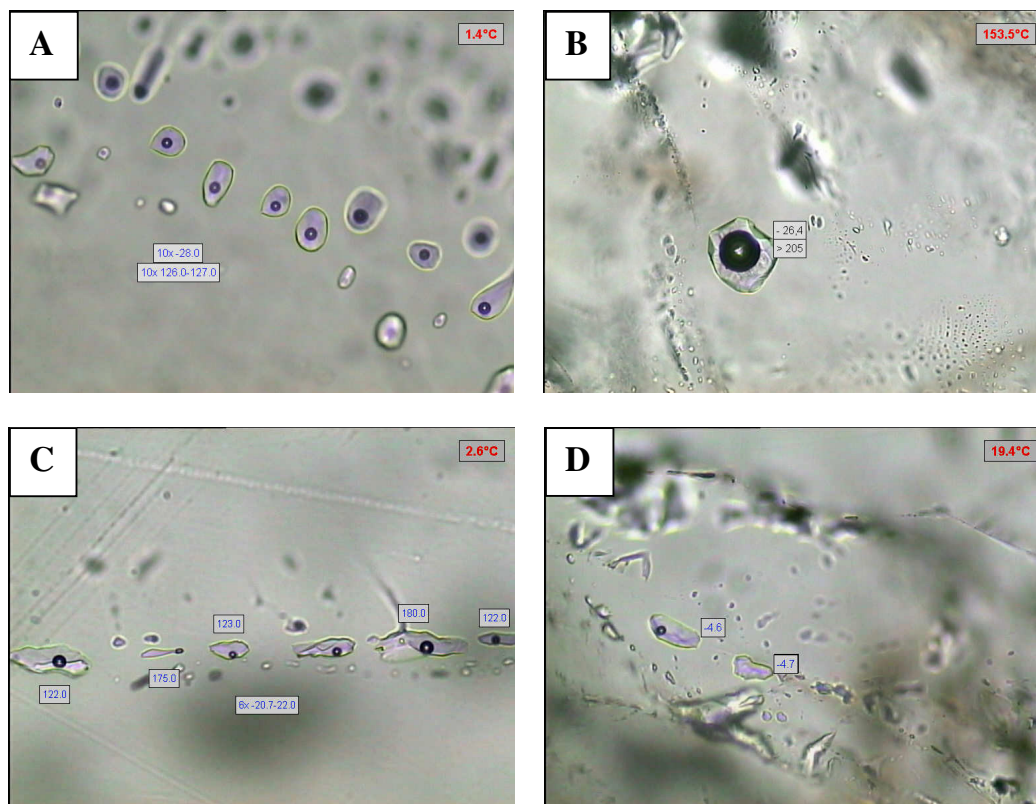
Figure 10. Photomicrographs showing principal fluid inclusion types in stage I and II fluorites of post-Variscan hydrothermal deposits, Schwarzwald. (**A**). Type 1 fluid inclusions in fluorite. Sample: FCH-1, Friedrich-Christian deposit. (**B**). Isolated type 1 fluid inclusion with lower degree of fill (CO_2) in fluorite. Sample: BTR-

26, Neuglück deposit. **(C)**. Type 1 fluid inclusions along the trail in fluorite. Sample: BTR-28, Käfersteige deposit. **(D)**. Mono-phase type 2 fluid inclusions in stage II fluorite. Sample: BTR-4, Teufelsgrund deposit. The temperatures are T_m and T_h. Size of inclusions range 20-25µm.

Microthermometry

Based on the measured range in salinities, all post-Variscan fluid inclusions can be divided into two distinct groups, which correspond to the types identified according to their petrographic characteristics.

Type 1. High-salinity aqueous fluid inclusions.

Generally, a consistent sequence of phase transitions was observed, comprising initial melting of ice, final melting of ice, final melting of hydrohalite (not clearly visible in all inclusions) and total homogenization. Initial ice melting temperatures of aqueous inclusions are in the range of –57 to –45°C, which correspond well to the eutectic temperature of the ternary H_2O-NaCl-$CaCl_2$ system at –52°C (Borisenko 1977). In this type of aqueous fluid inclusions, the final melting temperatures of ice range from -28 to -20°C, which corresponds to salinities of 22.4 to 24.7 wt.% eqv. NaCl. Hydrohalite as the last melting phase was only observed in 17 samples, with temperatures ranging from -18.5 to -7°C. In samples where both the final melting of ice (in the temperature range of -27.5°C to -22.0°C) and final melting of hydrohalite (in the temperature range of -18.5°C to -7°C), were observed, the fluid composition can be derived from the relevant ternary H_2O-NaCl-$CaCl_2$ phase diagram (Borisenko 1977; Zwart and Touret 1994). The resulting calculated fluid compositions are in the range of 11-22 wt.% NaCl and 3-17 wt.% $CaCl_2$. The total homogenization of high salinity aqueous fluid inclusions occurred exclusively into the liquid phase. Measured homogenization temperatures show considerable variation from 90 to 200 °C, with about 80 % of the data being located in the range of 100-160°C (Figs. 11 and 12; Table 7).

Type 2. Low salinity aqueous fluid inclusion.

This fluid inclusion type is exclusively present in late-stage quartz, fluorite, and calcite samples. Only the final melting of ice and total homogenization could be observed. The final ice melting temperatures range from -11.1 to 0°C, corresponding to salinities of 0 to 15.0 wt.% eqv. NaCl. The fluid inclusions always homogenize to the liquid phase, with homogenization temperatures between 110-200°C. Rarely, final ice melting temperatures were observed above 0°C, which is likely related to the presence of metastable superheated ice (Roedder 1984). Homogenization of vapour-richer inclusions occurred mostly to the liquid phase, with slightly higher homogenization temperatures in the range of 185-250°C.

Type 3. Monophase Inclusions.

In the monophase fluid inclusions, only initial and final melting of ice could be observed. Initial ice melting temperatures are in the range of -55 to -40°C, corresponding to the eutectic temperature of the ternary H_2O-NaCl-$CaCl_2$ system. Final melting temperatures of ice show a wide range, from -22.5 to -1.5°C, which corresponds to salinities of 2.5 to 24.0 wt.% eqv. NaCl.
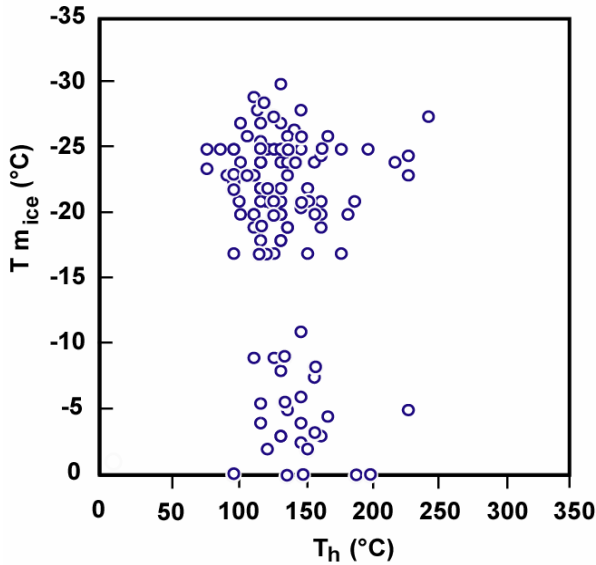
Figure 11. T_m vs. T_h diagram for the post-Variscan fluid inclusions in fluorite.
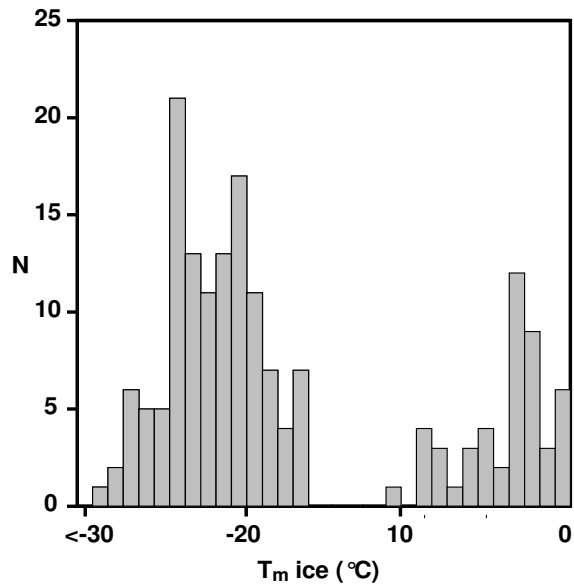
Figure 12. Histogram showing the range of all ice melting temperatures (T_m) from post-Variscan hydrothermal veins in the Schwarzwald.

The microthermometric data obtained from the different types of fluid inclusions are summarized in Table 7. Frequency distributions of the final ice melting and homogenization temperatures for individual samples generally show a rather narrow range, indicating the presence of a comparatively homogeneous hydrothermal fluid during a single mineralization event (Figs. 11 and 12). On a T_m-T_h diagram (Fig. 11), the post-Variscan inclusions show a significant variation in salinity, whereas the homogenization temperatures have a much smaller range.

Representative fluid inclusions from the microthermometrically distinguishable groups were analyzed with Laser Raman spectroscopy. Laser Raman spectroscopy was used to determine the presence of other components in addition to CO_2 and methane in the fluid

inclusions. Aqueous inclusions in fluorite and quartz were examined. Raman spectra from fluorite hosted fluid inclusions contain a peak for CO_2. These analyses show that CO_2 is the only detectable volatile species in the vapour phase (Fig. 13). They do not show any indication of methane, hydrocarbon, N_2, or H_2S in the aqueous inclusions.

Table 7. Summary of microthermometric data and compositional data of fluid inclusions from the post-Variscan hydrothermal veins of the Schwarzwald.

Locality	No. of deposit	Sample ID	Host mineral	Type of inclusion	N	T_mHH (°C)	T_mice (°C)	T_h (°C)	Salinity NaCl (wt.%)	CaCl$_2$ (wt.%)
Aitern Süd	45	44	Fluorite	Type 1	6		-16.6	116	19.9	
				Type 2	6		-9.4	115	13.2	
Artenberg	28	BTR-35	Fluorite	Type 1	20	-17.0	-26.4	227	11.0	17.0
				Type 1	15		-23.6	105	24.7	
		BTR-13	Fluorite	Type 1	97		-29.3	114	28.2	
		XSA-15	Quartz	Type 1	7		-22.9	87	24.3	
				Type 3	5		-16.9	-	20.1	
		BTR-1	Calcite-Late	Type 2	17		-5.6	207	8.7	
		BTR-35	Calcite	Type 1	30		-27.6	221	27.2	
		XSA-66	Calcite	Type 1	39		-28.1	125	27.5	
		BTR-13	Calcite	Type 1	42		-27.9	155	27.4	
		XSA-47	Calcite	Type 1	5		-28.0	115	27.4	
Badenweiler	36	BTR-39	Fluorite	Type 2	61		-5.3	199	8.0	
		BTR-38	Quartz	Type 2	8		-5.5	141	8.5	
		BTR-39	Quartz	Type 2	29		-4.2	162	6.7	
Badenweiler	36	41	Fluorite	Type 2	6		-2.9	170	4.8	
Barbara	26	GS 196	Fluorite	Type 2	222		-2.6	116	4.3	
Baumhalde	42	GS 71	Fluorite	Type 1	20		-20.0	131	22.4	
				Type 2	24		-3.9	119	6.3	
		GS 71	Quartz	Type 1	25		-21.2	154	23.2	
				Type 1	9		-16.5	131	19.8	
		M 31	Fluorite	Type 1	46		-14.6	-	18.3	
				Type 2	34		-5.7	-	8.8	
Brandenberg	43	GS 83	Fluorite	Type 1	115		-20.4	159	22.6	
		GS 91	Fluorite	Type 1	27		-22.9	121	24.3	
				Type 1	80		-20.1	161	22.4	
		GS 91	Quartz	Type 1	41		-21.9	125	23.6	
				Type 1	15		-20.5	143	22.7	
		GS 99	Fluorite	Type 1	44		-21.6	134	23.4	
		GS 99	Quartz	Type 1	27		-18.7	127	21.5	
		GS 99	Barite	Type 1	21		-21.8	218	23.6	
		GS 99	Calcite	Type 1	87		-22.0	145	23.7	
		GS 100	Fluorite	Type 3	6		-20.8	-	22.9	
		GS 111	Fluorite	Type 1	40		-20.0	165	22.4	
		GS 111	Quartz	Type 1	20		-20.0	150	22.4	
Brenden	56	GS 10	Fluorite	Type 1	31		-19.9	112	22.3	
		GS 10	Quartz	Type 1	10		-16.2	88	19.6	
		GS 15	Fluorite	Type 1	13		-22.4	120	24.0	
		GS 15	Quartz	Type 1	41		-20.5	95	22.7	
		GS 24	Fluorite	Type 1	110		-20.5	138	22.7	
Bleilersgrund, Wittichen	15	30	Fluorite	Type 1	6		-23.7	77	24.8	
Burgfelsen, Ilse, Wittichen	17	14	Fluorite	Type 1	6		-23.5	100	24.6	
Dorothea	4	BTR-14	Fluorite	Type 1	33	-17.7	-25.4	178	13.0	13.0

Location	No	Sample	Mineral	Type	n					
		QDC-52	Barite	Type 1	16	-17.3	-23.9	175	13.5	13.0
Drey	25	GS 151	Fluorite	Type 2	107		-3.1	163	5.1	
		GS 154	Fluorite	Type 2	47		-3.4	119	5.6	
Egghalde		4	Fluorite	Type 1	20		-22.5	128	24.0	
				Type 2	6		0.0	149	0.0	
Erzengel Gabriel	29	34	Fluorite	Type 2	6		-8.3	133	12.1	
Friedrich-Christian	11	M 5	Calcite	Type 1	27		-26.5	98	26.5	
		GS 135	Fluorite	Type 1	116		-23.0	145	24.3	
		GS 135	Quartz	Type 1	30		-22.5	110	24.0	
		GS 137	Fluorite	Type 1	82	-17.8	-24.1	140	12.0	14.0
		FCH 1	Fluorite	Type 1	50		-26.4	138	26.4	
		FCH-2	Fluorite	Type 1	56		-26.4	129	26.4	
		FST	Fluorite	Type 1	30		-25.0	135	25.6	
Fortuna near Wolfach	32	37	Fluorite	Type 2	23		-3.9	136	6.3	
Friedenweiler, Eisenbach	3	48	Fluorite	Type 1	6		-25.0	200	25.6	
Gottesehre near Urberg	51	10	Fluorite	Type 1	6		-28.2	172	27.5	
Hausen im Wiesental	58	9	Fluorite	Type 1	3		-20.5	220	22.7	
				Type 2	6		-4.0	146	6.4	
Heiligenwald, Pforzheim	2	11	Fluorite	Type 1	5		-29.5	135	28.4	
				Type 2	4		-8.9	135	12.7	
Herrmann	47	M 829	Fluorite	Type 1	9		-21.0	125	23.0	
		M 831	Fluorite	Type 1	21		-19.1	123	21.8	
		GS 67	Fluorite	Type 1	81		-18.0	135	21.0	
		GS 68	Fluorite	Type 1	26		-24.9	137	25.5	
				Type 1	20		-21.7	128	23.5	
Herzog Friedrich	20	24	Fluorite	Type 1	6		-21.4	220	23.3	
Hesselbach	8	31	Fluorite	Type 1	7	-17.0	-24.8	157	13.0	13.0
		7	Fluorite	Type 1	7	-17.0	-24.5	80	13.0	13.0
Hohberg, near Wolfach	34	23	Fluorite	Type 1	6		-24.9	139	25.5	
				Type 2	5		-0.1	97	0.2	
Igelschlatt	57	GS 37	Fluorite	Type 1	71		-22.6	138	24.1	
		GS 37	Quartz	Type 1	19		-20.8	125	22.9	
		GS 42	Fluorite	Type 1	76		-20.0	161	22.4	
Ilse im Kaltbrunn	16	5	Fluorite	Type 1	6		-25.0	92	25.6	
Johannes, Wittichen	13	WJB-2	Fluorite	Type 1	47	-17.0	-22.9	144	12.0	14.0
		WJB-4	Fluorite	Type 1	27	-17.0	-20.7	123	12.0	14.0
		WJB-17	Quartz	Type 1	43		-23.2	82	24.5	
		WJB-2	Barite	Type 1	13		-24.5	165	25.3	
Käfersteige	1	BTR-29	Fluorite	Type 1	86		-21.4	138	23.3	
		BTR-28	Fluorite	Type 1	80	-16.0	-20.7	131	19.0	7.0
Königswart	87	SW-23	Quartz	Type 1	21		-26.7	116	26.6	
König David, Gallenbach	18	6	Fluorite	Type 1	3		-25.3	120	25.8	
				Type 1	3		-20.0	115	22.4	
Laßgrund near Hausach	30	20	Fluorite	Type 2	6		-11.1	150	15.0	
Ludwigs Trost	33	33	Fluorite	Type 2	6		-8.6	135	12.4	
		45	Fluorite	Type 1	6		-25.4	143	25.8	
Michael im Weiler	65	GMW121	Quartz	Type 2	13		-4.2	110	6.4	
Mühlsteinbruch	63	26	Fluorite	Type 2	6		-1.0	123	1.8	
Neubergmännisch Glück	22	35	Fluorite	Type 1	6		-22.0	137	23.7	
Neubulach	64	BTR-32	Quartz	Type 1	41	-16.0	-25.8	114	12.5	13.0
Neuglück, Wittichen	14	BTR-37	Fluorite	Type 1	38	-16.1	-22.3	101	18.0	10.0
		BTR-26	Fluorite	Type 1	5		-24.3	178	25.1	
				Type 1	13		-23.1	215	24.4	
		BTR-37	Quartz	Type 3	9		-22.2	-	23.8	
				Type 1	1		-21.0	104	23.0	
		WNS-9	Barite	Type 1	14	-16.0	-23.6	227	12.0	14.0
		BTR-41	Quartz	Type 1	22		-23.6	87	24.7	

Location			Mineral	Type	n					
Nöggenschwiel	61	16	Fluorite	Type 1	6		-26.8	111	26.7	
Ohlsbach	7	2	Fluorite	Type 1	6		-18.4	159	21.2	
Ödsbach	9	8	Fluorite	Type 1	7		-17.1	160	20.3	
Riedlingen	48	19	Fluorite	Type 1	5		-25.8	86	26.1	
Ruprechtgangzug	52	GS 27	Fluorite	Type 1	73		-20.7	115	22.8	
		GS 29b	Fluorite	Type 1	26		-19.8	141	22.2	
				Type 2	25		0.0	152	0.0	
		GS 35a	Quartz	Type 1	107		-18.7	147	21.5	
		GS 36a	Fluorite	Type 1	16		-21.6	154	23.4	
		GS 36a	Quartz	Type 1	7		-22.1	129	23.8	
Schauinsland	67	BTR-40	Quartz	Type 2	34		-9.6	113	13.5	
				Type 1	16		-22.2	113	23.8	
		BTR-40	Calcite	Type 1	28		-23.7	116	24.8	
Schlechthalde, Wittichen	23	36	Fluorite	Type 1	6		-17.0	103	20.2	
Schönau	46	32	Fluorite	Type 1	6		-21.7	143	23.5	
				Type 2	6		-1.8	181	3.1	
Segen Gottes	27	56	Fluorite-Late	Type 2	30		-2.5	132	4.2	
		XSG-15	Fluorite	Type 2	23		-3.0	169	5.0	
		BTR-45	Quartz	Type 2	6		0.0	212	0.0	
		BTR-47	Quartz	Type 2	19		-1.9	147	3.2	
				Type 3	11		-1.7	-	2.9	
Silberbrünnle, Seebach	88	BTR-31	Quartz	Type 1	44		-24.5	140	25.3	
Silbergründle, Seebach	86	SW-24	Quartz	Type 1	20		-23.8	128	24.8	
Sophia Wittichen	12	BTR-17	Fluorite	Type 1	103	-15.5	-24.3	243	12.0	14.0
		BTR-46	Barite	Type 1	12		-21.3	220	23.2	
				Type 1	8		-20.6	118	22.6	
		BTR-41	Barite	Type 1	26		-25.8	151	26.1	
		M-207	Fluorite	Type 1	53	-16.0	-23.3	115	12.0	14.0
		WSB-13	Quartz	Type 1	12		-23.4	76	24.6	
				Type 3	8		-19.2	-	21.8	
		BTR-41	Calcite	Type 1	14	-14.0	-24.6	184	12.0	15.0
Sulzburg	62	13	Fluorite	Type 1	6		-20.3	133	22.6	
Sulzburg	62	SW-25a	Quartz	Type 1	16		-24.8	120	25.5	
Sulzburg	62	SW-25M	Quartz	Type 1	13		-23.0	124	24.3	
Tannenboden, Wieden	41	38	Fluorite	Type 1	6		-18.5	146	21.3	
				Type 2	4		-7.0	150	10.5	
Tennenbronn	35	28	Fluorite	Type 1	6		-24.9	144	25.5	
		YOB 11	Fluorite	Type 1	6		-19.8	160	22.2	
Teufelsgrund	40	BTR-9	Fluorite-Late	Type 2	49		-6.3	164	9.2	
		BTR-4	Fluorite	Type 1	35		-16.9	114	20.1	
		BTR-7	Fluorite	Type 1	30		-20.3	154	22.5	
		BTR-7	Quartz	Type 1	41	-18.1	-21.2	127	13.2	13.0
		BTR-6	Quartz	Type 1	33		-23.5	151	24.7	
		BTR-5	Calcite-Late	Type 2	29		-0.2	166	0.4	
Wehratal, Nöggenschwiel	59	15	Fluorite	Type 1	6		-18.4	137	21.2	
Wenzel	31	49	Fluorite	Type 1	6		-27.1	123	26.9	
Wenzel	31	BTR-42	Calcite	Type 1	23		-27.3	135	27.0	
		BTR-18	Calcite	Type 1	32		-27.5	126	27.1	
		BTR-43	Barite	Type 1	25		-22.4	191	23.9	
Wittenweiler	5	1	Fluorite	Type 1	5	-17.5	-25.2	133	13.0	13.0
Zunsweier	6	12	Fluorite	Type 1	25		-24.7	158	25.4	
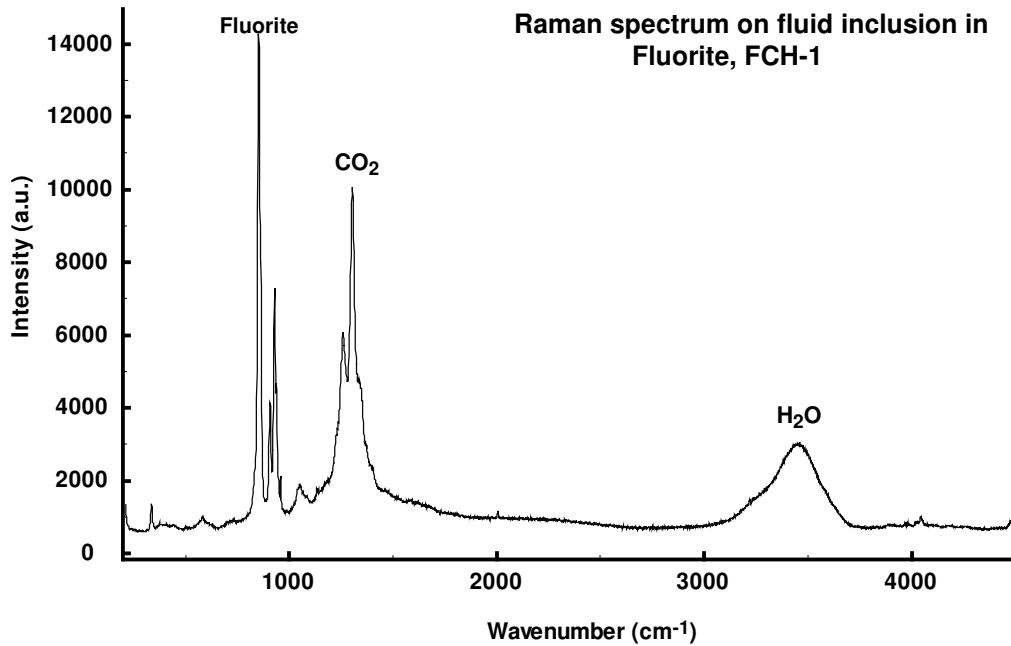
Figure 13. Typical RAMAN spectra of fluid inclusions in fluorites. They show the dominant CO_2 peak at 1285 cm^{-1} together with H_2O bands.

5.2.2. OXYGEN ISOTOPE DATA OF VEIN QUARTZ

The results of the oxygen isotope analyses are summarized in Table 4. All $\delta^{18}O$ values of quartz of the fluorite-bearing veins range between +11.1 and +19.5 ‰, with 75 out of 83 values being in a narrow interval between +14 and +18 ‰ (Fig. 14). Euhedral quartz crystals present as secondary overprint within few of the Variscan quartz veins (e.g., Holderpfad, St. Ulrich, Münstergrund, Ludwig/Adlerbach deposits) have $\delta^{18}O$ values between +14.6 and +17.8 ‰ and are consistent with the typical data range for the post-Variscan veins.
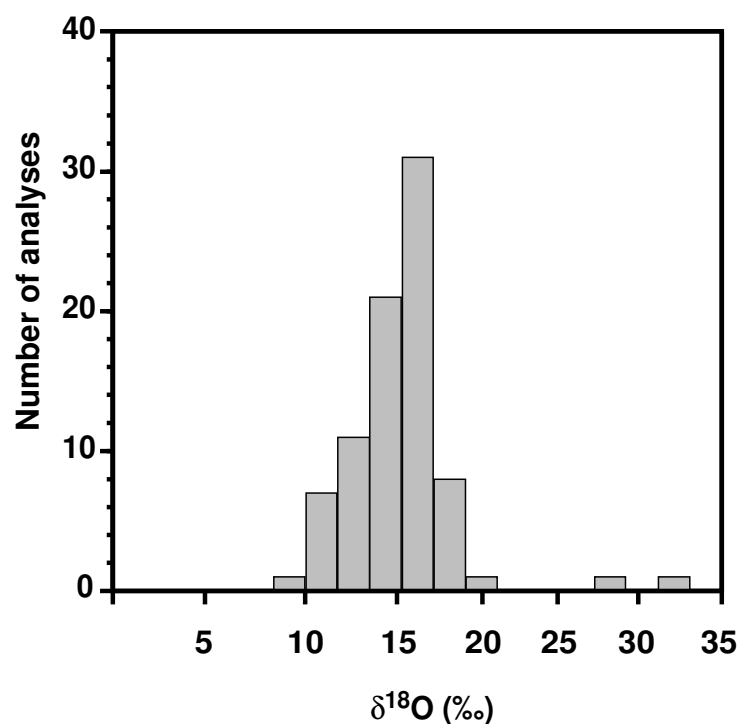
Figure 14. Histogram showing the ranges of measured $\delta^{18}O_{quartz}$ (SMOW) from the post-Variscan hydrothermal veins in the Schwarzwald.

The range in $\delta^{18}O$ values for quartz from post-Variscan veins found in this study is in good agreement with previously reported data from the Schauinsland and Menzenschwand deposits, which are in the range of +15.5 to +19.4 ‰, and +15.3 to +20.0 ‰, respectively (Weber 1997; Hofmann 1989). In comparison, carneol from feldspatic sandstone (Silberberg Mountain, near Wittichen) and agate from a Perminan rhyolite (Geisberg near Schweighausen) have significantly higher $\delta^{18}O$ values of +33.4 ‰ and +28.9 ‰, respectively. Combining measured $\delta^{18}O$ values of quartz from the fluorite veins with the respective fluid inclusion homogenization temperatures, calculated $\delta^{18}O_{H2O}$ (using the experimental quartz-water fractionation of Matsuhisa *et al.* 1979) range between –7.5 and +2.1 ‰ (Table 4).

Table 4. Summary of oxygen isotopic data for analyzed quartz samples and calculated isotopic composition of the fluid from the post-Variscan hydrothermal veins of the Schwarzwald.

No.	No. of deposit	Deposit	Sample ID	Description	$\delta^{18}O$ (‰)	T_h (°C)	$\delta^{18}O_{H2O}$ (‰)
1	1	Käfersteige	BTR-29	Milky fine grained quartz	17	130	-0.2
2	1	Käfersteige	BTR-33	Chalcedony	17.6		
3	4	Dorothea	QDC-69	Milky fine grained quartz	18.7		
4	4	Dorothea	BTR-34		17.6		
5	11	Friedrich-Christian	GS 135	Euhedral crystals	16.4	110	-3.0

6	11	Friedrich-Christian	GS 135	Coarse grained vein quartz	14.4	110	-5.0
7	11	Friedrich-Christian	GS 119	Qtz pseudomorph after barite	17.8		
8	11	Friedrich-Christian	GS 131	Greenish chert	17.1		
9	11	Friedrich-Christian	GS 131	Euhedral crystals	17.2		
10	11	Friedrich-Christian	GS 123	Quartz from gneiss-host	12.5		
11	12	Sophia, Wittichen	484	Euhedral crystals	17.6		
12	12	Sophia, Wittichen	WSB-26	Euhedral crystals	19.2		
13	12	Sophia, Wittichen	WSB-13	Smoky quartz	19.5	80	-4.6
14	13	Johannes, Wittichen	WJB-2	Fine grained vein quartz	17.2		
15	13	Johannes, Wittichen	WJB-17	Euhedral crystals	17.9	85	-5.3
16	14	Neuglück, Wittichen	BTR-37	Euhedral crystals	19	105	-1.2
17	19	Hilfe Gottes	PHG-153	Euhedral crystals	11.1		
18	19	Hilfe Gottes	PHG-134	Dense quartz vein in granite	14.5		
19	19	Hilfe Gottes	PHG-190	Chert	16.4		
20	27	Segen Gottes	BTR-47-II	Late stage quartz veinlet	14.1	147	-1.5
21	28	Artenberg	BTR-48	Coarse grained vein quartz	12.1		
22	28	Artenberg	XSA-15	Euhedral crystals	16.9	87	-5.5
23	31	Wenzel	OWF-111	Single grains in barite	14.3		
24	31	Wenzel	OWF-12	Euhedral crystals	17.6		
25	36	Badenweiler	BTR-39	Milky fine grained quartz	16.4	162	2.1
26	36	Badenweiler	BTR-34	Dense, milky quartz	17.6		
27	40	Teufelsgrund	BTR-6	Quartz druse, crystal	13.9	151	-1.4
28	40	Teufelsgrund	BTR-6	Blue chalcedony	14.7	151	-0.6
29	40	Teufelsgrund	BTR-7	Late-quartz, euhedral crystals	14.7	127	-2.8
30	42	Baumhalde	GS 71	Veinlet with euhedral crystals	11.8	154	-3.2
31	42	Baumhalde	GS 72	Fine grained vein quartz	14.7		
32	42	Baumhalde	GS 76	Chalcedony	13.7		
33	43	Brandenberg	GS 111	Qtz pseudomorph after barite	12.5		
34	43	Brandenberg	GS 99	Fine grained vein quartz	13.4	127	-4.1
35	43	Brandenberg	GS 91	Chalcedony	13.8	130	-3.4
36	43	Brandenberg	GS 91	Chalcedony	15	130	-2.2
37	43	Brandenberg	GS 91	Euhedral crystals	15.3	130	-1.9
38	43	Brandenberg	GS 91	Coarse grained vein quartz	13.9	130	-3.3
39	43	Brandenberg	GS 91	Euhedral crystals	13.5	130	-3.7
40	43	Brandenberg	GS 103	Qtz from gneiss, 4 cm apart from vein	9.7		
41	47	Herrmann	GS 67	Coarse grained vein quartz	14.4		
42	47	Herrmann	GS 70	Coarse grained vein quartz	14.6		
43	47	Herrmann	GS 68	Euhedral crystals	14.9		
44	53	Schwarzwaldsegen	GS 29c	Euhedral crystals	17.6		
45	54	Neue Hoffnung	GS 35	Euhedral crystals	11.9		
46	54	Neue Hoffnung	GS 34	Qtz pseudomorph after barite	17.1		
47	56	Brenden	GS 15	Qtz pseudomorph after barite	14.7	95	-6.6
48	56	Brenden	GS 15	Qtz pseudomorph after barite	13.8	95	-7.5
49	56	Brenden	GS 15	Qtz pseudomorph after barite	15.4	95	-5.9
50	56	Brenden	GS 4	Euhedral crystals	15.7		
51	57	Igelschlatt	GS 42	Qtz pseudomorph after barite	16.3		
52	57	Igelschlatt	GS 37	Purple quartz	16.8	125	-1.0
53	57	Igelschlatt	GS 37	Qtz from granite, 1 cm apart from vein	10.8	125	-7.0
54	57	Igelschlatt	GS 37	Qtz from granite, 6 cm apart from vein	10.7	125	-7.1
55	57	Igelschlatt	GS 41	Qtz from granite, 1 cm apart from vein	10.5		

56	57	Igelschlatt	GS 41	Qtz from granite, 8 cm apart from vein	10.9		
57	57	Igelschlatt	GS 41	Coarse grained vein quartz	13.7		
58	62	Sulzburg	SW-25a	Euhedral crystals	18.2	120	-0.1
59	62	Sulzburg	SW-25M	Dense, milky quartz	16.4	124	-1.5
60	64	Neubulach	919	Euhedral crystals	16.8		
61	64	Neubulach	BTR-32	Euhedral crystals	16.9	114	-2.1
62	65	Michael im Weiler	566	Blueish, dense quartz	18		
63	65	Michael im Weiler	GMW-121	Smoky quartz	16.3	110	-3.1
64	66	Geigeshalde	TGH-30	Euhedral crystals	15.8		
65	67	Schauinsland	BTR-40	Euhedral crystals	14.4	113	-4.7
66	69	Menzenschwand	GMS 03	Euhedral crystals	19		
67	69	Menzenschwand	GMS 07	Euhedral crystals	20.9		
68	69	Menzenschwand	GMS 08	Reddish chalcedony	16.9		
69	86	Silbergründle	SW-24	Euhedral crystals	16.2	128	-1.2
70	87	Königswart	SW-23	Euhedral crystals	17.1	116	-1.6
71	88	Silberbrünnle	BTR-31	Qtz pseudomorph after barite	16.5		
72	88	Silberbrünnle	YSB-195	Euhedral crystals	14.2		
73	88	Silberbrünnle	BTR-31	Chalcedony	14.6		
74	88	Silberbrünnle	BTR-31	Coarse grained vein quartz	15.7	132	-1.3
75	88	Silberbrünnle	YSB-235	Euhedral crystals	16.6		
76	88	Silberbrünnle	BTR-31	Blueish chalcedony	17.2		
77	88	Silberbrünnle	YSB-195	Blueish, dense quartz	18.2		
78	88	Silberbrünnle	BTR-31	Yellow chalcedony	16.5		
79	89	Lorenz	BTR-24	Euhedral crystals	15.9		
80	89	Lorenz	BTR-36	Euhedral crystals	17		
81	q-4	Ludwig/Adlersbach*	GS 160	Dense milky quartz	18.8		
82	q-4	Ludwig/Adlersbach*	GS 161	Dense milky quartz	15.1		
83	q-4	Ludwig/Adlersbach*	GS 162	Dense milky quartz	18.4		
84	q-13	Holderpfad **	GS 208	Euhedral crystals	17.8	102	-2.6
85		Silberberg, Wittichen	SW-01	Sedimentary carneol	33.4		
86		Steinbruch Feist, Geisberg	SW-15	Secondary agate from rhyolite	28.9		

Note: $\delta^{18}O_{H2O}$ were calculated using the equation of Matsuhisa *et al*. (1979) and temperatures (T_h) from fluid inclusions. In some sample, the T_h was not determined due to too small inclusions.
* Variscan vein with post-Variscan overprint.   ** Late drusy quartz in Variscan vein.

5.2.3. OXYGEN, HYDROGEN AND CARBON ISOTOPE SYSTEMATICS OF FLUID INCLUSIONS

Oxygen, hydrogen and carbon isotope compositions of directly extracted fluid inclusion water from fluorites are listed in Table 8. The $\delta^{18}O$ values of fluid inclusion water range from -11.6 to -3.0 ‰ (with most data lying between -6 and -3 ‰), which is very consistent with the $\delta^{18}O_{H2O}$ values calculated from the measured $\delta^{18}O_{Quartz}$ of vein quartz and fluid inclusion homogenization temperatures in the same samples (Table 8 and Fig. 15). Water yields and the δD values of inclusion fluids from hydrothermal fluorite, calcite and quartz samples are shown in Table 8 and Figure 16.
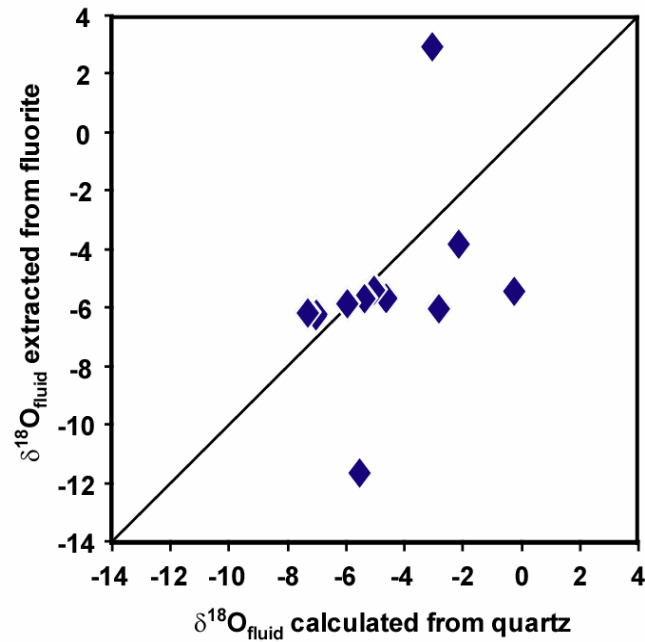
Figure 15. Diagram of $\delta^{18}O_{fluid}$ directly measured from fluid inclusion water (extracted from fluorite) vs. $\delta^{18}O_{fluid}$ calculated from quartz using the equation of Matsuhisa *et al*. (1979).
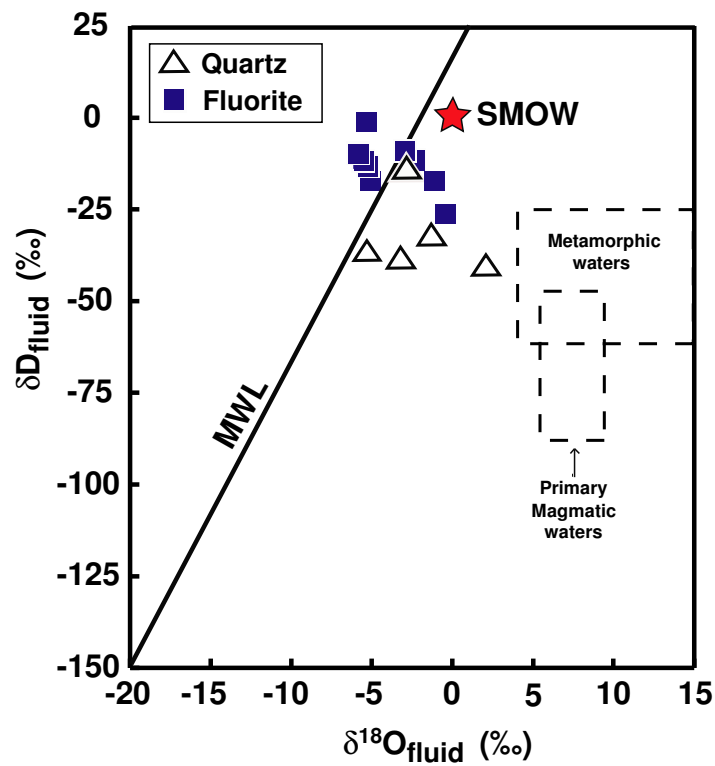
Figure 16. Fluid δD and $\delta^{18}O$ characteristics of post-Variscan hydrothermal veins, with superposed fields of estimated isotopic compositions of primary magmatic and metamorphic fluids (Sheppard 1986). $\delta^{18}O_{fluid}$ for

fluorites were measured from directly extracted fluid inclusion water, whereas $\delta^{18}O_{fluid}$ for quartz were calculated using the equation of Matsuhisa *et al*. (1979). MWL- Meteoric Water Line.

The δD values for water extracted from fluid inclusions in fluorites define a range between -29 and -1 ‰. In comparison, fluid inclusion water from quartz samples generally has much more variable and more negative δD values between -63 and +9 ‰, with 7 out of 12 values lying between -63 and -32 ‰. The only exception is a sample from the Neubulach deposit, which has a much higher δD value of +54 ‰. The δD values of fluid inclusion water extracted from primary calcite samples range between -26 and -15 ‰, very similar to the data from primary fluorite. In contrast, late-stage calcite samples have significantly heavier δD values in the range between -5 and +70 ‰ (Table 8). The carbon isotope data of fluid inclusion gas (mainly CO_2) show considerable variation, with $\delta^{13}C$ values between -21.4 and -6.7 ‰. The heaviest value of -6.7 ‰ was obtained from a late stage fluorite sample from the Teufelsgrund deposit.

Table 8. Summary of stable isotope data for post-Variscan ore forming hydrothermal fluids in the Schwarzwald.

Locality	No. of deposit	Sample ID	Mineral	H$_2$O content (%)	H$_2$O		CO$_2$
					$\delta^{18}O$	δD	$\delta^{13}C$
					(‰ VSMOW)		(‰ VPDB)
Artenberg	28	BTR-35	Fluorite	0.019	-11.6		-10.2
Artenberg	28	BTR-1	Calcite	0.032		-24	
Artenberg	28	BTR-13	Calcite-Late	0.192		-22	
Badenweiler	36	BTR-39	Quartz	0.085		-40	
Baumhalde	42	GS-71	Quartz	0.066		-38	
Brandenberg	43	GS-111	Fluorite		-1.0	-17	-7.5
Brandenberg	43	GS-91	Quartz	0.033		-9	
Brenden	56	GS-24	Fluorite	0.161	-3.3	-11	-18.3
Brenden	56	GS-4	Quartz	0.035		9	
Dorothea	4	BTR-14	Fluorite	0.068	-3.3		-21.3
Drey	25	151	Fluorite	0.057	-7.4		-15.6
Friedrich Christian	11	FCH-1	Fluorite	0.025	-5.4	-12	-21.4
				0.057	-3.0		-20.9
Friedrich Christian	11	FCH-2	Fluorite	0.02	-2.6	-12	-19.5
Friedrich Christian	11	GS-135	Fluorite		-2.3		
Friedrich Christian	11	GS-119	Quartz-Late	0.117		-62	
Friedrich Christian	11	GS-131	Quartz	0.068		-63	
Friedrich Christian	11	38 Cc-I	Calcite	0.059		-26	
Gottesehre near Urberg		53	Calcite	0.343		-25	
Igelschlatt	57	GS-37	Quartz	0.044		-47	
Igelschlatt	57	GS-37	Fluorite	0.153	-0.2	-29	-11.8

Johannes, Wittichen	13	WJB-2	Fluorite	0.11	-5.6	-12	-19.2
Johannes, Wittichen	13	WJB-17/4	Quartz	0.158		-36	
Käfersteige	1	BTR-28	Fluorite	0.142	-5.4	-17	-16.4
Michael im Weiler	65	GMW102	Quartz	0.055		-28	
Neu Bergmännisch Glück	22	814	Fluorite	0.1	-3.8		-17.8
Neubulach	64	815	Quartz	0.056		53	
Schauinsland	67	17	Calcite	0.094		-25	
Schauinsland	67	446	Quartz	0.037		-22	
Silberbrünnle	88	BTR-31	Quartz	0.049		-32	
Sophia Wittichen	12	BTR-50	Fluorite	0.091	-5.6		-9.2
Sophia Wittichen	12	198	Calcite-Late	0.035		70	
Teufelsgrund	40	BTR-7	Fluorite	0.105	-6.0	-1	-11.5
Teufelsgrund	40	BTR-9	Fluorite-Late	0.096	-9.0		-6.7
Teufelsgrund	40	BTR-8	Calcite-Late	0.052		-4	
Tunnelbau Hausach	29b	HTB-13	Calcite-Late	0.036		48	
Wenzel	31	BTR-42	Calcite	0.166		-15	

5.2.4. DEPENDENCE OF MEASURED δD OF FLUID INCLUSION WATER ON EXTRACTION TEMPERATURES

Fluid inclusion water was extracted from all fluorite samples at 400 °C and 650 °C. The δD values for water extracted from fluid inclusions in fluorites at 400 °C ranged widely between -60 and +82 ‰, with 10 of the 12 values between -29 and +22 ‰. At 650 °C, the values ranged from -78 to +40 ‰, with 10 of the 12 values between -47 and +17 ‰ (Table 9). Only one late fluorite from Teufelsgrund, BTR-9 shows lower δD values at both extraction temperatures (at 400°C, -58 ‰ and at 650 °C, -78 ‰) than primary hydrothermal fluorites. The δD at 650 °C vs. at 400 °C diagram (Fig. 17) shows that all δD values of water extracted from fluid inclusions in fluorites at 650 °C are systematically to lower (by upto -55 ‰) than those of water extracted at 400 °C. The δD values from rest gases oxidized by CuO to H_2O were always lower than extracted molecular water. We assume that most of the fluid inclusions in fluorites, which were decrepitated up to 400 °C, released only molecular water.
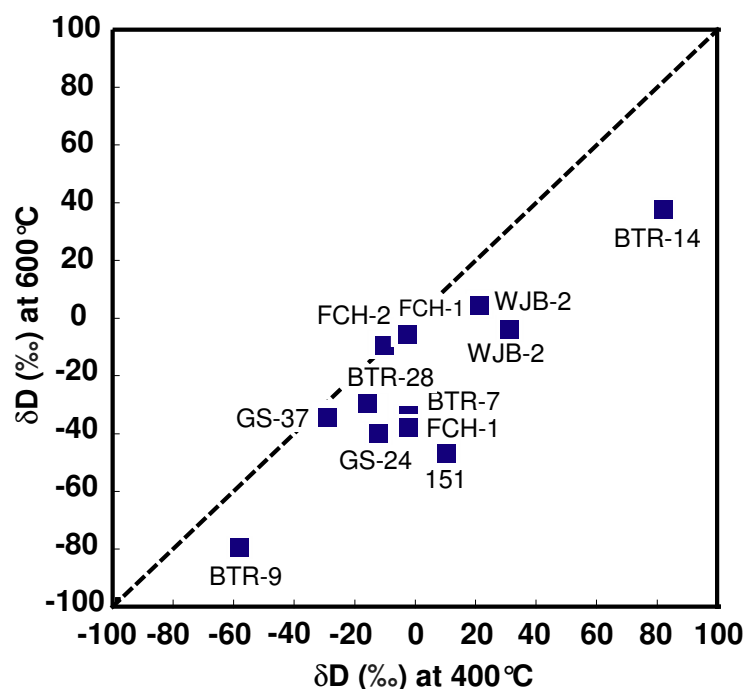
Figure 17. The δD values of fluid inclusion water released at 650 °C vs. δD values of fluid inclusion water released at 400 °C.

Table 9. Summary of stable isotope data for ore forming hydrothermal fluids in the Schwarzwald.

No. of deposit	Locality	Sample ID	Mineral	without CuO, 650°C		without CuO, 400°C
				$\delta^{18}O$	δD	δD
1	Käfersteige	BTR-28	Fluorite	-5.4	-30.0	-17.9
4	Dorothea	BTR-14	Fluorite	-3.3	38.0	81.5
11	Friedrich Christian	FCH-1	Fluorite		-42	-12.0
11	Friedrich Christian	FCH-1	Fluorite		-5.5	-6.3
11	Friedrich Christian	FCH-2	Fluorite	-2.6	-10.0	-12.1
13	Johannes, Wittichen	WJB-2	Fluorite	-5.6	6.0	22.2
13	Johannes, Wittichen	WJB-2	Fluorite		-2.9	25.6
25	Drey	GS-151	Fluorite	-7.4	-47.0	9.7
40	Teufelsgrund	BTR-7	Fluorite	-6.5	-36.0	-0.6
40	Teufelsgrund	BTR-9	Fluorite-Late	-9.0	-78.0	-58.1
56	Brenden	GS-24	Fluorite	-5.8	-41.0	-11.5
57	Igelschlatt	GS-37	Fluorite	-6.2	-36.0	-29.3

5.2.5. INFRARED SPECTRA AND WATER CONTENT OF FLUORITES

Fourier transformation infrared (FTIR) analyses in the IR wavelength region (2500 cm^{-1} to 5500 cm^{-1}) were scanned through the fluid inclusions and host fluorite mineral. In the infrared spectrum from the fluid inclusions in fluorite samples obtained at room temperature, two dominant broad absorbance bands at about 3400 cm^{-1} are present that indicate molecular water and structurally bound water (Aines and Rossman 1984). A smaller band was scanned at about 5200 cm^{-1} that can be identified as hydrogen in molecular water (O-H vibrations). In the spectrum obtained at room temperature from a fluid inclusion free area in the fluorite samples, the bands were observed with less intensity or no peak observed at 5200cm^{-1}. In the spectrum of primary fluorite sample GS-37, Igelschlatt deposit (Fig. 18), two dominant absorption bands were scanned at 3400 and 5210 cm^{-1} in fluid inclusions, whereas in fluid inclusion free area (fluid inclusion host), almost no peak observed at 5200cm^{-1}. This confirms that fluid inclusion or molecular water is absent in this area. A small peak scanned around 3400cm^{-1} in host that indication of no structurally bound water in host mineral. We obtained higher intensity sharp bands at 3400 and 5210cm^{-1} from the spectrum in fluid inclusions in fluorite sample BTR-7, Teufelsgrund deposit. Broadband was observed at 3400cm^{-1} in host fluorite that indicate amount of structurally bound water in host mineral. There was no molecular water observed (at 5210cm^{-1}) in host mineral of primary fluorite sample BTR-7, Teufelsgrund. It shows that there is water in fluorite not only in fluid inclusions, but also in structurally incorporated. Polarized FTIR absorption spectra at room temperature of fluid inclusions and host mineral of fluorite samples are presented in Figure 18.
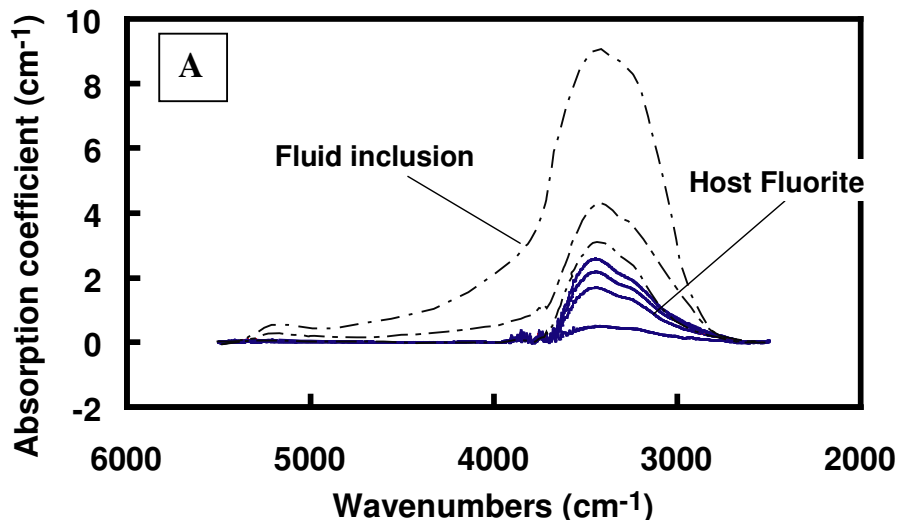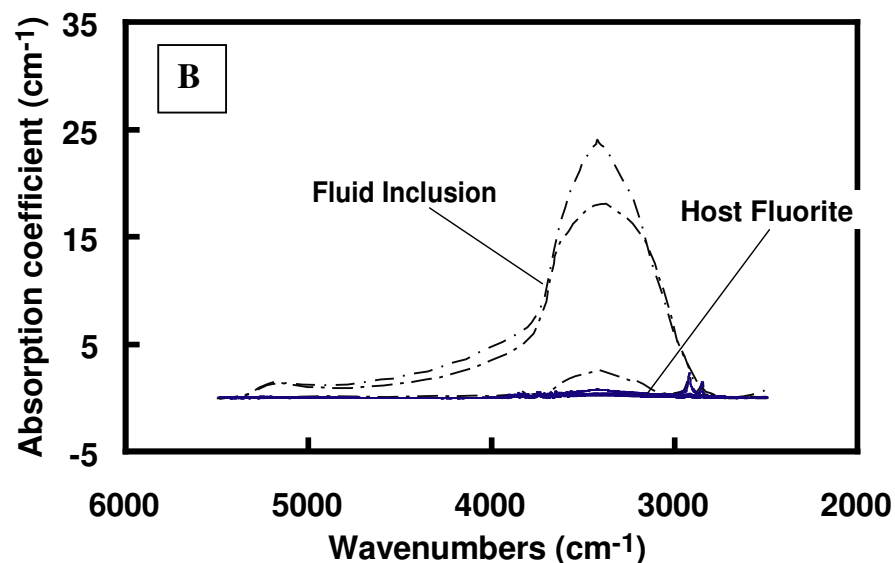
Figure 18. Infrared spectra of fluorite from post-Variscan hydrothermal veins. **(A)**. Sample BTR-7, Teufelsgrund deposit. Broadband was observed at 3400cm^{-1} in host. **(B)**. Sample GS-37, Igelschlatt deposit. The band at 3400cm^{-1} is absent in host. See the explanation in the text.

5.2.6. SULFUR ISOTOPES

The results of the δ^{34}S measurements are listed in Table 10 together with equilibrium temperatures of texturally coexisting mineral pairs calculated after Ohmoto and Goldhaber (1997). The δ^{34}S values of galena, chalcopyrite, and barite are summarized in Figure 19. Most of the barite data range between +9 and +15 ‰, with only 8 samples having slightly higher or lower δ^{34}S values (Fig. 19). Within individual veins, remobilized late-stage barite (Fig. 19, upside-down triangles) shows typically lower δ^{34}S values than the primary barite generation. The galena and chalcopyrite data cover a range of -14.1 to -1.6 ‰ and of –14.4 to +1.7 ‰, respectively. In the deposits Friedrich-Christian, Brandenberg, and Brenden, where multiple measurements of both principal sulfide minerals could be performed, the δ^{34}S values of cogenetic galena and chalcopyrite show a relatively broad overlap (Table 10). Sphalerite and pyrite samples show distinctively higher δ^{34}S values of -3.2 to +1.5 ‰ and +0.8 to +2.9 ‰.

Table 10. Summary of the δ^{34}S values and calculated equilibrium temperatures (using fractionation factors listed in Ohmoto and Goldhaber, 1997).

No.	Deposit (No. of deposit)	Sample ID	Mineral	δ^{34}S (V-CDT)	Temp. (°C); sulfide pairs [1]	Temp. (°C); sulfide-sulfate [1]
1	Käfersteige (1)	BTR-30	Barite	10.7		287 (1-3)
2	Käfersteige (1)	BTR-33	Barite	17.2		208 (2-3)
3	Käfersteige (1)	BTR-34a	Chalcopyrite	−11.6		
4	Dorothea (4)	QDC-69	Barite	10.4		
5	Dorothea (4)	M-33	Chalcopyrite	−14.4		245 (3-4)
6	Friedrich-Christian (11)	GS-129	Galena	−6.4	reversed (6-7)	359 (6-8)
7	Friedrich-Christian (11)	GS-129	Chalcopyrite	−7.5		314 (7-8)
8	Friedrich-Christian (11)	GS-129	Barite	12.0		
9	Friedrich-Christian (11)	GS-118	Galena	−10.0	255 (9-10)	302 (9-8)
10	Friedrich-Christian (11)	GS-118	Chalcopyrite	−7.9		308 (10-8)
11	Friedrich-Christian (11)	MSchl-389	Galena	−5.6	>1000 (11-12)	374 (11-8)
12	Friedrich-Christian (11)	MSchl-389	Pyrite	−4.9		352 (12-8)
13	Friedrich-Christian (11)	M-3	Galena	−7.7		338 (13-8)
14	Friedrich-Christian (11)	GS-129	Galena	−8.2	156 (14-15)	328 (14-8)
15	Friedrich-Christian (11)	GS-129	Chalcopyrite	−5.1		356 (15-8)
16	Friedrich-Christian (11)	GS-142	Galena	−9.3	reversed (16-17	312 (16-8)
17	Friedrich-Christian (11)	GS-142	Chalcopyrite	−9.7		283 (17-8)
18	Friedrich-Christian (11)	GS-135	Chalcopyrite	−7.6		313 (18-8)
19	Sophia (12)	WSB-181	Barite	13.1		
20	Sophia (12)	KL-1/63	Barite	14.2		
21	Sophia (12)	WSB-249	Barite	12.8		
22	Sophia (12)	5/97	Chalcopyrite	−1.8		401 (22-19)
23	Johann (13)	WJB-2	Chalcopyrite	−9.4		272 (23-24)
24	Johann (13)	WJB-2	Barite	13.2		
25	Johann (13)	WJB-59	Galena	−9.1	reversed (24-25	300 (25-24)
26	Johann (13)	WJB-59	Chalcopyrite	−13.0		232 (26-24)
27	Johann (13)	910	Chalcopyrite	−12.7		234 (27-24)
28	Drey (25)	GS-151	Galena	−4.3		343 (28-29)
29	Drey (25)	GS-151	Barite	15.0		
30	Drey (25)	GS-151	Galena	−5.5		325 (30-29)
31	Drey (25)	GS-154	Galena	−5.4		326 (31-29)
32	Drey (25)	GS-151	Galena	−5.7		322 (32-29)
33	Segen Gottes (27)	XSG-20	Sphalerite	−1.9		372 (34/35-33)
34	Segen Gottes (27)	XSG-20	Barite	14.3		
35	Segen Gottes (27)	XSG-15	Barite	14.0		
36	Segen Gottes (27)	XSG-30	Chalcopyrite	−3.8	287 (35-36)	341 (34/35-36)
37	Segen Gottes (27)	BTR-3	Galena	−5.7		336 (34/35-37)
38	Artenberg (28)	XSA-66	Barite	12.4		
39	Artenberg (28)	BTR-13	Chalcopyrite	−8.4		294 (38-39)
40	Wenzel (31)	OWF-18	Barite	8.5		
41	Wenzel (31)	OWF-56	Galena	−1.6	147 (41-43)	455 (41-42)
42	Wenzel (31)	OWF-56	Barite	12.4		
43	Wenzel (31)	OWP-86	Chalcopyrite	1.6		525 (43-42)

44	Wenzel (31)	BTR-19	Galena	−1.7	143 (43-44)	453 (44-42)
45	Teufelsgrund (40)	BTR-8	Barite	20.0		
46	Teufelsgrund (40)	BTR-4	Galena	−8.3	66 (46-48)	267 (46-47)
47	Teufelsgrund (40)	BTR-4	Barite	16.7		
48	Teufelsgrund (40)	BTR-27	Chalcopyrite	−3.3		307 (48-47)
49	Teufelsgrund (40)	BTR-7	Sphalerite	−3.2		303 (49-47)
50	Teufelsgrund (40)	BTR-6	Galena	−5.4		
51	Baumhalde (42)	GS-77	Galena	−10.2		
52	Baumhalde (42)	M-ZBH-31	Galena	−14.1	65 (52-53)	
53	Baumhalde (42)	M-ZBH-31	Chalcopyrite	−9.1		
54	Baumhalde (42)	MSchl-585	Galena	−13.2	97 (53-54)	
55	Brandenberg (43)	GS-93	Galena	−8.5	89 (55-60)	284 (55-62)
56	Brandenberg (43)	GS-98	Galena	−7.0	340 (56-60)	304 (56-62)
57	Brandenberg (43)	GS-91	Galena	−8.2		288 (57-62)
58	Brandenberg (43)	MSchl-584	Galena	−5.6	reversed (58-59	323 (58-62)
59	Brandenberg (43)	MSchl-584	Chalcopyrite	−5.7		298 (59-62)
60	Brandenberg (43)	GS-78	Chalcopyrite	−4.1		321 (60-62)
61	Brandenberg (43)	GS-86	Sphalerite	0.2		400 (61-62)
62	Brandenberg (43)	GS-86	Barite	15.0		
63	Brandenberg (43)	M"CuK/ZnS"	Sphalerite	−2.9		334 (63-62)
64	Brandenberg (43)	M-649	Barite	12.7		
65	Brandenberg (43)	GS-99	Barite-II	9.7		
66	Brandenberg (43)	GS-99-Sph	Sphalerite	−0.3		388 (66-62)
67	Herrmann (47)	GS-68	Galena	−2.6		600 (67-68)
68	Herrmann (47)	GS-68	Barite	8.3		
69	Gottes Ehre, Urberg (51)	M-810	Galena	−10.3	218 (69-70)	286 (69-77)
70	Gottes Ehre, Urberg (51)	M-810	Chalcopyrite	−7.9		294 (70-77)
71	Neuglück (52)	GS-26	Galena	−5.9		349 (71-77)
72	Neuglück (52)	M-UNG-9	Galena	−10.2	130 (72-73)	324 (72-77)
73	Neuglück (52)	M-UNG-9	Chalcopyrite	−6.7		320 (73-77)
74	Schwarzwaldsegen (53)	GS-28b	Galena	−7.0		330 (74-77)
75	Schwarzwaldsegen (53)	GS-28a	Galena	−8.5		309 (75-77)
76	Neuhoffnung (54)	GS-31	Galena	−10.0		288 (76-77)
77	Neuhoffnung (54)	GS-32	Barite	13.0		
78	Brenden (56)	GS-15	Galena	−10.5		303 (78-95)
79	Brenden (56)	GS-24	Galena	−11.1		295 (79-93)
80	Brenden (56)	GS-24	Galena	−11.0		295 (80-94)
81	Brenden (56)	GS-25	Galena	−9.7		315 (81-95)
82	Brenden (56)	GS-26	Galena	−9.9		313 (82-95)
83	Brenden (56)	GS-27	Galena	−10.1		309 (83-95)
84	Brenden (56)	MS-33	Galena	−11.4	380 (84-85)	292 (84-95)
85	Brenden (56)	MS-33	Chalcopyrite	−10.0		285 (85-95)
86	Brenden (56)	MS-35	Galena	−10.8	327 (86-87)	299 (86-95)
87	Brenden (56)	MS-35	Chalcopyrite	−9.3		296 (87-95)
88	Brenden (56)	MS-501	Galena	−11.6	215 (88-89)	289 (88-95)
89	Brenden (56)	MS-501	Chalcopyrite	−9.2		297 (89-95)
90	Brenden (56)	MS-564	Galena	−11.3	645 (90-91)	292 (90-95)
91	Brenden (56)	MS-564	Chalcopyrite	−10.6		278 (91-95)
92	Brenden (56)	MS-1466	Chalcopyrite	−9.0		300 (92-95)

93	Brenden (56)	GS-24	Barite	10.8	
94	Brenden (56)	GS-24	Barite	11.4	
95	Brenden (56)	GS-11	Barite	14.4	
96	Igelschlatt (57)	GS-42-2	Galena	–7.7	330 (96-102)
97	Igelschlatt (57)	GS-42-3	Galena	–8.9	312 (97-102)
98	Igelschlatt (57)	GS-42-4	Galena	–9.2	306 (98-102)
99	Igelschlatt (57)	GS-43	Galena	–8.8	315 (99-102)
100	Igelschlatt (57)	GS-57	Galena	–9.3	305 (100-102)
101	Igelschlatt (57)	GS-57	Galena	–8.0	325 (101-102)
102	Igelschlatt (57)	GS-57	Barite	13.4	
103	Igelschlatt (57)	GS-57	Barite	12.5	
104	Igelschlatt (57)	GS-45	Barite	12.3	
105	Michael im Weiler (65)	566	Galena	–4.5	355 (105-107)
106	Michael im Weiler (65)	566	Barite	14.2	
107	Michael im Weiler (65)	566	Barite	15.9	
108	Michael im Weiler (65)	782	Sphalerite	–0.1	
109	Kobaltgrube (68)	BTR-10	Barite	13.1	
110	Kobaltgrube (68)	DSB-29	Barite	12.9	
111	Kobaltgrube (68)	DSB-15	Galena	–4.2	382 (109/110-111)
112	Menzenschwand (69)	GMS-03	Barite	1.5	
113	Menzenschwand (69)	GMS-04	Barite	12.0	
114	Menzenschwand (69)	GMS-05	Barite	14.6	
115	Menzenschwand (69)	GMS-06	Barite	7.6	
116	Menzenschwand (69)	GMS-06	Pyrite	1.0	765 (116-114)

[1] Numbers in brackets refer to analyis numbers in column 1.

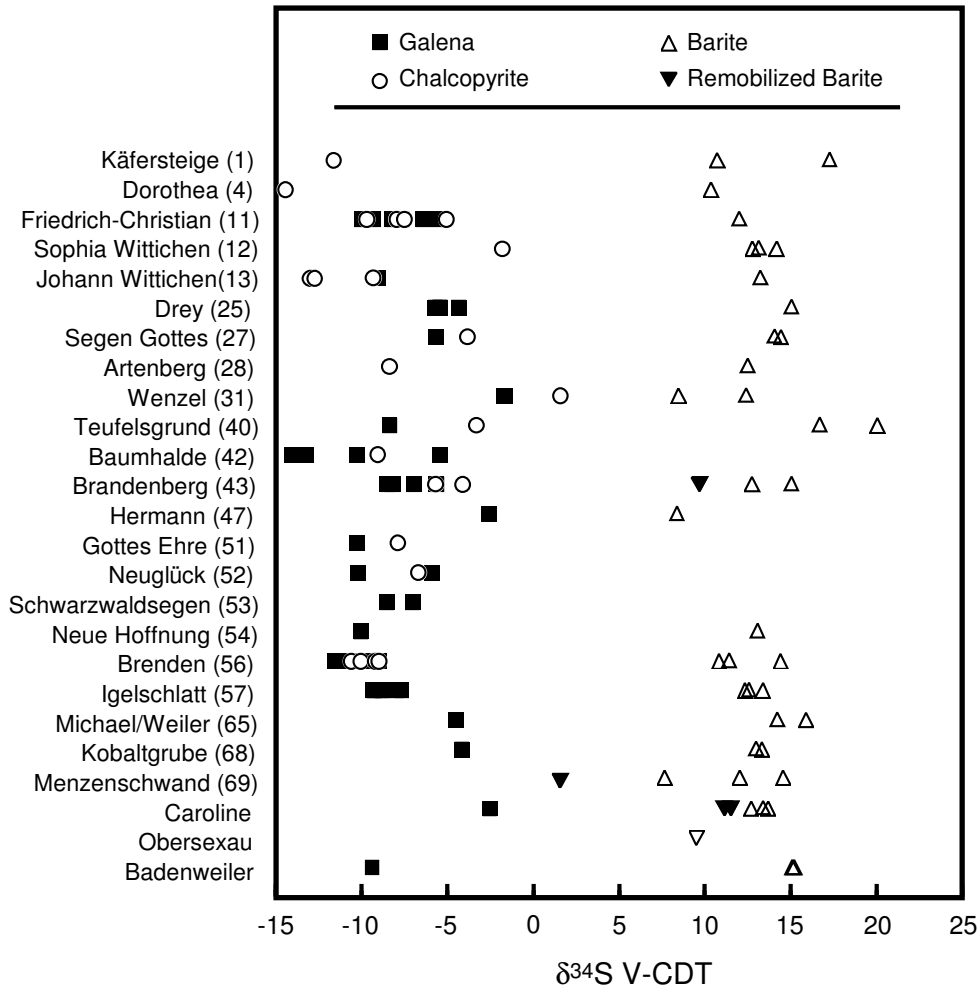**Figure 19.** Plot of the δ^{34}S values of sulfides and barite: galena (squares), chalcopyrite (circles), barite (triangles), and remobilized barite (upside-down triangles). Data for sphalerite and pyrite are not shown.

5.2.7. CARBON AND OXYGEN ISOTOPES OF CALCITES

The carbon and oxygen isotope data are summarized in Table 11. Figure 20 displays all measurements of petrographically primary (circles) and remobilized (squares) calcites. Primary calcites show a positive correlation in the δ^{13}C vs δ^{18}O space, ranging from -12.2 to -3.0 ‰ and from +12.0 to +18.5 ‰, respectively. Relatively late calcite generations within the veins (filled squares) display significantly higher δ^{13}C values of -12 to -1 ‰ and δ^{18}O values of +20 to +25 ‰. Sub-recent calcite sinters (open squares) show very high δ^{18}O values around +24 ‰. Mesozoic Muschelkalk limestone of the sedimentary cover (filled stars) show relatively high δ^{13}C values of -5 to +2 ‰. In contrast, calcites from a metamorphic vein

hosted by crystalline basement rocks and Paleozoic limestone from the Badenweiler-Lenzkirch zone (open star) have comparatively low $\delta^{13}C$ values.

Table 11. Summary of the carbon and oxygen isotope data of post-Variscan hydrothermal calcite samples from the Schwarzwald district.

No	No. of deposit	Deposit	Sample ID	Calcite stage	$\delta^{13}C$ (V-PDB)	$\delta^{18}O$ (V-SMOW)
1	1	Käfersteige	1/41	Cc II	–9.8	24.9
2	1	Käfersteige	1_BTR-30	Cc II	–9.4	24.7
3	10	Clara	10/43	Cc I	–10.3	14.3
4	10	Clara	10/44	Cc I	–9.1	15.2
5	10	Clara	10/45	Cc II	–4.9	21.5
6	11	Friedrich-Christian	11/36	Cc I	–6.1	18.2
7	11	Friedrich-Christian	11/37	Cc IV	–6.4	23.5
8	11	Friedrich-Christian	11/38	Cc I	–7.5	17.1
9	11	Friedrich-Christian	11/39	Cc II	–3.5	20.9
10	11	Friedrich-Christian	11/74	Cc IV	–1.3	23.7
11	11	Friedrich-Christian	12/54	Cc I	–10.7	15.2
12	12	Sophia	12_198	Cc II	–4.5	23.5
13	12	Sophia	12_BTR-35a	Cc II	–2.5	22.5
14	12	Sophia	12_KL-1/63	Cc I	–9.9	13.8
15	12	Sophia	12_BTR-41	Cc I	–10.8	14.9
16	12	Wittichen area (Sophia)	10	Cc II or III	–2.1	21.0
17	12	Wittichen area	13	Cc II	–9.5	20.6
18	12	Wittichen area	14	Cc II	–10.8	14.4
19	13	Johannes	13/8	Cc I	–10.0	15.0
20	13	Johannes	13_WJB-90	Cc II	–6.0	23.7
21	28	Artenberg	28/55	Cc I	–8.5	13.3
22	28	Artenberg	28/56	Cc II	–9.6	15.3
23	28	Artenberg	28/57	Cc III	–11.6	24.1
24	28	Artenberg	28_BTR-13	Cc I	–10.1	13.8
25	28	Artenberg	28_XSA-47	Cc I	–11.3	11.8
26	28	Artenberg	28_XSA-47	Cc II	–11.4	24.0
27	29b	Tunnel near Hausach	11	Cc II	–6.3	22.6
28	31	Wenzel	31/19	Cc II	–10.2	21.4
29	31	Wenzel	31/33	Cc I	–8.1	14.7
30	31	Wenzel	31/34	Cc I	–11.2	14.5
31	31	Wenzel	31/50	Cc II	–6.5	21.6
32	31	Wenzel	31/51	Cc I	–12.8	13.7
33	31	Wenzel	31_BTR-18	Cc I	–11.9	13.1
34	31	Wenzel	31_BTR-18	Cc II	–6.7	20.7
35	35	Tennenbronn	35/66	Cc I	1.5	19.9
36	37	Sulzburg	37/68	Cc IV	–3.1	23.8
37	40	Teufelsgrund	40/58	Cc II	–3.5	17.2
38	40	Teufelsgrund	40/59	Cc II	–4.4	17.3

39	40	Teufelsgrund	40_BTR-5	Cc I	−4.4	17.1
40	40	Teufelsgrund	40_BTR-8	Cc I	−3.2	16.9
41	43	Brandenberg	43/60	Cc II	−3.7	17.0
42	43	Brandenberg	43/61	Cc II	−3.9	17.7
43	43	Brandenberg	43/62	Cc II	−3.7	18.3
44	51	Gottes Ehre	51/21	Cc II	−3.4	19.7
45	51	Gottes Ehre	51/22	Cc III	−6.2	21.4
46	51	Gottes Ehre	51/53	Cc I	−11.1	12.7
47		Mühlsandstein	63/25	Cc I	−9.0	20.1
48	64	Neubulach	64/42	Cc II	−6.5	24.1
49	64	Neubulach	64_BTR-20	Cc II	−7.2	23.9
50	64	Neubulach	64_BTR-22	Cc II	−8.0	23.8
51	67	Schauinsland	67/17	Cc I	−12.2	12.1
52	67	Schauinsland	67/18	Cc I	−12.1	12.5
53	67	Schauinsland	67/20	Cc II	−4.1	20.9
54	67	Schauinsland	67/28	Cc II	−4.5	21.3
55	67	Schauinsland	67_BTR-40	Cc I	−10.8	13.3
56	70	Daniel/Dehs	70/3	Cc I	−9.9	14.4
57	70	Daniel/Dehs	70/70	Cc II	−3.6	22.2
58	70	Daniel/Dehs	70/72	Cc I	−9.3	15.9
59	70	Daniel/Gallenbach	21/2	Cc II	−7.1	17.5
60	71	Johann Baptist	71/69	Cc IV	−4.6	22.2
61	72	Anton/Heubach	72/30	Cc II	−1.4	23.3
62	72	Anton/Heubach	72/73	Cc IV	0.1	24.5
63	73	Bernhard/Hauserbach	73/23	Cc II	−4.6	21.8
64	73	Bernhard/Hauserbach	73/52	Cc II	−8.0	23.2
65	74	Maria Theresia	74/47	Cc II	−4.3	21.3
66	75	Katharina/Trillengrund	75/27	Cc I	−10.4	14.6
67	75	Katharina/Trillengrund	75/75	Cc IV	−7.9	23.9
68	76	Rötenbach quarry	76/24	Cc II	−1.0	22.6
69	77	Christina/Wittichen	77/6	Cc II	−5.2	23.3
70	78	Simson/Wittichen	78/7	Cc I	−8.1	15.9
71	81	Giftgrube/Kaltwasser	81/29	Cc II	−4.3	16.5
72	82	Fahl	82/35	Cc II	−5.4	22.0
73	83	Gschwend	83/63	Cc II	−7.1	22.1
74	84	Herrenwald	84/15	Cc II or III	−3.3	15.1
75	85	Anton/Wieden	85/5	Cc II	−5.4	22.4
76	90	Tunnel near Waldkirch	12	Cc II	−4.6	21.4
77	91	Merzhausen near Freiburg	16	Cc II	−3.7	20.4
78	92	Tunnel near Hornberg	46	Cc II	−6.9	23.7
79	93	Hechtsberg quarry	48	Cc II	−8.7	22.8
80	93	Hechtsberg quarry	49	Cc II	−10.2	23.8
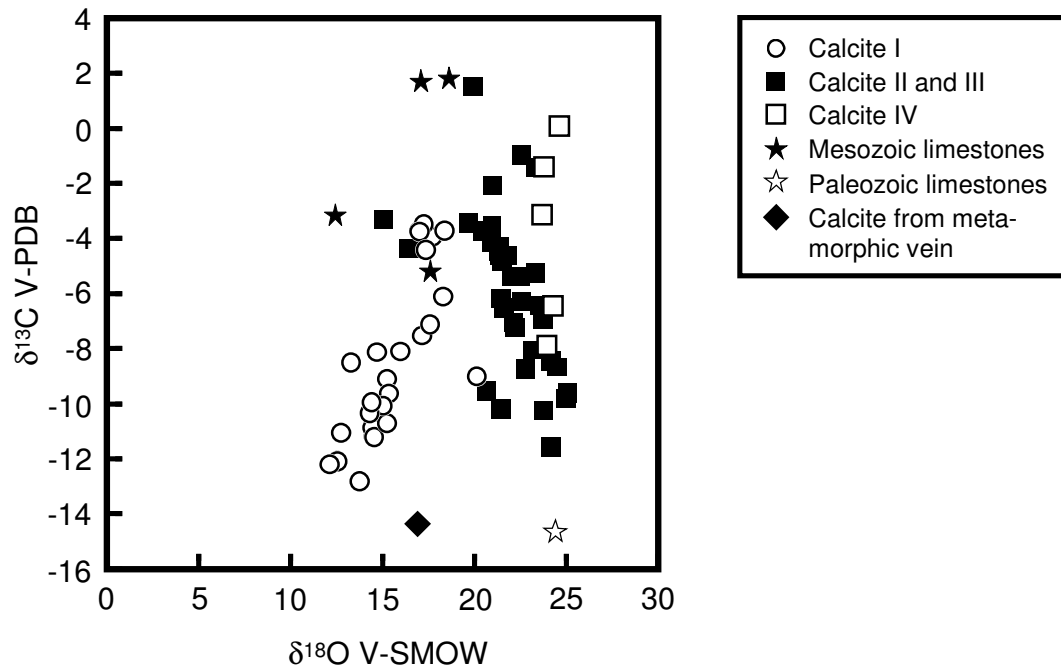
Figure 20. Plot of the $\delta^{13}C$ and $\delta^{18}O$ values of primary hydrothermal calcites (circles) and remobilized calcites (squares) from the deposits. Open squares are very late, possibly recent sinters. Additional data are calcites from Mesozoic (solid-stars) and Paleozoic (open-stars) limestones and calcite from a Variscan calcite-prehnite-pectolite vein (rhomb).

6. DISCUSSION

6.1. VARISCAN VEINS

6.1.1. PRESSURE-TEMPERATURE CONDITIONS OF VARISCAN MINERALIZATION

Based on the fluid inclusion and stable isotope data presented above, the Variscan and post-Variscan fluid systems in the Schwarzwald are very different. Variscan aqueous fluids are generally of low-salinity. The initial melting temperatures of ice indicate the presence of NaCl-KCl-rich compositions, whereas $CaCl_2$ appears to be absent. In addition, a second distinct group of fluid inclusions with predimonantly CO_2 and CH_4 ($\pm N_2$) is present. These characteristics conform to the results of fluid inclusion studies in altered granites from the Schwarzwald area, which indicate that low-salinity fluids (0 to 10 wt.% equivalent NaCl) with homogenization temperatures of 200-400 °C were responsible for early high-temperature alteration of the granites (Simon and Hoefs 1987; Hofmann and Eickenberg 1991). Behr *et al.* (1987) concluded that the Variscan hydrothermal fluids in Germany are characterized by a clear dominance of CO_2 and N_2-CH_4 mixtures. The origin of the CH_4-CO_2-N_2 gas-rich component is assumed to be related to Variscan metamorphism of lithologically highly variable rocks of the crystalline basement (Behr *et al.* 1987). Hydrothermal alteration of Variscan granites was most effective in the temperature range between 200-500 °C at rather shallow levels corresponding to pressures of 1-2 kbar, as estimated from various geothermobarometers (Simon 1990). Oxygen isotope systematics and calculations of both closed- and open-system models for fluid-rock interaction indicate that the hydrothermal fluids responsible for the widespread granite alteration were unequivocally of meteoric origin (having original $\delta^{18}O$ values around -12 ‰). Progressive interaction with the granites resulted in oxygen exchange and a systematic shift towards higher values (Simon 1990). The Variscan mineralizations have homogenization temperatures between 150 and 350°C. Since there is no evidence that the Variscan fluid system has ever been open to the surface, these values need to be corrected for lithostatic pressure. Behr *et al.* (1987) estimated the maximum trapping temperatures (250-400°C) in Variscan mineralizations based on the estimated thickness of overburden. These conditions are in good agreement with the reconstructed P-T conditions of syn- to late-orogenic Au- and Sb-bearing vein systems in other parts of the Variscan belt, e.g. the French Massif Central (Boiron *et al.* 2003; Vallance *et al.* 2004), the Rheinish Massif (Wagner and Cook 2000), Cornwall (Wilkinson *et al.* 1995) and Spain (Germann *et al.* 2003; Sanchez-Espana *et al.* 2003).

6.1.2. ISOTOPIC COMPOSITION OF THE VARISCAN HYDROTHERMAL SOLUTIONS

All $\delta^{18}O$ values of quartz of the Variscan veins are in a range between +2.8 and +14.5 ‰ (Table 3). Heavier $\delta^{18}O$ values were observed from the deposits Ludwig im Adlersbachtal (+15.1 to +18.8 ‰) and St. Ulrich (+13.7 and +14.7 ‰), which are related to a low temperature fluid and are believed to reflect a Post-Variscan hydrothermal overprint of the Variscan vein, which is not surprising given the great abundance of post-Variscan fluorite-barite veins in the Schwarzwald area. The calculated oxygen isotope composition of the fluids varies between -12.5 and +4.4 ‰ using the mode of the homogenization temperatures, whereas for the maximum homogenization temperatures the $\delta^{18}O$ values of the fluids are shifted towards slightly heavier values. Thus, the calculated $\delta^{18}O$ values of the fluids cover the range estimated for regional metamorphic fluids or for mixtures between metamorphic fluid and seawater (e.g., Sheppard 1986). The δD values are consistent with the trend displayed by the oxygen isotope data.

6.2. POST-VARISCAN VEINS

Many ideas and discussions on the stable isotope study and the mixing calculations resulted from the close collaboration with my co-PhD student Gregor Schwinn.

6.2.1. PRESSURE-TEMPERATURE CONDITIONS OF POST-VARISCAN MINERALIZATION

The results of the integrated fluid inclusion and stable isotope studies of the post-Variscan veins allow a reconstruction of the pressure-temperature conditions prevalent during their formation. Combining the measured $\delta^{18}O$ data of quartz and directly extracted fluid inclusion water for pairs of texturally coexisting quartz and fluorite, the equilibrium temperatures were calculated. By combination with the trapping temperatures of the fluid inclusions, the corresponding pressure can then be calculated from the intersection with the respective isochores of the fluid inclusions, which establishes the P-T conditions of the vein formation (Fig. 21). It is important to note that fluid inclusion petrography and the microthemometric data demonstrate the contemporaneous formation of texturally coexisting quartz-fluorite pairs. Figure 22 shows a hand specimen from the Brandenberg deposit with histograms of the final

ice melting temperatures of fluid inclusions in quartz and fluorite, which demonstrates that both minerals were apparently precipitated from the same hydrothermal fluid.

Figure 22. Cogenetic quartz and fluorite in sample GS-111 with histograms of fluid inclusion melting temperatures in both minerals.
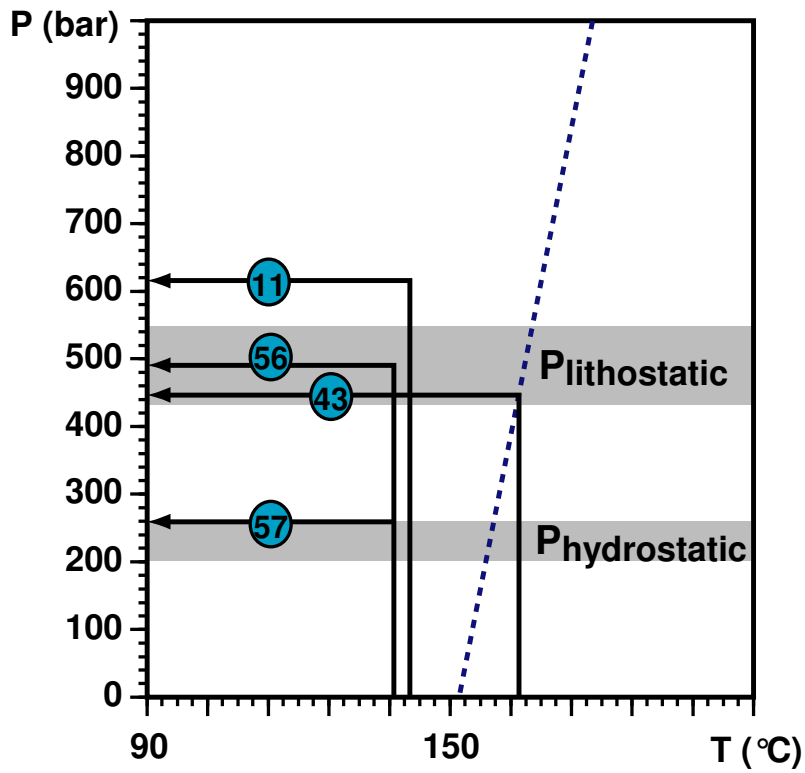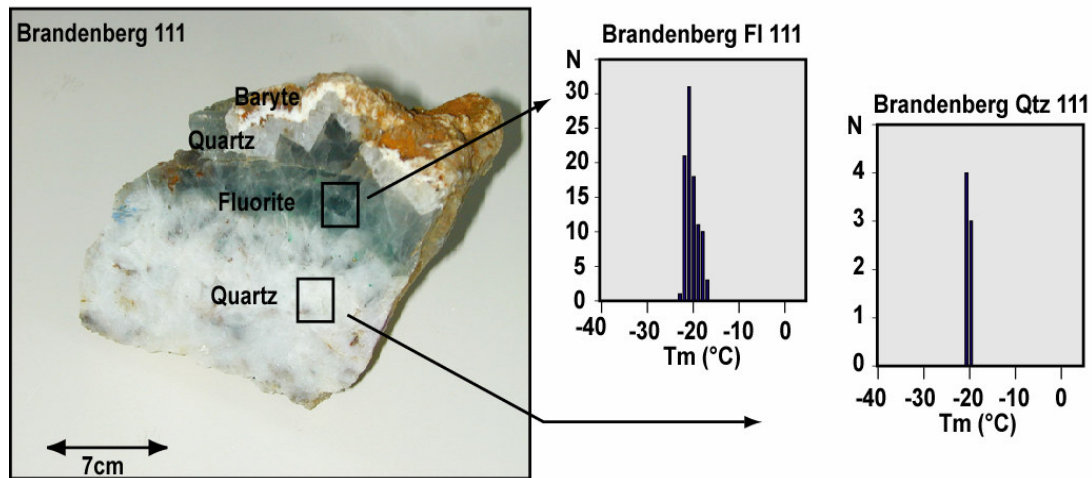

Figure 21. P-T diagramm with conditions of crystallization of four deposits (see map for locations). The pressure was calculated by intersecting isotope equilibrium temperatures with isochores (dotted line as example)

Oxygen isotope equilibrium temperatures between bulk quartz and the hydrothermal fluid from fluid inclusions were calculated after Matsuhisa *et al.* (1979), and the corresponding isochores were calculated after Brown and Hageman (1995). The results and the input parameters for the calculation of the isochores are given in Table 12.

Table 12. Temperature and pressure of formation from $\delta^{18}O$ ratios and microthermometric data from post-Variscan veins in the Schwarzwald.

No. of deposits	Locality	Sample ID	$\delta^{18}O_{Quartz}$ (V-SMOW)	$\delta^{18}O_{Fluid}$ (V-SMOW)	T_m (°C)	T_h (°C)	$T_{formation}$ (°C)	$P_{formation}$ (bar)
11	Friedrich-Christian	GS 135	14.3	-2.3	-23	110	137	610
43	Brandenberg	GS 111	12.5	-1.0	-20	165	173	450
56	Brenden	GS 24/GS 15	13.8	-3.3	-20	135	132	490
57	Igelschlatt	GS 37	16.8	-0.2	-22	135	133	260

Note: $\delta^{18}O_{Fluid}$ measured from extracted fluid inclusions from fluorite.

In order to determine the error interval associated with our calculations, error ranges of the measured fluid inclusion homogenization temperatures (± 5 °C) and the $\delta^{18}O$ equilibrium temperatures (± 5 °C, corresponding to approximately ± 0.5 ‰ $\delta^{18}O$) have been considered. The calculated formation pressures range from 260 to 610 bars (Fig. 21 and Table 12), with the error interval being about ± 125 bar. The sedimentary overburden in the area where the deposits formed prior to the subsidence of the Rheingraben structure can be reconstructed from the regional geology (Geyer and Gwinner 1986) and lithostatic and hydrostatic pressure conditions can be calculated from the barometric equation. For example, the Friedrich-Christian deposit was covered by approximately 1800-2000 m of basement rocks and sediments. With assumed rock and fluid densities of 2.7 and 1.2 g/cm³ respectively, one can estimate that the hydrostatic pressure should have been around 220 bar and the lithostatic regime around 500 bar (shaded areas in Fig. 21). Comparison of the vein formation pressures determined from fluid inclusion and oxygen isotope data with the litho- and hydrostatic pressures reconstructed from geological constraints shows that the actual pressure conditions apparently varied between lithostatic as hydrostatic pressure conditions.

6.2.2. ISOTOPIC COMPOSITION OF THE POST-VARISCAN HYDROTHERMAL FLUIDS

The oxygen isotopic composition of the hydrothermal fluids was calculated from the measured range of isotopic compositions of quartz within distinct veins and the corresponding pressure-corrected fluid inclusion temperatures (Table 4). The resulting equilibrium $\delta^{18}O_{H2O}$ values are within a relatively narrow range between -7.5 to +2.1 ‰. This data range is very consistent with the measured $\delta^{18}O_{H2O}$ values (-11.6 to -3.0 ‰) of water directly extracted from fluorite-hosted fluid inclusions. Consequently, the initial $\delta^{18}O$ values of the primary hydrothermal fluids are estimated to be in the range between -10 and 0 ‰. The $\delta^{18}O$ values of the surface-derived meteoric waters can vary along the meteoric water line from 0 ‰ to negative values. Integrating the $\delta^{18}O$ data of vein quartz, fluid inclusion homogenization temperatures, and calculated and measured fluid isotopic compositions, all available information points to formation of the post-Variscan vein deposits from saline brines with quite homogeneous geochemical characteristics. The δD (-10 to -40 ‰) and $\delta^{18}O$ (-11.6 to -3.0 ‰) values of fluid inclusion water directly extracted from the vein minerals ($\delta^{18}O$ from fluorite, δD from fluorite, quartz and calcite) are well within the range typical of meteoric water. The deep saline brine is most likely of meteoric or seawater origin (Behr and Gerler 1987; von Gehlen 1987; Hofmann 1989; German *et al.* 1994; Werner *et al.* 2000; 2002), but was extensively modified through water-rock reactions in the crystalline basement. During high-temperature water-rock interaction with crystalline rocks, the $\delta^{18}O$ of water is generally shifted towards higher values (Taylor 1997). The oxygen data indicate that the hydrothermal fluids have partly exchanged oxygen through progressive fluid-rock interaction in the crystalline basement (Fig.16). Considering the trends of both $\delta^{18}O$ and δD of the post-Variscan hydrothermal veins, it appears that the meteoric contribution to the isotopic budget is certainly dominant. The oxygen isotope signature, however, was compositionally modified during fluid ascent and interaction with the surrounding rocks. Schwinn *et al.* (in press) have applied both closed- and open-system scenarios (Taylor 1977; 1997) to model the isotopic exchange between water of meteoric origin (with $\delta^{18}O$ between -5 and 0 ‰) and typical granites of the Schwarzwald area having average primary $\delta^{18}O$ values of 10 ‰ (Hoefs and Emmermann 1983; Simon and Hoefs 1987). The resulting $\delta^{18}O$ values of the deep saline brine are in the range between -1.2 and 5.3 ‰ for geologically reasonable water/rock ratios between 0.01 and 1.0 and an exchange temperature of 300°C.

The $\delta^{13}C$ values of directly extracted fluid inclusion gas, which are in the range between -21.4 and -6.7 ‰, are systematically lower than the values for primary hydrothermal calcites from the post-Variscan veins, which range between -12.0 and -3.0 ‰ (Schwinn *et al.* in press). This difference cannot be explained through equilibrium fractionation between calcite and dissolved inorganic carbon species in the fluids in the temperature interval 150-200 °C. Applying equilibrium fractionation factors for both CO_2 (aq) and HCO_3^- (Ohmoto and Goldhaber 1997), which are most likely the predominant dissolved carbon species in the fluids, results in calculated $\Delta_{CAL-CO2}$ of 0.9 to –0.7 ‰, and $\Delta_{CAL-HCO3}$ of 1.1 to 2.0 ‰. This range is much narrower than the observed difference in carbon isotope composition between the bulk fluid inclusion gas and the hydrothermal calcites. Although the dominant carbon component in the fluid inclusions is CO_2, as shown by the Raman spectra, it appears probable that minor amounts of a second carbon component with significantly more negative $\delta^{13}C$ values contribute to the bulk composition of carbon isotope of the fluid inclusion gas. A likely candidate for this component is gaseous CH_4, which has been found at detectable concentrations in fluid inclusions from the Schauinsland deposits (Werner *et al.* 2002). Based on mass balance considerations, even small amounts of CH_4 with very negative $\delta^{13}C$ values could shift the bulk carbon isotopic composition of the fluid inclusions towards more negative values. This, in turn, would have no impact on the $\delta^{13}C$ values of the hydrothermal calcites, because in comparatively rapid processes such as fluid migration and fluid mixing, CH_4 would not equilibrate with oxidized aqueous carbon species due to kinetic restrictions (Ohmoto and Goldhaber 1997).

6.2.3. SULFUR ISOTOPE SYSTEMATICS

Equilibrium temperatures of sulfide-sulfide and sulfate-sulfide mineral pairs were calculated using fractionation factors given in Ohmoto and Goldhaber (1997). Most interestingly, the calculated temperatures of texturally coexisting sulfide ore minerals cover a temperature range from less than 100 upto 400 °C and more (Fig. 23A), whereas sulfide-sulfate temperatures show a distinct maximum of the temperature distribution around 300-350 °C (Fig. 23B). The isotopic temperatures contrast with the formation temperatures (150-200 °C) of the hydrothermal ore deposits, which are well established from fluid inclusion studies (Behr and Gerler 1987; Behr *et al.* 1987; von Gehlen 1989; Werner *et al.* 1990; Hofmann and Eikenberg 1991; German *et al.* 1994; Lippolt and Werner 1994; Lüders 1994; Ritter 1995;

Weber 1997; Werner *et al*. 2000; 2002). This indicates that ore precipitation occurred under conditions where a sulfur isotope equilibrium could not be established.

We hypothesize that the temperature range of 300-350 °C calculated from sulfide-sulfate equilibria could reflect the aquifer paleotemperature of the deep saline brine, which was preserved during fluid migration. This assumption is corroborated by calculations applying the kinetic model of sulfur isotope fractionation of Ohmoto and Lasaga (1982). Assuming a near-neutral pH and a total sulfur concentration of 500-1000 ppm, the time required to establish a degree of equilibrium of 95 % at 300-350 °C, i.e. at conditions prevalent in the deep fluid aquifer, is less than one year. At temperatures of 150-200 °C, which correspond to the formation temperatures of the deposits, re-establishment of the sulfide-sulfate equilibria needs 3000 to 7000 years. Considering the hydrodynamics of fluid migration within the fault zones, it appears plausible that fluid mixing and mineral deposition processes were too fast for re-equilibration of sulfur isotopes at formation temperatures. Relatively fast ascent of deep-sourced fluids through open fractures is consistent with the tectonic setting of the hydrothermal mineralizations in the Schwarzwald district (Franzke, 1992; Werner and Franzke, 2001).

Although the homogeneous sulfate-sulfide isotopic temperatures indicate a common deep source for both aqueous sulfate and sulfide, they do not exclude that at least part of the sulfate budget was derived from mixing with meteoric waters. Such a model has been favored by different authors for the Schauinsland deposit (Weber 1997; Werner *et al*. 2002). If barite precipitation occurred as a response to instantaneous fluid mixing, the barite should then reflect the δ^{34}S value of dissolved aqueous sulfate of the meteoric fluids and fingerprint their source rocks. In this case, the observed consistent isotope temperatures would be purely coincidental. However, the sedimentary cover of the crystalline basement contains different sulfate-bearing units (Triassic to Jurassic evaporites) with very heterogeneous δ^{34}S values ranging between 12 and 21 ‰ (Müller *et al*. 1966). Considering the relatively variable δ^{34}S values of potential sulfate sources and the fact that ore-forming processes in the Schwarzwald district were operative over more than 100 Ma, we would not expect the observed narrow range of sulfate-sulfide isotope fractionation by mixing of deep brines with meteoric waters.

Another possible model for sulfate deposition is oxidization of aquoeus sulfide being supplied by a reduced, saline brine through mixing with meteoric water. In this case, the instantaneous oxidation and precipitation processes are too fast for establishment of isotopic equilibrium between dissolved sulfide and the aqueous sulfates formed via oxidation.
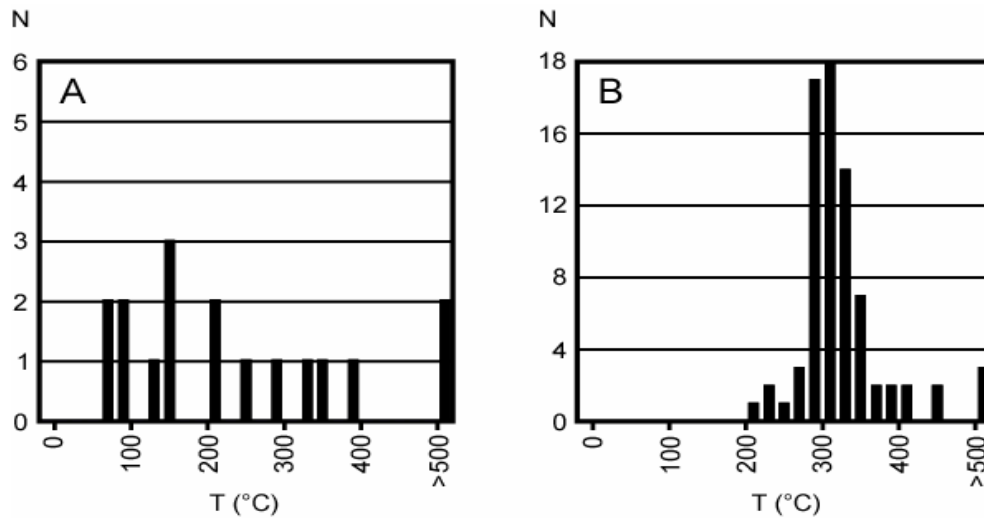
Figure 23. Calculated sulfur isotope equilibrium temperatures for **(A)** sulfide-sulfide and **(B)** sulfide-sulfate pairs (fractionation factors from Ohmoto and Goldhaber, 1997).

The sulfide ore minerals should then display isotopic compositions very similar to barite, with only a very small fractionation between sulfide and sulfate minerals detectable (Ohmoto and Goldhaber 1997). However, the observed sulfur isotope systematics, i.e., the consistently different $\delta^{34}S$ values of sulfides and barite from the Schwarzwald area, argues against such a model.

6.2.4. MIXING CALCULATIONS INVOLVING SULFUR ISOTOPES

To strengthen our point, we have assessed the potential effect of contamination of a high-temperature brine transporting aqueous sulfate and sulfide in isotopic equilibrium by mixing with sulfate from meteoric water. Quantification of such a process requires reasonable estimates of the equilibrium temperatures, the sulfate concentrations and sulfur isotope composition of both end-member fluids and the fluid mixing ratio. We know from fluid inclusion studies that the temperatures of formation of the hydrothermal vein deposits range from 150 to 200°C at depths of around 1.5 km, and the salinities of primary fluid inclusions range from 20 to 33 wt.% equivalent (eqv.) NaCl (Behr and Gerler 1987; Behr *et al.* 1987; von Gehlen 1989; Werner *et al.* 1990; Hofmann and Eikenberg 1991; Lüders 1994; Ritter 1995; *this study*, Table 13).

Table 13. Summary of fluid inclusion data from post-Variscan hydrothermal veins in the Schwarzwald district.

Mineralization stage	Host mineral	T_m ice (°C)	Salinity (wt.%)	T_h (°C)
Main stage	Fluorite	–27.0 to –20.0	22.4–26.8	120–175
	Quartz	–26.0 to –20.0	22.4–26.2	80–150
	Barite	–25.8 to –21.8	23.6–26.1	150–220
	Calcite	–28.1 to –22.0	23.7–27.5	100–180
Late stage	Fluorite	–9.4 to –1.0	1.7–13.3	120–160
	Quartz	–5.5 to –1.1	1.9–8.5	140–250
	Calcite	–5.6 to –0.2	0.4–8.7	160–200

The highest salinities that were found in primary fluid inclusions of the main stage (fluorite-barite) are around 33 wt.% eqv. NaCl. Considering that this fluid composition does certainly not represent the unmodified deep saline brine (prior to any mixing with meteoric water), we used an estimate of 40 wt.% eqv. NaCl for modeling. This should be very close to the true composition of the original deep-sourced brine. In order to make some reasonable assumptions on the paleo-hydrothermal system, we will compare the paleo-system with the recent conditions in the Schwarzwald area. This is valid because (1) the area has been tectonically active recently and hosts numerous thermal springs, and (2) these thermal and mineral waters show REE patterns, which are identical to patterns, preserved in fluorites from the post-Variscan deposits of the Schwarzwald (Schwinn and Markl 2005). Assuming an elevated geothermal gradient of 40°C/km due to the intense tectonic activity of the area, the temperature of a meteoric water at 1 km depth should be close to 50°C. Temperatures of 300 °C in the deep aquifer would be reached at depths around 7- 8 km. The migrating saline brine will probably cool during the ascent from at least 7 km to the vein-forming level at 1 km depth. Hydrological data from recent geothermal wells from the Schwarzwald area show very little cooling of thermal waters during ascent on the order of 5-10 °C from 1.5 km depth (He *et al*. 1999). Therefore, it seems reasonable to assume cooling of the saline brine down to a temperature of about 250 °C during ascent from the deep aquifer. Using these temperature estimates for both fluid end-members, mixing calculations of a saline brine with total dissolved solutes of 40 wt.% equivalent NaCl and a temperature of 250°C with meteoric water having a temperature of 50°C reproduces the measured range of salinities and homogenization temperatures found in fluid inclusions (Fig. 24). The calculated mixing ratios

(meteoric water/saline brine) would range between 1 and 0.33, which corresponds to mass fractions of the deep saline brine between 0.5 and 0.75.
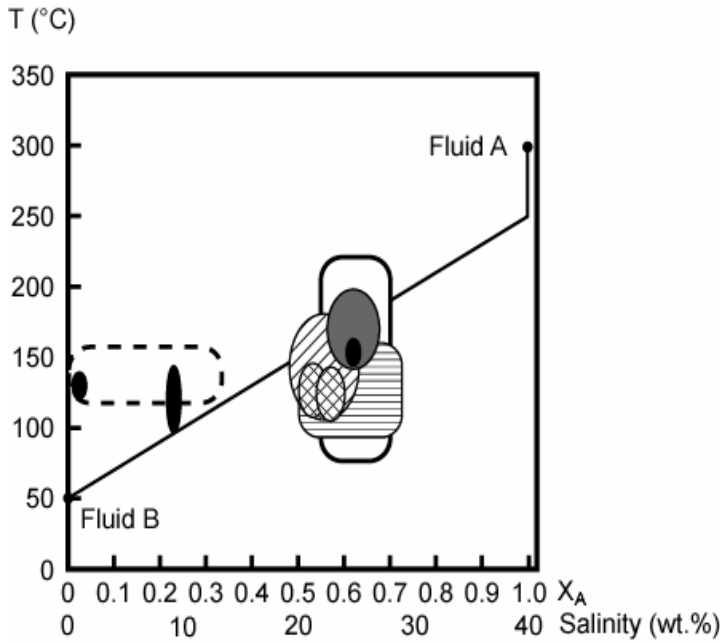

Figure 24. Temperature of a mixed fluid plotted as a function of the mixing ratio of fluid A (deep saline brine) with fluid B (meteoric water), and superimposed fluid inclusion data from the Schwarzwald district. Both the mass fraction of fluid A and the resulting salinity (given as wt.% equivalent NaCl) are given on the abscissa. Fluid inclusion data are from Werner *et al.* (2000) and Mittelstädt (1987) (Schauinsland deposit, horizontal lines), Werner et al. (2000) (Teufelsgrund deposit, cross-hatched), Lüders (1994) (Badenweiler, black), Behr *et al.* (1987) (several post-Variscan deposits, diagonal lines), Hofmann and Eikenberg (1991) (Krunkelbach deposit, dark gray), and our data from primary fluorite, calcite, quartz, and barite (thick solid line), and late stage fluorite and calcite (thick dashed line).

Using these data as a basis, we can evaluate how robust the calculated sulfate-sulfide equilibrium temperatures are against meteoric contamination. Contamination of an equilibrated sulfate-sulfide system in the deep saline brine by sulfate supplied by mixing with surface-derived meteoric waters would result in a significant displacement of the calculated equilibrium temperatures. The impact of this contamination depends (1) on the mixing ratio of the two fluids, (2) on the concentrations of sulfate in the brine and the meteoric water, and (3) on the difference between the $\delta^{34}S$ values of aqueous sulfates in the brine and the meteoric source. For estimating this effect, we will assume that aqueous sulfate and sulfide were equilibrated in the deep aquifer with $\delta^{34}S$ values of 13 ‰ and –9.2 ‰ at a temperature of 300 °C and then calculate the shift in the resulting equilibrium temperature for variations in these parameters.

In order to constrain the concentration ratio of aqueous sulfate in meteoric water and brine, $Rs = mSO4_{METEORIC} / mSO4_{BRINE}$, we first assume that the meteoric water is saturated with gypsum, which is, based on the abundance of sulfate-rich evaporitic series in the rock sequences through which those meteoric waters percolate, the most likely source of sulfur. Calculated sulfate concentrations at 50 °C are around 0.005 mol/kg. Crush-leach analysis of

fluid inclusions from several ore deposits shows that total sulfur concentrations are around 500-1000 ppm or 0.008-0.015 mol/kg. Because the hydrothermal fluid trapped in fluid inclusions is already a mix of the deep saline brine and the meteoric water, the total sulfur concentrations in the deep saline brine were most likely even higher. Therefore, it seems reasonable to assume that the ratio Rs is lower or equal to 0.5.

Mixing with sulfate derived from Triassic sediments having a $\delta^{34}S$ value of 21 ‰ would have the largest effect on the resulting (in this case apparent) calculated temperatures. Figure 25 shows mixing lines calculated for a saline brine with a $\delta^{34}S_{SULFATE}$ value of 13 ‰ with meteoric water with a $\delta^{34}S_{SULFATE}$ of 21 ‰ for a wide range of different sulfate concentration ratios Rs. We have already estimated that the fluid mixing ratios were in the range between 0.5 and 0.75 from the reconstructed paleo-geothermal conditions and fluid inclusion information. A shift of the $\delta^{34}S$ value of the $\delta^{34}S_{SULFATE}$ from 13 to 14.5 ‰ would result in a displacement of the calculated equilibrium temperatures by about 20°C. Any $\delta^{34}S_{SULFATE}$ of the mixed fluid, which is located inside the shaded area in Figure 25, will change the resulting equilibrium temperature by not more than 20°C. It can be seen from Figure 25 that a meteoric fluid at the assumed maximum sulfate concentration ratio Rs of 0.5 could change the equilibrium temperature of the deep saline brine at mixing fractions lower than 0.7 beyond this 20°C range. At sulfate ratios Rs lower than 0.25, the effect on the equilibrium temperatures will be below 20°C for all possible mixing fractions. If the isotopic composition of the sulfate in the meteoric water is lower than 21 ‰, even higher concentration ratios will not shift the resulting equilibrium temperatures considerably. These calculations support the idea that the observed consistent sulfate-sulfide temperatures of 300-350°C reflect equilibrium conditions established in the deep-sourced aquifer.
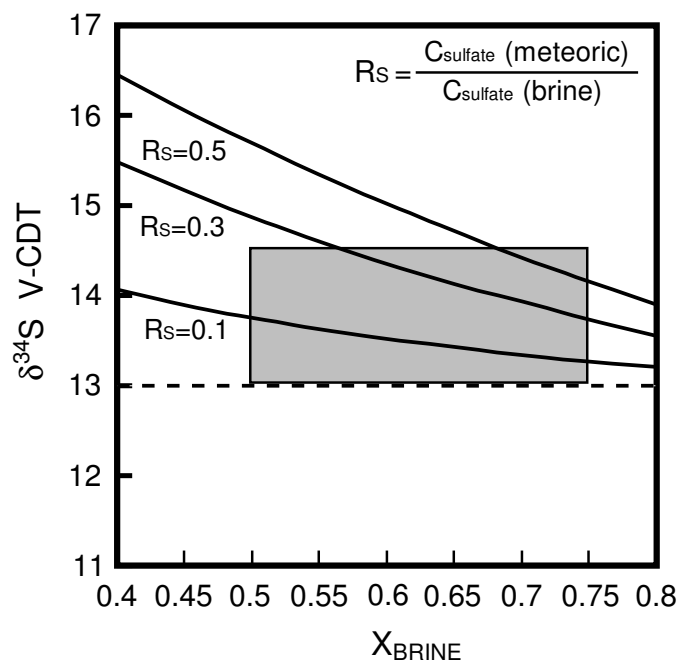
Figure 25. Calculated mixing lines between a sulfate-bearing deep saline brine with a $\delta^{34}S$ of 13 ‰ and a meteoric fluid having a $\delta^{34}S$ of 21 ‰ at different sulfate concentration ratios Rs. See text for explanations.

6.2.5. MODELING OF THE CARBON AND OXYGEN ISOTOPE COMPOSITION OF MIXED FLUIDS

The measured $\delta^{13}C$ and $\delta^{18}O$ values of the primary calcites show a significant covariation, which must reflect a systematic change in the carbon and oxygen isotope composition of the hydrothermal solutions and/or temperature during progressive precipitation. In order to constrain the nature of this isotopic evolution, we have quantitatively modeled the isotopic effects of mixing and cooling processes. Zheng and Hoefs (1993c) have derived a two-component model to describe the covariation of $\delta^{13}C$ and $\delta^{18}O$ values of hydrothermal calcites, which assumes mixing between a high-temperature and a low-temperature end-member fluid. Although this model has reasonably described the isotopic variation of carbonates in the Bad Grund Pb-Zn deposit (Harz Mountains, Germany), it has several limitations and simplifications, which preclude universal application to fluid mixing processes in hydrothermal systems. The model by Zheng and Hoefs (1993c) does not consider the effect of salinity on the oxygen concentration in the two fluids, which can be important for mixing between a saline brine and dilute meteoric water. The concentration of oxygen in concentrated brines with e.g. 20-40 wt.% equivalent NaCl will be much lower than in meteoric waters, and

this difference has to be accounted for in the isotopic mass balance equations. Calculations assuming solute concentrations of 10 mol/kg in the brine show that this effect is about 0.2-0.3 ‰ per 5 per mil difference in oxygen isotope composition of the two fluid end-members. For a difference of 20 ‰, the effect is already on the order of 1 ‰. Most importantly, the model by Zheng and Hoefs (1993c) assumes that the predominant aqueous carbon species in the high-temperature and low-temperature end-members are CO_2 (aq) and HCO_3^-. Mixing is then calculated as a purely physical process, ignoring the temperature and pH dependence of the CO_2-HCO_3^- equilibria.

To overcome these limitations, we have derived a modified and improved set of equations, which we have combined with calculations using a speciation and reaction path modeling code. The results of these calculations predict the aqueous carbon speciation more accurately and incorporate the effects of different starting pH values of both end-member fluids. The speciation calculations for several mixing scenarios were performed with the HCh software package (Shvarov and Bastrakov 1999), which models heterogeneous equilibria by minimization of the Gibbs free energy of the total system (Shvarov 1978). Thermodynamic data for aqueous species were taken from the SUPCRT92 database (Johnson *et al.* 1991; Shock *et al.* 1997; Sverjensky *et al.* 1997), while the thermodynamic data for solid phases came from Robie and Hemingway (1995), Holland and Powell (1998). In the following section, we will derive the set of equations used to calculate the effect of fluid mixing on the $\delta^{13}C$ and $\delta^{18}O$ values of hydrothermal carbonates.

For the mixing of two fluids having different isotope compositions, the isotopic mass balance for carbon isotopes is given by (Criss 1999):

(1) $\qquad \delta^{13}C_M = X_A\, \delta^{13}C_A + X_B\, \delta^{13}C_B$

where $\delta^{13}C_A$, $\delta^{13}C_B$ and $\delta^{13}C_M$ are the carbon isotope compositions of fluids A, B and the mixture. X_A and X_B are the mole fractions of carbon contributed from fluids A and B in the mixture. If the carbon concentrations in both fluids were identical, the mole fractions of carbon would be equal to the mole fractions of the two fluids in the mixture, f_A and f_B, where $f_B = 1 - f_A$. Now we introduce the concentration dependence in terms of molalities, and the mixing equation for carbon isotopes then becomes

(2) $\quad \delta^{13}C_M = \dfrac{m_A f_A}{m_A f_A + m_B(1-f_A)}\delta^{13}C_A + \dfrac{m_B(1-f_A)}{m_A f_A + m_B(1-f_A)}\delta^{13}C_B$

where m_A and m_B are the molalities (mol/kg) of carbon in fluids A and B, respectively. However, if the salinities of both fluids are quite different, such as for mixing between a deep-sourced saline brine and dilute meteoric water, this simplified version of the mixing equation does not hold true and has to be corrected for total solute concentrations. To accomplish this, a conversion is introduced, which relates the molalities to the total number of moles of solvent+solutes in the end-member fluids

(3) $\quad m_A^* = \dfrac{m_A}{n_w + \Sigma m_{i,A}}$

where n_w is the total number of moles H_2O in 1 kg of water, and $\Sigma m_{i,A}$ is the sum of the molalities of all solutes in fluid A. Applying these conversion factors, the mixing equation for carbon is then re-written as follows

(4) $\quad \delta^{13}C_M = \dfrac{m_A^* f_A}{m_A^* f_A + m_B^*(1-f_A)}\delta^{13}C_A + \dfrac{m_B^*(1-f_A)}{m_A^* f_A + m_B^*(1-f_A)}\delta^{13}C_B$

A similar equation can be derived for oxygen isotopes, which takes into account the oxygen concentrations (corrected for total solutes) in both end-member fluids. With these equations, $\delta^{13}C$ and $\delta^{18}O$ values of the mixed fluid can be modeled. For calculating the isotopic composition of hydrothermal calcites, H_2O is the principal reservoir of oxygen, with $\delta^{18}O_{H2O} = \delta^{18}O_M$. Consequently, only the fractionation factor between calcite (and any other carbonate mineral) and liquid H_2O at the temperature of mixing has to be applied (Ohmoto and Goldhaber 1997).

To calculate the carbon isotope composition of calcite, the species distribution for dissolved inorganic carbon has to be considered. For geologically reasonable pH and redox conditions, CO_2 (aq) and HCO_3^- are the predominant species, whereas the concentrations of CO_3^{2-} and CH_4 (aq) are several orders of magnitude smaller. Consequently, the contribution of these species to the carbon isotope mass balance can be neglected for most cases. However, CO_3^{2-} becomes important in very alkaline solutions, so the model we present will account for all four principal species. The isotopic mass balance for the distribution of carbon isotopes between the aqueous species is given by the equation

(5) $\delta^{13}C_{\Sigma C} = X_{CO2}\,\delta^{13}C_{CO2} + X_{HCO3}\,\delta^{13}C_{HCO3} + X_{CO3}\,\delta^{13}C_{CO3} + X_{CH4}\,\delta^{13}C_{CH4}$

where, X_{CO2}, X_{HCO3}, X_{CO3} and X_{CH4} are the mole fractions of CO_2 (aq), HCO_3^-, CO_3^{2-} and CH_4 (aq) in the mixed fluid, which are defined in terms of molalities. For this system, the mass balance equation for carbon takes the form $m_{\Sigma C} = m_{CO2} + m_{HCO3} + m_{CO3} + m_{CH4}$. The expressions for the isotopic fractionation factors between HCO_3^-, CO_3^{2-} and CH_4 (aq) and CO_2 (aq) are substituted into equation (5), which is then rearranged and solved for the carbon isotope composition of CO_2 (aq)

(6) $\delta^{13}C_{CO2} = \dfrac{\delta^{13}C_{\Sigma C} - 1000\,X_{HCO3}(\alpha_{HCO3-CO2}-1) - 1000\,X_{CO3}(\alpha_{CO3-CO2}-1) - 1000\,X_{CH4}(\alpha_{CH4-CO2}-1)}{X_{CO2} + X_{HCO3}\alpha_{HCO3-CO2} + X_{CO3}\alpha_{CO3-CO2} + X_{CH4}\alpha_{CH4-CO2}}$

For equilibrium conditions, the isotopic composition of calcite (or any other carbonate mineral) can then be calculated from the composition of CO_2 (aq) using the equilibrium fractionation factor (Ohmoto and Goldhaber 1997).

We have performed a number of model calculations applying the above equations, using the carbon isotope fractionation factors $\alpha_{HCO3\text{-}CO2}$ and $\alpha_{CAL\text{-}CO2}$ from Ohmoto and Goldhaber (1997) and the oxygen isotope fractionation factor $\alpha_{CAL\text{-}H2O}$ from Clayton and Kieffer (1991). Concentrations of total carbon in the two end-member fluids have been estimated by solubility calculations. The meteoric water has been saturated with calcite at a temperature of 50 °C and the system was considered to be open to the atmosphere, i.e. CO_2 and O_2 fugacities were set to atmospheric values. These calculations result in a carbon concentration of 0.00068 mol/kg in the meteoric fluid at 50°C (Table 14). Estimations of the total carbon concentrations of the deep saline brine are more difficult. Saturation of the brine with calcite leads to rather high total carbon concentrations, which most likely do not reflect the conditions in the deep aquifer. We assumed that the pH of the hydrothermal fluid in the aquifer is primarily controlled by water-rock reactions with the crystalline host rocks and not by calcite saturation. Carbon-dissolving reactions in the aquifer, such as dissolution of carbonates and oxidation of graphite, would then not significantly modify the fluid pH. For reference, we have calculated the pH value of the saline fluid in equilibrium with a granitic assemblage, i.e., muscovite-quartz-albite-microcline, at 300-350°C and a pressure of 1 kbar. For further calculations, we constructed a series of model fluids by adding different CO_2

concentrations and adjusting the pH back to the granite-buffered value. The most likely model setup, where calcite would be allowed to dissolve without changing the pH significantly, results in a total carbon concentration of 0.005 mol/kg (Table 14). Our model calculations show that CO_2 (aq) and HCO_3^- are by far the dominant carbon species to be considered.

Table 14. Chemical and isotopic composition of model fluids used in mixing calculations.

Parameter	Model A, meteoric	Model A, brine	Model B, meteoric	Model B, brine	Model C, meteoric	Model C, brine
T (°C)	50	350	50	350	50	350
P (bar)	Sat.	1000	Sat.	1000	Sat.	1000
pH	8.3	4.9	8.3	4.9	8.3	4.9
H_2O (kg)	1.0	1.0	1.0	1.0	1.0	1.0
CO_2 (mol)	0.00068	0.005	0.00068	0.05	0.00068	0.5
NaCl (mol)	0	7.6	0	7.6	0	7.6
KCl (mol)	0	0.62	0	0.62	0	0.62
$CaCl_2$ (mol)	0	1.7	0	1.7	0	1.7
HCl (mol)	0	0.000095	0	0	0	0
NaOH (mol)	0	0	0	0.00012	0	0.0023
$Ca(OH)_2$ (mol)	0.00015	0	0.00015	0	0.00015	0
$\delta^{13}C$ (V-PDB)	0.0	–17.0	4.0	–16.0	4.0	–16.0
$\delta^{18}O$ (V-SMOW)	–3.5	3.5	–5.0	4.0	–6.0	4.0

Using the reconstructed model fluids, we have calculated different fluid mixing scenarios. Figure 26 shows the relative species distribution of CO_2 (aq) and HCO_3^- during progressive mixing of the two fluids. Rc is the concentration ratio of total dissolved carbon in both fluids, $Rc = m_{BRINE} / m_{METEORIC}$. This ratio has been estimated at around 7 for the most likely case of calcite dissolution without saturation. For comparison, both ten times higher and lower concentrations of total dissolved carbon in the brine were considered, resulting in Rc values of 70 and 0.7.
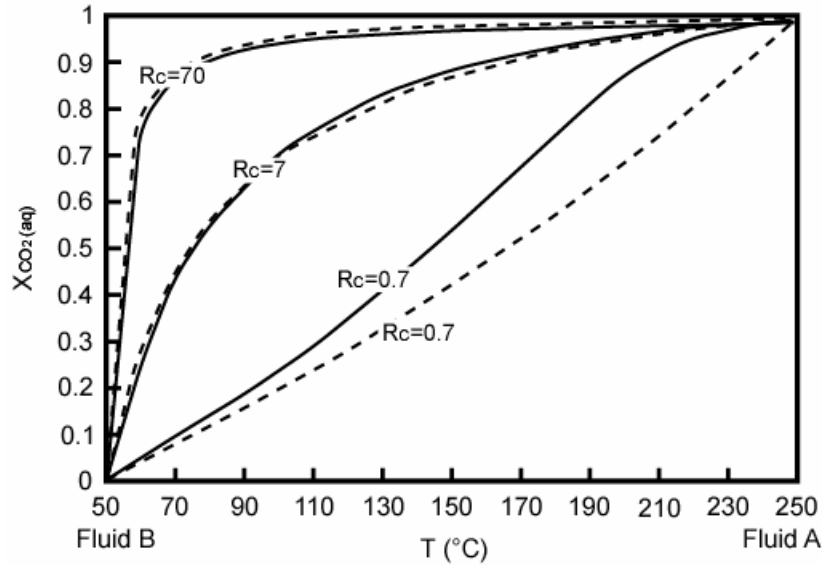
Figure 26. Speciation of carbon given as fraction of CO_2 (aq) resulting from mixing of the two model fluid end-members at different total carbon concentration ratios Rc. The calculated carbon speciation (solid lines) is compared with the purely physical mixing model (dashed lines).

It can be seen from Figure 26 that the calculated speciation (solid lines) differs significantly from the ideal (physical) mixing model (dashed lines) if the concentrations of total dissolved carbon in the high-temperature brine are equal or lower than in the low-temperature meteoric water. The ideal speciation model is reasonably consistent with the calculated speciation lines only for high values of Rc. Figure 27 shows the isotopic composition of calcite, precipitated from the mixing of two hypothetical fluid end-members. It was assumed that the deep saline brine has a $\delta^{13}C$ of -16 ‰ and a $\delta^{18}O$ of 5 ‰, whereas the meteoric water has a $\delta^{13}C$ of -2 ‰ and a $\delta^{18}O$ of -5 ‰. It is clear that the concentration ratio Rc has a significant effect on the curvature of the mixing line. Consequently, the measured covariation of the $\delta^{13}C$ and $\delta^{18}O$ values in the calcites contains intrinsic information, which can be used to constrain the carbon concentrations in the end-member fluids.

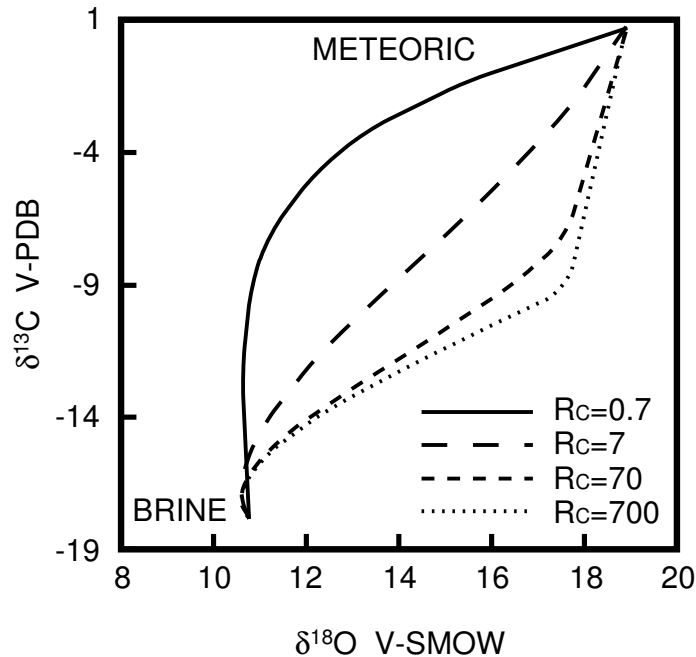**Figure 27.** Isotopic compositions of calcite precipitated via mixing of two model fluids having $\delta^{13}C = -16\ \text{‰}$, $\delta^{18}O = 5\ \text{‰}$ (deep saline brine) and $\delta^{13}C = -2\ \text{‰}$, $\delta^{18}O = -5\ \text{‰}$ (calcite-saturated meteoric fluid).

6.2.6. CARBON AND OXYGEN ISOTOPE VARIATION IN HYDROTHERMAL CALCITES

To model the isotopic data of primary calcites from the Schwarzwald district, reasonable estimations of the isotopic compositions of the two fluid end-members have to be made. The selected values should reflect the isotopic compositions of the most likely sources for both fluids, as constrained by the available geological and isotopic information. The meteoric water was probably in contact with the marine limestones of the Mesozoic sedimentary units covering the crystalline basement. Surface waters from limestone aquifers show typical $\delta^{13}C$ values of -8 to 4 ‰ (Ohmoto 1986). The $\delta^{13}C$ values of granites in the Schwarzwald vary between -10 and -26 ‰ (Hoefs 1973). Sedimentary protoliths of the gneisses will probably contained carbon originating from organic matter, which usually has $\delta^{13}C$ values of around -25 ‰ (Ohmoto and Goldhaber 1997). Volatilization during metamorphism leads to a slight enrichment in ^{13}C compared to the sedimentary protoliths (Ohmoto 1986). Therefore, an isotopically light composition of the carbon in the deep saline brine of around -15 ‰ or even lower can be assumed.

The $\delta^{18}O$ values of the surface-derived meteoric waters can vary along the meteoric water line from 0 ‰ to negative values. Considering the paleogeography of the Schwarzwald area and modern oxygen isotopic trends in meteoric precipitation (e.g., Bowen and Wilkinson 2002), the original $\delta^{18}O$ values of the meteoric fluid end-member are estimated to have been in the range between -5 to 0 ‰. The deep saline brine is most likely of meteoric origin (Behr and Gerler 1987; von Gehlen 1987; Hofmann 1989; German *et al*. 1994; Werner *et al*. 2000; 2002), but was extensively modified through water-rock reactions in the crystalline basement. During high-temperature water-rock interaction with crystalline rocks, the $\delta^{18}O$ of water is generally shifted towards higher values (Taylor 1997). We have applied both closed- and open-system scenarios (Taylor 1977; 1997) to model the isotopic exchange between water of metoric origin (with $\delta^{18}O$ between -5 and 0 ‰) and typical granites of the Schwarzwald area having average primary $\delta^{18}O$ values of +10 ‰ (Hoefs and Emmermann 1983; Simon and Hoefs 1987). The resulting $\delta^{18}O$ values of the deep saline brine are in the range between -1.2 and +5.3 ‰ for geologically reasonable water/rock ratios between 0.01 and 1.0 and an exchange temperature of 300 °C.

Using the estimated temperatures of both end-member fluids, the modeled carbon speciation during mixing (Table 15), the concentrations of total dissolved carbon in both fluids and the likely isotopic compositions of the two fluids, the compositional range of the hydrothermal calcites can be reproduced with our mixing model (Fig. 28).
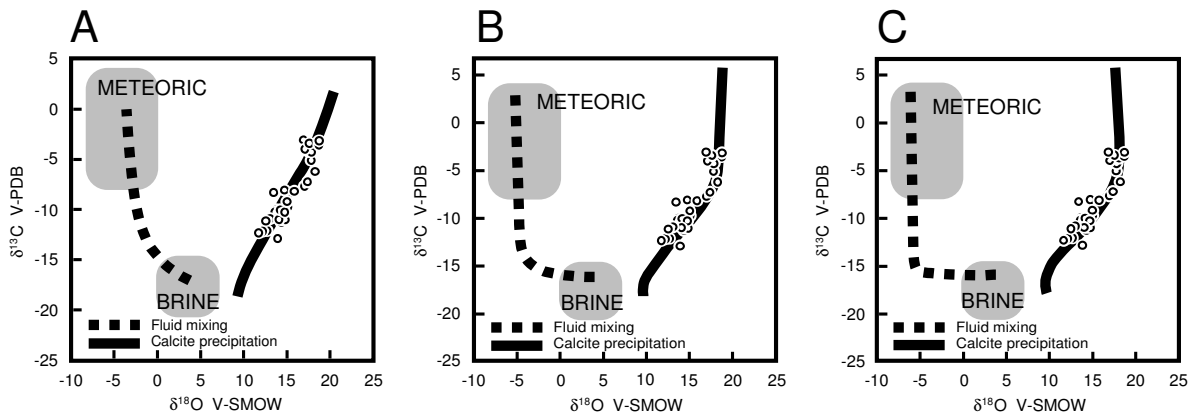

Figure 28. Plot of the $\delta^{13}C$–$\delta^{18}O$ covariation of primary hydrothermal calcites from the Schwarzwald district compared to the results of the fluid mixing calculations. The shaded areas A and B indicate the likely range of isotopic compositions of the two fluids, constrained by the isotopic data of geologically reasonable fluid sources in the literature. The dashed lines show the mixing trends for the fluids, whereas the solid lines indicate the isotopic compositions of the corresponding calcites, precipitated from the mixed fluid. **A**: Rc = 7, **B**: Rc = 70, **C**: Rc = 700.

The shaded areas A and B in Figure 28 show the likely range of the isotopic compositions of the two fluids A (deep saline brine) and B (meteoric water). The mixing lines are given as dashed lines; the isotopic compositions of the two end-member fluids used are within the geologically reasonable ranges. Figure 28A was calculated for a total carbon concentration in the deep saline brine of 0.005 mol/kg, i.e. a ratio Rc of 7. Because a saline brine at the given temperature could possibly have even higher carbon concentrations, if calcite would be a solubility-controlling phase in the aquifer, mixing lines were also calculated using ratios of Rc of 70 (Fig. 28B) and 700 (Fig. 28C). Figure 28 shows that the trend of primary calcites can be explained well by the mixing of two fluids.

The compositional range of secondary or remobilized calcites can be explained by low-temperature reaction and isotopic exchange with meteoric waters. Remobilization of calcite having a $\delta^{13}C$ of about -2 ‰ through interaction with a bicarbonate-dominated meteoric water at temperatures around 50 °C will shift the $\delta^{13}C$ value of precipitating secondary calcites to – 0.3 ‰.

Table 15. Main results of the mixing calculations using model fluid compositions A, B and C (see Table 14 for composition). Concentrations of principal aqueous carbon species are given in molalities.

T (°C)	Model A			Model B			Model C		
	pH	HCO_3^-	CO_2 (aq)	pH	HCO_3^-	CO_2 (aq)	pH	HCO_3^-	CO_2 (aq)
250	4.6	0.0001	0.0049	4.4	0.0004	0.0495	4.2	0.0030	0.4976
240	4.6	0.0001	0.0047	4.3	0.0004	0.0471	4.2	0.0029	0.4727
230	4.6	0.0001	0.0045	4.3	0.0005	0.0446	4.1	0.0028	0.4478
220	4.6	0.0001	0.0042	4.3	0.0005	0.0421	4.0	0.0028	0.4229
210	4.7	0.0002	0.0040	4.2	0.0005	0.0396	4.0	0.0027	0.3980
200	4.7	0.0002	0.0038	4.2	0.0005	0.0371	3.9	0.0026	0.3731
190	4.7	0.0002	0.0035	4.2	0.0005	0.0347	3.9	0.0025	0.3482
180	4.8	0.0002	0.0033	4.2	0.0005	0.0322	3.8	0.0024	0.3233
170	4.8	0.0003	0.0030	4.1	0.0005	0.0297	3.8	0.0023	0.2984
160	4.9	0.0003	0.0028	4.1	0.0006	0.0272	3.7	0.0022	0.2735
150	4.9	0.0003	0.0025	4.2	0.0006	0.0248	3.7	0.0021	0.2486
140	5.0	0.0004	0.0023	4.2	0.0006	0.0223	3.7	0.0020	0.2237
130	5.0	0.0004	0.0020	4.2	0.0006	0.0198	3.7	0.0019	0.1988
120	5.1	0.0004	0.0018	4.2	0.0006	0.0173	3.7	0.0017	0.1739
110	5.2	0.0005	0.0015	4.3	0.0006	0.0148	3.7	0.0016	0.1491
100	5.3	0.0005	0.0013	4.4	0.0006	0.0124	3.8	0.0015	0.1242
90	5.4	0.0006	0.0010	4.5	0.0007	0.0099	3.8	0.0013	0.0993
80	5.6	0.0006	0.0007	4.7	0.0007	0.0074	3.9	0.0012	0.0745
70	5.8	0.0006	0.0005	4.9	0.0007	0.0049	4.1	0.0010	0.0496
60	6.2	0.0007	0.0002	5.2	0.0007	0.0025	4.3	0.0009	0.0248
50	8.1	0.0007	0.0000	8.1	0.0007	0.0000	8.1	0.0007	0.0000

Assuming an $\delta^{18}O$ value of roughly 0 ‰ for meteoric water, the remobilization will result in $\delta^{18}O$ values of the secondary calcites of around 24 ‰. The remobilization trend indicated in Figure 29 shows that the direction of this shift is quite distinct from the primary calcite trend. Individual measurements of different calcite generations from the Friedrich-Christian and Wenzel deposits substantiate the remobilization model (Fig. 29). The low-temperature remobilization proves that the isotopic compositions of all secondary calcites are shifted towards higher $\delta^{13}C$ and $\delta^{18}O$ values, in contrast to the primary hydrothermal calcites.
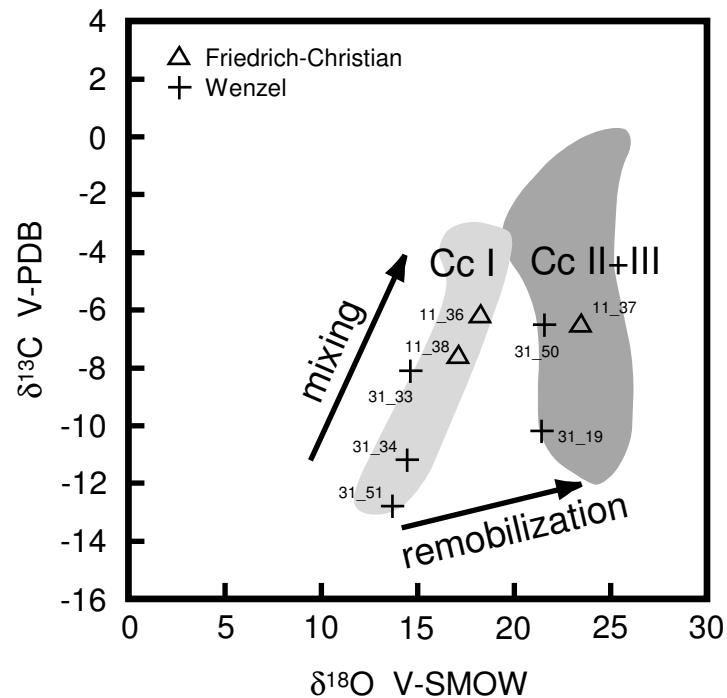
Figure 29. Binary diagram of the $\delta^{13}C$ and $\delta^{18}O$ values of primary and remobilized hydrothermal calcites, showing the principal mixing and remobilization trends.

6.2.7. THE POST-VARISCAN FLUID SYSTEM

Isotopic characteristics of this study are in good agreement with the post-Variscan fluid system in the Schwarzwald area, which have been reported from other hydrorthermal fluids originating in crystalline basement rocks. Fluids sampled during pumping tests of the KTB (Continental Deep Borehole-in Bavarian Oberpfalz) pilot hole have δD and $\delta^{18}O$ values in the range between –32 to –27 ‰ and between –5.8 to –5.7 ‰, respectively (Lodemann *et al.* 1997). Simon and Hoefs (1991) postulated a direct relationship between the fluids responsible

for vein mineralization visible throughout the KTB drillcore profile and the fluids encountered at 4000m by KTB. Based on a comprehensive fluid inclusion study, Behr *et al.* (1993a, 1994) concluded that fluids with Ca-Na-Cl characteristics are compositionally very similar to the present fracture fluids, indicating a common primary fluid source. Below about 6000 m, Ca-Na-Cl fluid inclusions with homogenization temperatures up to 250 °C dominate and represent a young fluid system, probably of late Cretaceous age (Behr *et al.* 1994). This fluid system and the associated fracture mineralization are clearly related to extensional fault tectonics and are also recorded in post-Variscan hydrothermal mineralizations in different areas of Germany. Highly saline brines (Ca-Na-Cl) are typically found at depths of some kilometers in the continental crystalline basement of the Canadian (Fritz and Frape 1982; Frape and Fritz 1987), Fennoscandian (Nurmi *et al.* 1988) and Ukrainian shields (Vovk and Vysotskii 1982) and elsewhere in the world (Kloppmann *et al.* 2002). In the Schwarzwald area, which is part of the central European continental crust, TDS (total dissolved solids) concentrations of typical Na-Cl-type groundwater are more than 5 g/kg at 2-3 km below the surface. The observed pH ranges from 6 to 8 (Stober 2004). Stober (1999) concluded that the deep waters in the crystalline basement of the Schwarzwald area with a mean Cl/Br ratio of 295 must have been of predominantly marine origin.

Our extensive fluid inclusion study of hydrothermal veins demonstrates that post-Variscan fluids originate from deep highly saline $NaCl-CaCl_2-H_2O$ brines that mixed with low salinity meteoric water (Fig. 11). The temperature of the $NaCl-CaCl_2$ fluid prior to mixing cannot be directly determined by means of fluid inclusions. Based on isotope temperature calculations from sulfide-sulfate equilibria and paleogeothermal considerations, the aquifer paleotemperatures of the deep saline brine are estimated at 300-350°C (Schwinn *et al.* in press). The $NaCl-CaCl_2-H_2O$ brines responsible for hydrothermal vein formation in the Schwarzwald area compare well with post-Variscan fluids found in other ore districts in Germany such as the Harz and Rheinish Massif and widespread Pb-Zn mineralization in Belgium, Ireland and south England (Behr *et al.* 1984; Behr and Gerler 1987; Wilkinson 1995; Reilly 1997; Muchez *et al.* 1994b, 1998). A number of studies have identified cases where the δD values of basinal brines are lower than those of meteoric water (Fallick *et al.* 1993; Munoz 1994; Wilkinson *et al.* 1995) and this is frequently explained by derivation of the hydrogen from alteration of organic matter (Sheppard 1986). There is, however, accumulating evidence that structurally bound water in quartz might have hydrogen isotopic signatures systematically shifted towards negative values compared to the original fluid inclusion water (Ishiyama *et al.* 1999; Simon 2001; Faure 2003; this study). If contributions

of such structurally bound water to the bulk isotopic signature are significant, this might equally well explain anomalously low δD values of post-Variscan hydrothermal systems.

7. CONCLUSIONS

By combining stable isotope and fluid inclusion techniques, it has been possible to decipher the complexities of prolonged hydrothermal activity in the Schwarzwald ore district, SW Germany. Two distinct fluid types, distinguished on the basis of vein chronology, fluid inclusion and stable isotope characteristics, have been identified.

- Fluid inclusion and stable isotope data support a metamorphic origin for the high-temperature (approximately 250-400°C), low to moderate salinity (<15 wt.% eqv. NaCl) Variscan to late-Variscan H_2O-NaCl-(KCl) fluid type. This fluid is closely associated with gas-rich fluid inclusions, characterized by predominance of CO_2-CH_4. It is found in Sb (±Au and Ag) –bearing quartz veins.

- In contrast to that, the second fluid belongs to the NaCl-$CaCl_2$-H_2O type, is generally of higher salinity (20-25 wt.% eqv. NaCl) and lower temperature (100-160°C). Late-stage mineral generations in the post-Variscan veins host secondary fluid inclusions of lower salinity, but with similar homogenization temperatures. Both the fluid inclusion and oxygen and hydrogen isotope systematics suggest that the post-Variscan fluid originated from large-scaling mixing of a deep-sourced saline brine with surface-derived meteoric water. It led to the formation of Pb±Zn±Cu-barite-fluorite veins.

An overprint by a second fluid event is indicated according to different textural features and fluid inclusions. Comparing the fluid inclusion and isotopic characteristics of the post-Variscan fluids, this overprinting event can be clearly related to the post-Variscan hydrothermal regime. This demonstrates the importante of combining detailed deposit-scale studies (involving a small-scale resolution of individual vein generations) with a district-scale characterization of fluid types for understanding the complex history of hydrothermal processes.

Consistent sulfide-sulfate equilibrium temperatures of about 300°C from several locations within the entire Schwarzwald district demonstrate the existence of a large homogeneous fluid reservoir at a depth of around 7-10 km. Integration of several datasets including fluid inclusion salinities, deposit formation temperatures and calculated aquifer temperatures is used to derive a model of district-scale fluid mixing between a deep saline brine and surface-

derived meteoric waters. Calculations indicate that mass fractions of the high-salinity end-member were on the order of 0.5 to 0.75.

The isotopic compositions of hydrothermal calcites precipitated via mixing of the two fluids have been modeled by a combination of isotopic mass balance equations and speciation calculations. Geologically reasonable estimates for the isotopic compositions of the two fluid end-members have been integrated into the model, permitting reconstruction of paleo-mixing-lines that reproduce the measured covariation of δ^{13}C and δ^{18}O of the calcites. This confirms that mixing of homogeneous deep saline brines with surface-derived meteoric water was a large-scale process responsible for the formation of most hydrothermal ore deposits in the Schwarzwald district. Many similar geochemical characteristics, such as salinities and compositions of fluids, homogenization temperatures of fluid inclusions, stable isotope compositions of oxygen, sulfur, and carbon, REE pattern of fluorites (Schwinn and Markl 2005) of the hydrothermal deposits over a large area are attributed to this large-scale convection system.

Most likely, this hydrothermal system has been active since the Mesozoic. A major Jurassic alteration event, which affected the crystalline basement and the Triassic sedimentary cover (Zuther and Brockamp 1988; Lippolt and Kirsch 1994; Meyer *et al*. 2000), demonstrates the influx of a meteoric fluid, possibly seawater, into the crust. This seawater was modified by water-rock interaction and stored as deep groundwater in the crystalline basement, where recent thermal waters show a fossil seawater component (Stober and Bucher 1998; He *et al*. 1999). During times of increased tectonic activity, pathways allowed the ascent of this brine to the subsurface. Mixing with meteoric waters (e.g. Werner *et al*. 2002) leads to the formation of the post-Variscan fluorite-barite-quartz veins of the Schwarzwald district.

By integrating all data from this study with additional isotopic datasets from previous work, a consistent model for post-Variscan hydrothermal mineralization can be developed. This model envisages upward circulation of 300-350 ° C hot saline brine (NaCl-CaCl$_2$-H$_2$O) through strike-slip fault systems. During periods of increased tectonic activity, efficient mixing of this brine with low-temperature surface-derived meteoric water was facilitated. This mixing process resulted in precipitation of the major fluorite-barite-quartz generation of the post-Variscan veins. This fluid system was active over an area of 120 by 40 km and over at least 100 Ma.

REFERENCES

Aines RD, Rossman GR. (1984) Water in minerals? A peak in the infrared. Journal of Geophysical research, **89**, 4059-4071.

Anderson GM. (1975) Precipitation of Mississippi Valley-type ores. *Econ. Geol*. **70**, 937-942.

Barker AJ, Bennett DG, Boyce AJ, Fallick AE. (2000) Retrogression by deep infiltration of meteoric fluids into thrust zones during late-orogenic rapid unroofing. *Journal of Metamorphic Petrology*, **18**, 307-318.

Barret TJ, Anderson GM. (1982) The solubility of sphalerite and galena in NaCl brines. *Econ. Geol*. **77**, 1923-1933.

Behr HJ, Gerler J. (1987) Inclusions of sedimentary brines in post-Variscan mineralizations in the Federal Republic of Germany: A study by Neutron Activation Analysis. *Chemical Geology*. **61**, 65-77.

Behr HJ, Gerler J, Hein UF, Reutel CJ. (1993a) Tectonic Brines und Basement Brines in den mitteleuropäischen Varisziden: Herkunft, metallogenetische Bedeutung und geologische Aktivität. *Göttinger Arb. Geol. Paläont*. **58**, 3-28.

Behr HJ, Horn EE, Frenzel-Beyme K, Reutel C. (1987) Fluid inclusion characteristics of the Variscan and post-Variscan mineralizing fluids in the Federal Republic of Germany. *Chemical Geology*, **61**, 273-285.

Behr HJ, Horn EE, van den Kerkhof AM, Reutel C, Topp J. (1993b) Geoscientific Investigations - Crustal fluids of the continental deep drilling project (KTB) at 0-7000 m. *KTB Report*, **93-2**, 451-454.

Behr HJ, Reutel C, Horn EE, van den Kerkhof AM. (1994) The fluid research program of the Continental Deep Drilling Project KTB (Germany): II. Ca-Na-Cl basement brines as tracers of fluid activity and mineralization in an orogenic collapse system. *In: PACROFI V, Cuernavaca*, 8.

Bethke CM. (1996) *Geochemical reaction modelling*. Oxford University Press, New York.

Blakeman RJ, Ashton JH, Boyce AJ, Fallick AE, Russell MJ. (2002) Timing of interplay between hydrothermal and surface fluids in the Navan Zn-Pb orebody, Ireland: Evidence from metal distribution trends, mineral textures, and δ^{34}S analyses. *Econ. Geol*. **97**, 73-91.

Bliedtner M, Martin M. (1988) Erz- und Minerallagerstätten des Mittleren Schwarzwaldes. *Geologisches Landesamt Baden-Wuerttemberg*, Freiburg i.Br.

Bodnar RJ, Vityk MO. (1994) Interpretation of microthermometric data for H_2O-NaCl fluid inclusions. *in* Fluid Inclusions in Minerals, Methods and Applications, B. De Vivo and M. L. Frezzotti, eds., *pub. by Virginia Tech, Blacksburg, VA*, 117-130.

Boiron MC, Cathelineau M, Banks DA, Fourcade S, Vallance J. (2003) Mixing of metamorphic and surficial fluids during the uplift of the Hercynian upper crust: consequences for gold deposition. *Chemical Geology*, **194**, 119-141.

Borisenko AS. (1977) Study of the salt composition of solutions in gas-liquid inclusions in minerals by the cryometric method. *Soviet Geoogy and Geophysics,* **18**. 11-19.

Bowen GJ, Wilkinson B. (2002) Spatial distribution of δ^{18}O in meteoric precipitation. *Geology,* **30**, 315-318.

Brockamp O, Clauer N, Zuther M. (2003) Authigenic sericite record of a fossil geothermal system: the Offenburg trough, central Black Forest, Germany. *Int J Earth Sci (Geol Rundsch)*, **92**, 843-851.

Brown EB, Lamb WM. (1989) *P-V-T* properties of fluids in the system H_2O-CO_2-NaCl: new graphical presentations and implications for fluid inclusion studies. *Geochimica et Cosmochimica Acta*, **53**, 1209-1221.

Brown PE, Hagemann SG. (1995) Fluid inclusion data reduction and interpretation using MacFlinCor on the Macintosh. XIII ECROFI Symposium, Barcelona, *Boletin de la Sociedad Espaola de Mineralogia*, **18-1**, 32-33.

Brown PE, Hagemann SG. (1995) MacFlinCor and its application to fluids in Archean lode-gold deposits. *Geochimica Cosmochimica Acta,* **59**, 3943-3952.

Bucher K, Stober I. (2000) The composition of groundwater in the continental crystalline crust. *Hydrogeology of Crystalline rocks*. 141-175.

Burke EAJ. (2000) Raman microspectrometry of fluid inclusions. *Lithos*, **55**, 139-158.

Canals A, Cardellach E. (1993) Strontium and sulfur isotope geochemistry of low-temperature barite-fluorite veins of the Catalonian Coastal Ranges (NE Spain): a fluid mixing model and age constraints. *Chemical Geology*, **104**, 269-280.

Charef A, Sheppard SMF. (1988) The Malines Cambrian carbonate-shale-hosted Pb-Zn deposit, France: thermometric and isotopic (H,O) evidence for pulsating hydrothermal mineralization. *Mineralium Deposita*, **23**, 86-95.

Clauer N, O'Neil JR, Furlan S. (1995) Clay minerals as record of temperature conditions and duration of thermal anomalies in the Paris basin, France. *Clays and Clay Minerals*, **30**, 1-13.

Clayton RN, Kieffer SW. (1991) Oxygen isotopic thermometer calibrations. In *Isotope Geochemistry: A Tribute to Samuel Epstein* (eds. H.P. Taylor, J.R. O'Neil, and I.R. Kaplan). Geochem. Soc. Spec. Publ. **3**, 3-10.

Craig H. (1961) Isotopic variations in meteoric waters. *Science*, **133,** 1702-1703.

Craig H. (1961) Standards for reporting concentrations of deuterium and oxygen 18 in natural waters. *Science*, **133**, 1833-1834.

Criss R.E. (1999) *Principles of stable isotope distribution*. Oxford University Press, New York-Oxford, 264.

Demeny A. (1995) H isotope fractionation due to hydrogen-zinc reactions and its implications on D/H analysis of water samples. *Chemical Geology*, **121**, 19-25.

Donald E. White. (1974) Diverse Origins of Hydrothermal Ore Fluids. *Economic Geology,* **69**, 954-973.

Douglas TA, Chamberlain CP, Poage MA, Abruzzese M, Shultz S. (2003) Fluid flow and the Heart Mountain fault: A stable isotopic, fluid inclusion, and geochronologic study. *Geofluids,* **3**, 13-32.

Echtler H, Chauvet A. (1992) Carboniferous convergence and subsequent crustal extension in the southern Schwarzwald (SW Germany). *Geodin Acta*, **5**, 37-49.

Fallick AE, Macaulay CI, Haszeldine RS. (1993) Implications of linearly correlated oxygen and hydrogen isotopic compositions for kaolinite and illite in the Magnus sandstone, North Sea. *Clays Clay Miner*. **41**, 184-190.

Faure K. (2003) δD values of fluid inclusion water in quartz and calcite ejecta from active geothermal system: Do values reflect those of original hydrothermal water? *Economic Geology*, **98**, 657-660.

Franzke HJ. (1992) Die strukturelle Enwicklung mineralisierter Störungszonen im Schwarzwald. *Technical report, GFZ-Postdam*, Germany.

Franzke HJ, Ahrendt H, Kurz S, Wemmer K. (1996) K-Ar Datierungen von Illiten aus Kataklasiten der Floßbergstörung im südöstlichen Thüringer Wald und ihre geologische Interpretation. *Zeitschrift für geologische Wissenschaften*, **24**, 441-456.

Frape SK, Fritz P. (1987) Geochemical trends for groundwaters from the Canadian Shield. *In Saline Water and Gases in Crystalline rocks* (eds P. Fritz and S.K. Frape). *Geol. Assoc. Canad. Spec. Pap*. **33**, 19-38.

Friedman I. (1953) Deuterium content of natural water and other substances. *Geochimica et Cosmochimica Acta*, **4**, 89-103.

Fritz P, Frape SK. (1982) Saline groundwaters in the Canadian Shield. A first overview. *Chem. Geol*. **36**, 179-190.

German A, Lang R, Werner W, Friedrich G. (1994) Zur Mineralogie und Geochemie der Erzgänge im Bergbaurevier Freiamt- Sexau, Mittlerer Schwarzwald. In: D.H. Storch and W. Werner (Editors), Die Erz- und Mineralgänge im alten Bergbaurevier "Freiamt- Sexau", Mittlerer Schwarzwald. *Abhandlungen des Geologischen Landesamtes Baden-Württemberg,* **14**, 119-155.

Germann K, Lüders V, Banks DA, Simon K, Hoefs J. (2003) Late Hercynian polymetallic vein-type base-metal mineralization in the Iberian Pyrite Belt: fluid-inclusion and stable isotope geochemistry (S-O-H-Cl). *Mineralium Deposita*, **38**, 953-967.

Geyer OF, Gwinner MP. (1986) Geologie von Baden-Württemberg. *Stuttgart.*

Giesemann A, Jäger H, Norman A, Brand W. (1994) On-line sulfur isotope determination using an element analyzer coupled to mass spectrometer. *Anal. Chem.* **66**, 2816-2819.

Gleeson SA, Yardley BWD, Boyce AJ, Fallick AE, Munz IA. (2000) From basin to the basement: The movement of surface fluids into the crust. *J. Geochem. Explor.* **69-70**, 527-531.

Gleeson SA, Yardley BWD, Munz IA, Boyce AJ. (2003) Infiltration of basinal fluids into high-grade basement, South Norway: Sources and behaviour of waters and brines. *Geofluids,* **3**, 33-48.

Gleeson SA, Wilkinson JJ, Shaw HF, Herrington RJ. (2000) Post-magmatic hydrothermal circulation and the origin of base metal mineralization. *Journal of the Geological Society, London*, **157**, 589-600.

Gleeson SA, Wilkinson JJ, Boyce AJ, Stuart FM. (1999) On the occurrence and wider implications of anomalously low δD fluids in quartz veins, South Cornwall, England. *Chemical Geology*, **160**, 161-173.

Grant K, Gleeson SA, Roberts S. (2003) The high-temperature behavior of defect hydrogen species in quartz: Implications for hydrogen isotope studies. *American Mineralogist*, **88**, 262-270.

Halliday AN, Mitchell JG. (1984). K-Ar ages of clay-size concentrates from the mineralisation of the Pedroches Batholith, Spain, and evidence for Mesozoic hydrothermal activity associated with the break up of Pangaea. *Earth and Planetary Science Letters,* **68,** 229-239.

Haynes FM, Kesler SE. (1987) Chemical evolution of brines during Mississippi Valley-type mineralization: Evidence from East Tennessee and Pine Point. *Econ. Geol.* **82**, 53-71.

He K, Stober I, and Bucher K. (1999) Chemical evolution of thermal waters from limestone aquifers of the Southern Upper Rhine Valley. *Appl. Geochem.* **14**, 223-235.

Hein UF. (1993) Synmetamorphic Variscan siderite mineralization of the Rhenish Massif, Central Europe. *Mineralogical Magazine*, **57**, 451-467.

Heinrich CA, Andrew AS, Knill MD. (2000) Regional metamorphism and ore formation: Evidence from stable isotopes and other fluid tracers. *Rev. Econ. Geol.* **11**, 97-117.

Hoefs J, Emmermann R. (1983) The Oxygen Isotope Compostion of Hercynian Granites and Pre- Hercynian Gneisses from the Schwarzwald, SW Germany. *Contributions to Mineralogy and Petrology*, **83**, 320-329.

Hoefs J. (1973) Ein Beitrag zur Isotopengeochemie des Kohlenstoffs in magmatischen Gesteinen. *Contrib. Mineral. Petrol.* **41**, 277-300.

Hoefs J. (1987) *Stable Isotope Geochemistry*. 3rd ed, Springer, Berlin Heidelberg New-York, 241.

Hofmann B. (1989) Genese, Alteration und rezentes Fliesssystem der Uran-Lagerstätte Krunkelbach, Menzenschwand, Südschwarzwald. *Technical Report 88-30, Mineralogisch-Petrographisches Institut, University of Bern, Switzerland.*

Hofmann B, Eikenberg J. (1991) The Krunkelbach Uranium Deposit, Schwarzwald, Germany. Correlation of Radiometric Ages, U-Pb, U-Xe-Kr, K-Ar, Th-U with Mineralogical Stages and Fluid Inclusions. *Economic Geology*, **86**, 1031-1049.

Holland TJB, Powell R. (1998) An internally consistent thermodynamic data set for phases of petrological interest. *J. Metamorph. Geol.* **16**, 309-343.

Horita J, Matsuo S. (1986) Extraction and isotopic analysis of fluid inclusions in halites. *Geochemical Journal*, **20**, 261-272.

Huck KH, Walther HW. (1984) Zur wirtschaftlichen Bedeutung der post-varistischen Mineralisation in Mitteleuropa. *Schriftenr GDMB*, **41**, 405-418.

Huston DL. (1999) Stable isotopes and their significance for understanding the genesis of volcanic-hosted massive sulfide deposits: A review. *Rev. Econ. Geol.* **8**, 157-179.

Ihinger PH, Zink SI. (2000) Determination of relative growth rates of natural quartz crystals. *Nature*, **404**, 865-869.

Ishiyama D, Shinoda K, Shimizu T, Matsubaya O, Aikawa N. (1999) Structural states and isotopic composition of water in hydrothermal quartz, Koryu deposit, Japan. *Economic Geology*, **94**, 1347-1352.

Jamtveit B, Hervig RL. (1994) Constraints on transport and kinetics in hydrothermal systems from zoned garnet crystals. *Science,* **263**, 505-508.

Jenkin GRT, Craw D, Fallick AE. (1994). Stable isotopic and fluid inclusion evidence for meteoric fluid penetration into an active mountain belt; Alpine Schist, New Zealand *J. metamorphic Geol.* **12,** 429-444.

Johnson JW, Oelkers EH, Helgeson HC. (1991) SUPCRT92, a software package for calculating the standard molal thermodynamic properties of minerals, gases, aqueous species, and reactions from 1 to 5000 bars and 0 to 1000 °C. *Comput. Geosci.* **18**, 899-947.

Jones HD, Kesler SE. (1992) Fluid inclusion gas chemistry in East Tennessee Mississippi Valley-type districts; evidence for immiscibility and implications for depositional mechanisms. *Geochim. Cosmochim. Acta,* **56**, 137-154.

Kalt A, Altherr R, Hanel M. (2000) The Variscan Basement of the Schwarzwald. *European Journal of Mineralogy, Beihefte*, **12**, 1-43.

Kishima N, Sakai H. (1980) Oxygen-18 and Deuterium Determination on a Single Water Sample of a few Milligrams. *Analytical Chemistry*, **52**, 356-358.

Kloppmann W, Girard JP, Negrel P. (2002) Exotic stable isotope compositions of saline waters and brines from the crystalline basement. *Chemical Geology*, **184**, 49-70.

Knauth LP, Eipstein S. (1975) Hydrogen and oxygen isotope ratios in silica from the Joides deep sea drilling project. *Earth and Planetary Science Letters*, **25**, 1-10.

Komninou A, Yardley BWD. (1997) Fuid-rock interaction in the Rhine Graben: A thermodynamic model of the hydrothermal alteration observed in deep drilling. *Geochim. Cosmochim. Acta* **61**, 515-531.

Lippolt HJ, Kirsch H. (1994) Isotopic Investigation of Post-Variscan Plagioclase Sericitization in the Schwarzwald Gneiss Massif. *Chemie der Erde*, **54**, 179-198.

Lippolt HJ, Werner O. (1994) Die Genetische Aussage von Blei- Isotopen- Verhältnissen in Bleiglanzen des Bergbaureviers Freiamt- Sexau, Mittlerer Schwarzwald. In: D.H. Storch and W. Werner (Editors), Die Erz- und Mineralgänge im alten Bergbaurevier "Freiamt- Sexau", Mittlerer Schwarzwald. *Abhandlungen des Geologischen Landesamtes Baden-Württemberg,* **14**, 191-205.

Lodemann M, Fritz P, Wolf M, Ivanovich M, Hansen BT, Nolte E. (1997) On the origin of saline fluids in the KTB (continental deep drilling project of Germany). *Applied Geochemistry*, **12**, 831-849.

Lüders V. (1994) Geochemische Untersuchungen an Gangartmineralen aus dem Bergbaurevier Freiamt- Sexau und dem Badenweiler- Quarzriff, Schwarzwald. In: D.H. Storch and W. Werner (Editors), Die Erz- und Mineralgänge im

alten Bergbaurevier "Freiamt- Sexau", Mittlerer Schwarzwald. *Abhandlungen des Geologischen Landesamtes Baden-Württemberg*, **14**, 173-191.

Lüders V, Franzke HJ. (1993) Formation of Hydrothermal Fluorite Deposits in the Southern Black Forest (SW Germany). *Part* **2***: Geochemical Features. In: Fenoll-Hach A, Torres-Ruiz J & Gervilla F (Eds.): Current Research in Geology Applied to Ore Deposits*, 739-742, Granada.

Lüders V, Möller P. (1992) Fluid evolution and ore deposition in the Harz Mountains (Germany). *European Journal of Mineralogy*, **4**, 1053-1068.

Lüders V, Ebneth J. (1993) Sulfur isotopes in shales and their relation to vein sulfides (and barite) of the Upper and Middle Harz Mountains. *Monogr. Ser. Mineral Deposits* **30**, 231-240.

Matsuhisa Y, Goldsmith HJR, Clayton RN. (1979) Oxygen isotopic fractionation in the system quartz-albite-anorthite-water. *Geochimica et Cosmochimica Acta,* **43**, 1131-1140.

McMillan PF. (1985) Raman and micro-Raman spectroscopy: EOS, *American Geophysical Union Transaction*, **66**, 1139.

McMillan PF. (1989) Raman spectroscopy in mineralogy and geochemistry: *Annual Review of Earth and Planetary Sciences*, **17**, 255-283.

Meshik AP, Lippolt HJ, Dymkov YM. (2000) Xenon geochronology of Schwarzwald pitchblendes. *Mineralium Deposita*, **35**, 190-205.

Metz R, Richter M, Schürenberg H. (1957) Die Blei-Zink-Erzgänge des Schwarzwaldes. *Beihefte Geologisches Jahrbuch*, **29**, 1-277.

Metz R. (1980) *Geologische Landeskunde des Hotzenwaldes*. Moritz Schauenburg Verlag, Lahr/Schwarzwald.

Meyer M, Brockamp O, Clauer N, Renk A, Zuther M. (2000) Further evidence for a Jurassic mineralizing event in central Europe. K-Ar dating of geothermal alteration an fluid inclusion systematics in wall rocks of the Käferteige fluorite vein deposit in the northern Black Forest, Germany. *Mineralium Deposita*, **35**, 754-761.

Mitchell JG, Halliday AN. (1976) Extent of Triassic-Jurassic hydrothermal ore deposits on the North Atlantic margins. *Transaction of the Institution of Mining and Metallurgy,* **B85**, 159-161.

Mittelstädt R. (1987) *Flüssigkeitseinschluss- und Isotopenuntersuchungen an Mineralen der Blei Zink-Lagerstätte Schauinsland im südlichen Schwarzwald*. Diploma thesis, University of Göttingen, Germany.

Möller P, Franzke HJ, Lüders V. (1994) Post-orogene intraformationale Bildung der hydrothermalen Pb-Zn, F und F-Ba Lagerstätten im Schwarzwald. *Technical report* **Mo 443/3** *and* **Fr 874/1***, Intraformationale Lagerstättenbildung, GFZ-Postdam, Germany.*

Muchez P, Sintubin M, Swennen R. (2000) Origin and migration of palaeofluids during orogeny: discussion on the Variscides of Belgium and northern France. *Journal of Geochemical Exploration*, **69-70**, 47-51.

Muchez P, Slobodnik M, Viaene W, Keppens E. (1994b) Mississippi Valley-type Pb-Zn mineralization in eastern Belgium: indications for gravity-driven flow. *Geology*, **22**, 1011-4.

Muchez P, Zhang Y, Dejonghe L, Viaene W, Keppens E. (1998) Evolution of palaeofluids at the Variscan thrust front in eastern Belgium. *Geologische Rundschau,* **87**, 373-380.

Müller G, Nielsen H, Ricke W. (1966) Schwefel-Isotopen-Verhältnisse in Formationswässern und Evaporiten Nord- und Süddeutschlands. *Chem. Geol.* **1**, 211-220.

Mullis J, Stalder HA. (1987) Salt-poor and salt-rich fluid inclusions in quartz from two boreholes in northern Switzerland. *Chemical Geology*, **61**, 263-272.

Munoz M, Boyce AJ, Courjault-Rade P, Fallick AE, Tollon F. (1994) Multi-stage fluid incursion in the Palaeozoic basement hosted Saint-Salvy ore deposit (NW Montagne Noire, southern France). *Appl Geochem*. **9**, 609-626.

Munoz M, Premo WR, Courjault-Rade. (2005) Sm-Nd dating of fluorite from the worldclass Montroc fluorite deposit, southern Massif Central, France. *Mineralium Deposita*, **39**, 970-975.

Nurmi PA, Kukkonen IT, Lahermo PW. (1988) Geochemistry and origin of saline groundwaters in the Fennoscandian Shield. *Appl. Geochem.* **3**, 185-203.

O'Reilly C, Jenkin GRT, Feely M, Alderton DHM, Fallick AK. (1997) A fluid inclusion and stable isotope study of 200 Ma of fluid evolution, Galway Granite, Connemara, Ireland. Contributions to Mineralogy and Petrology, **129**, 120-142.

Ohmoto H. (1986) Stable isotope geochemistry of ore deposits. In *Stable Isotopes in High-temperature Geological Processes* (eds. J.W. Valley, H.P. Taylor, and J.R. O'Neil), Rev. Mineral. **16**, 491-559.

Ohmoto H, Lasaga AC. (1982) Kinetics of reactions between aqueous sulfates and sulfides in hydrothermals systems. *Geochim. Cosmochim. Acta* **46**, 1727-1745.

Ohmoto H, Rye RO. (1979) Isotopes of sulfur and carbon. In *Geochemistry of Hydrothermal Ore Deposits* (ed. H.L. Barnes), 2 nd ed., Wiley, New York, 505-567.

Ohmoto H. Goldhaber MB. (1997) Sulfur and carbon isotopes. In *Geochemistry of Hydrothermal Ore Deposits* (ed. H.L. Barnes), **3rd ed**., Wiley, New York, 517-611.

Ritter J. (1995) Genese der Mineralistation Herrmanngang im Albtalgranit, SE-Schwarzwald und Wechselwirkungen mit dem Nebengestein. In: Puchelt (Editor), *Karlsruher Geochemische Hefte*, **8**, 1-132.

Robie RA, Hemingway BS. (1995) Thermodynamic properties of minerals and related substances at 298.15 K and 1 Bar (105 Pascals) pressure and at higher temperatures. *U.S. Geol. Surv. Bull.* **2131**, 461.

Roedder E. (1958) Technique for the extraction of fluid-filled inclusions from minerals. *Economic Geology*, **53**, 235-269.

Roedder E. (1979) Fluid Inclusions as Samples of Ore Fluids. Geochemistry of Hydrothermal Ore Deposits. *Wiley*. 684.

Roedder E. (1984) Fluid inclusions. *Reviews Mineralogy*, **12**, 644.

Rumble D III, Hoering TC. (1994) Analysis of oxygen and sulfur isotope ratios in oxide and sulfide minerals by spot heating with a carbon dioxide laser in a fluorine atmosphere . *Account of Chemical Research,* **27**, 237-241.

Rye RO. (1993) The evolution of magmatic fluids in the epithermal environment: the stable isotope perspective. *Econ. Geol.* **88**, 733-753.

Rye RO, Ohmoto H. (1974) Sulfur and carbon isotopes and ore genesis: A review. *Econ. Geol.* **69**, 826-842.

Sanchez-Espana J, Velasco F, Boyce AJ, Fallick AE. (2003) Source and evolution of ore-forming hydrothermal fluids in the northern Iberian Pyrite Belt massive sulphide deposits (SW Spain): evidence from fluid inclusions and stable isotopes. *Mineralium Deposita*, **38**, 519-537.

Schreiner A. (1991) Geologe und Landschaft. Das Markgräfler Land: Entwicklung und Nutzung. In Das Märkgräfler Land: Entwicklung und Nutzung (ed. A. Hoppe), pp. 11-24. *Naturforschende Gesellschaft Freiburg i. Br.* **81**.

Schuler C, Steiger RH. (1978) On the genesis of feldspar megcrysts in granites: Rb-Sr isotopic study. *4th Conf. Geochron. Isotope Geology, Ed. R.E. Zartmann*, 386-387.

Schwinn G, Markl G. (2005) REE systematics in hydrothermal fluorite. *Chem. Geol.* **216**, 225-248.

Schwinn G, Wagner T, Baatartsogt B, Markl G. (in press) Quantification of mixing processes in ore-forming hydrothermal systems by combination of stable isotope and fluid inclusion analyses. *Geochimica et Cosmochimica Acta*

Segev A, Halicz L, Lang B, Steinitz G. (1991) K-Ar dating of manganese minerals from the Eisenbach region, Black Forest, southwest Germany. *Schweizerische Mineralogische und Petrogaphische. Mitteilungen,* **71**, 101-114.

Sharp ZD. (1990) A laser-based microanalytical method for the in-situ determination of oxygen isotope ratios of silicates and oxides. *Geochemica et Cosmochimica Acta,* **54**, 1353-1357.

Sheets RW, Nesbitt BE, Muehlenbachs K. (1996) Meteoric water component in magmatic fluids from porphyry copper mineralization, Babine Lake area, British Columbia. *Geology*, **24**, 1091-1094.

Shepherd TJ, Rankin AH, Alderton DHM. (1985) A practical guide to fluid inclusion studies. *Blackie. London*.

Sheppard SMS. (1986) Characterization and isotopic variations of natural waters. In John W. Valley, H.P. Taylor Jr., and J.R.O'Neil, Eds., Stable isotopes in high temperature geological processes. *Reviews in Mineralogy, Mineralogical Society of America*. v. **16**, 165-183.

Shock EL, Sassani DC, Willis M, Sverjensky DA. (1997) Inorganic species in geological fluids: Correlations among standard molal thermodynamic properties of aqueous ions and hydroxide complexes. *Geochim. Cosmochim. Acta,* **61**, 907-950.

Shvarov YV, Bastrakov E. (1999) *HCh: A software package for geochemical equilibrium modeling. User's guide.* Australian Geological Survey Organisation, Department of Industry, Science and Resources.

Shvarov YV. (1978) Minimization of the thermodynamic potential of an open chemical system. *Geochem. Internat.* **15**, 200-203.

Simmons SF, Arehart GB, Simpson MP, Mark JL. (2000) Origin of Massive Calcite Veins in the Golden Cross Low-Sulfidation Epithermal Au-Ag Deposit, New Zealand. *Econ. Geol.* **95**, 99-112.

Simon K. (1990) Hydrothermal alteration of Variscan granites, southern Schwarzwald, Federal Republic of Germany. *Contributions to Mineralogy and Petrol*ogy, **105**, 177-196.

Simon K. (1997) H-isotope composition of different 'water' reservoirs in hydrothermal quartz. Terra Abstract, E.U.G. IX

Simon K. (2001) Does δD from fluid inclusion quartz reflect the original hydrothermal fluid? *Chemical Geology*, **177**, 483-495.

Simon K, Hoefs J. (1987) Effects of meteoric water interaction on Hercinian granites from the Südschwarzwald, southwest Germany. *Chemical Geology*, **61**, 253-261.

Simon K, Hoefs J. (1991) O,H,C-Isotope in Gesteinen und Mineralen der KTB-VB. In: *R. Emmermann, J. Lauterjung (Eds.):* **KTB-Report 91-1**, *Nds. Landesamt für Bodenforschung 91-1*, 359-378.

Simon K, Hoefs J. (1993) O, H, C isotope study of rocks from the KTB pilot hole: crustal profile and constraints on fluid evolution. *Contributions to Mineralogy and Petrol*ogy, **114**, 42-52.

Spötl C, Vennemann TW. (2003) Continuous-flow isotope ratio mass spectrometric analysis of carbonate minerals. *Rapid. Commun. Mass. Spectrom.* **17**, 1004-1006.

Stober I, Bucher K. (1999) Deep groundwater in the crystalline basement of the Balck Forest region. *Applied Geochemistry*, **14**, 237-254.

Stober I, Bucher K. (1999) Origin of salinity of deep groundwater in crystalline rocks. *Terra Nova,* **11**, 181-185.

Stober I, Bucher K. (2004) Fluid sinks within the earth's crust. *Geofluids*, **4**, 143-151.

Stober I, Richter A, Brost E, Bucher K. (1999) The Ohlsbach plume – discharge of deep saline water from the crystalline basement of the Black Forest, Germany. *Hydrogeol. J.* **7**, 273-283.

Stober I, Zhu Y, Bucher K. (2002) Water-Rock reactions in a Barite-Fluorite Underground Mine, Black Forest (Germany). *Water-Rock Interaction*, 171-187.

Sverjensky DA, Shock EL, Helgeson HC. (1997) Prediction of the thermodynamic properties of aqueous metal complexes to 1000 °C and 5 kb. *Geochim. Cosmochim. Acta,* **61**, 1359-1412.

Taylor HP Jr. (1974) The application of oxygen and hydrogen isotope studies to problems of hydrothermal alteration and ore deposition. *Economic Geology*, **69**, 843-883.

Taylor HP Jr. (1977) Water/rock interactions and the origin of H_2O in granitic batholiths. *Journal of the Geological Society London*, **133**, 509-558.

Taylor HP Jr. (1979) Oxygen and hydrogen isotope relationships in hydrothermal mineral deposits. In: *Geochemistry of hydrothermal ore deposits,* **2nd Ed.** *(ed. Barnes HL)*, 236-277.

Taylor HP Jr. (1997) Oxygen and hydrogen isotope relationships in hydrothermal mineral deposits, *In H. L. Barnes (ed.) Geochemistry of Hydrothermal Ore Deposits* **3rd Ed**. Wiley, New York, 229-302.

Thury M, Gautschi A, Mazurek M, Müller WH, Naef H, Pearson FJ, Vomvoris S, Wilson W. (1994) Geology and Hydrogeology of the Crystalline Basement of Northern Switzerland. *Synthesis of Regional Investigations 1981-1993 within the Nagra Radioactive Waste Disposal Programme. Nagra, Technical Report*, **93-01**, 1-347.

Todt W. (1976) Zirkon-U/Pb-Alter des Malsburger Granits vom Süd-Schwarzwald. *N. Jb. Miner., Mh.,* **H.12**, 532-544.

Upton P, Craw D, Caldwell TG, Koons PO, James Z, Wannamaker PE, Jiracek GJ, Chamberlain CP. (2003) Upper crustal fluid flow in the outboard region of the Southern Alps, New Zealand. *Geofluids,* **3**, 1-12.

Vallance J, Boiron M, Cathelineau M, Fourcade S, Varlet M, Marignac C. (2004) The granite hosted gold deposit of Moulin de Cheni (Saint-Yrieix district, Massif Central, France): petrographic, structural, fluid inclusion and oxygen isotope constraints. *Mineralium Deposita*, **39**, 265-281.

Vennemann TW, O'Neil JR. (1993) A simple and inexpensive method of hydrogen isotope and water analyses of minerals and rocks based on zinc reagent. *Chemical Geology*, **103**, 227-234.

von Gehlen K. (1962) Ore and Mineral Deposits of the Schwarzwald.

von Gehlen K. (1989) Ore and Mineral Deposits of the Schwarzwald. In: R. Emmermann and J. Wohlenberg (Editors), *The German Continental Deep Drilling Program, Springer Verlag*, 276-295.

von Gehlen K, Nielsen H, and Ricke W. (1962) S-Isotopen Verhältnisse in Baryt und Sulfiden aus hydrothermalen Gängen im Schwarzwald und jüngeren Barytgängen in Süddeutschland und ihre genetische Bedeutung. *Geochim. Cosmochim. Acta,* **26**, 1189-1207.

von Gehlen K. (1987) Formation of Pb-Zn-F-Ba mineralizations in SW Germany: a status report. *Fortschritte der Mineralogie*, **65**, 87-113

Vovk IF, Vysotskii VI. (1982) Isotopic composition and geochemical characteristics of subsurface waters of the Krivoi Rog Basin as indicators of their interrelation and origin. *Water Res*. **9**, 15-21.

Wagner T, Cook NJ. (2000) Late-Variscan antimony mineralization in the Rheinisches Schiefergebirge, NW Germany: Evidence for stibnite precipitation by drastic cooling of high-temperature fluid systems. *Mineralium Deposita*, **35**, 206-222.

Walther HW. (1981) Quantitative regionale Metallogenese als Beitrag zur Frage: Wo sind die Metalle der Zukunft? *Erzmetall,* **34**, 432-438.

Weber A. (1997) Geochemische Untersuchungen zur Genese der Blei-Zink-Lagerstätte am Schauinsland im Schwarzwald. *Diploma Thesis, Faculty of Geosciences, University of Tübingen, Germany*.

Werner W, Dennert V. (2004) *Lagestätten und Bergbau im Schwarzwald*. Freiburg.

Werner W, Franzke HJ. (2001) Postvariskische bis neogene Bruchtektonik und Mineralisation im südlichen Schwarzwald. *Zeitschrift der Deutschen Geoogischen. Gesellschaft*, **152/2-4**, 405-437.

Werner W, Franzke HJ, Lüders V. (2000) Zur Genese der Zink-Blei-Lagerstätte Schauinsland. *Erzmetall*, **53**, 273-285.

Werner W, Franzke HJ, Wirsing G, Jochum J, Lüders V, Wittenbrink J. (2002) Die Erzlagerstätte Schauinsland bei Freiburg im Breisgau. *Aedificatio Verlag, Freiburg i.Br.*

Werner W, Schlaegel-Blaut P, Rieken R. (1990) Verbreitung und Ausbildung von Wolfram-Mineralisationen im Kristallin des Schwarzwaldes. *Jahreshefte des geologischen Landesamtes Baden-Württemberg*, **32**, 17-61.

Wernicke RS, Lippolt HJ. (1993) Botryoidal hematite from the Schwarzwald, Germany. heterogenous U distributions and their bearing on the helium dating method. *Earth and Planetary Science Letters*, **114**, 287-300.

Wernicke RS, Lippolt HJ. (1997) U+Th-He evidence of a Jurassic continuous hydrothermal activity in the Schwarzwald basement, Germany. *Chemical Geology*, **138**, 273-285.

Wilkinson JJ, Boyce AJ, Earls G, Fallick AE. (1999) Gold remobilization by low temperature brines: evidence from the Curraghinalt gold deposit, Northern Ireland. *Economic Geology*, **94**, 289-296.

Wilkinson JJ, Jenkin GRT, Fallick AE, Foster RP. (1995) Oxygen and hydrogen isotopic evolution of the Variscan crustal fluids, south Cornwall, U.K. *Chemical Geology*, **123**, 239-254.

Zheng YF, Hoefs J. (1993a) Stable isotope geochemistry of hydrothermal mineralizations in the Harz Mountains: I. Carbon and oxygen isotopes of carbonates and implications for the origin of hydrothermal fluids. *Monogr. Ser. Mineral Deposits* **30**, 169-187.

Zheng YF, Hoefs J. (1993b) Stable isotope geochemistry of hydrothermal mineralizations in the Harz Mountains: II.Sufur and oxygen isotopes of sulfides and sulfate and constraints on metallogenic models. *Monogr. Ser. Mineral Deposits* **30**, 211-229.

Zheng YF, Hoefs J. (1993c) Carbon and oxygen isotopic covariations in hydrothermal calcites. Theoretical modeling on mixing processes and application to Pb-Zn deposits in the Harz Mountains, Germany. *Mineral. Deposita.* **28**, 79-89.

Zuther M, Brockamp O. (1988) The fossil geothermal system of the Baden-Baden Trough (Northern Black Forest, F.R. Germany). *Chemical Geology*, **71**, 337-353.

Zwart EW, Touret JLR. (1994) Melting behaviour and composition of aqueous fluid inclusions in fluorite and calcite: applications within the system H_2O-$CaCl_2$-NaCl. *European Journal of Mineralogy*, **6**, 773-786.

CURRICULUM VITAE

Name:	Baldorj Baatartsogt
Date and place of birth:	05. September 1973, Tuv Aimag (Mongolia)
Nationality:	Mongolian
Marital status:	Married, two children: son and daughter.

University Education

Since 04/2002	PhD study (Dr. rer. nat), Title: *Fluid inclusion and stable isotope studies of hydrothermal vein deposits, Schwarzwald, Germany*. (Supervision: Prof. Gregor Markl, University of Tübingen, Germany). DAAD-scholarship.
01/1999	MSc degree in Geology. MSc thesis: *The Ikh-Khairhan tungsten deposit's substantial composition and exploration method*.
09/1997 – 01/1999	Master of Science (MSc) course at the National University of Mongolia.
07/1997	Bachelor degree in Geology. Diploma thesis: *Geological and Mineralogical analysis of Ikh-Khairhan tungsten deposit*.
09/1993 - 06/1997	Studies of Geology at the Faculty of Earth Science, National University of Mongolia.
07/1997	Diploma of Interpreter of English.
10/1994 – 07/1997	Evening school of English at the School of Foreign Service, National University of Mongolia.

Experience

09/1999 – 05/2001	National University of Mongolia, Department of Geology and Mineralogy *Lecturer. Mineral exploration, Economic geology and Geochemistry*.
06/1997 – 09/1999	BHP minerals exploration Inc. and Ivanhoe Mines. Gold-Copper exploration in South-East and South Mongolia and Oyu Tolgoi gold-copper project. *Exploration-Geologist and GIS specialist*.

School

09/1982-06/1992	Secondary and High School, Ulaanbaatar, Mongolia

PUBLICATIONS

Baatartsogt B, Wagner T, Taubald H, Mierdel K, Markl G. (*in progress*) Hydrogen isotope determination of fluid inclusion water from hydrothermal fluorite: The results depend on extraction technique. *Chemical Geology.*

Baatartsogt B, Schwinn G, Wagner T, Taubald H, Markl G. (*submitted*) Contrasting paleofluid systems in the continental basement: a fluid inclusion and stable isotope study of hydrothermal vein mineralizations, Schwarzwald district, Germany. *Geofluids.*

Schwinn G, Wagner T, **Baatartsogt B**, Markl G. (*in press*) Quantification of mixing processes in ore forming hydrothermal systems by combination of stable isotope and fluid inclusion analyses. *Geochim. Cosmochim. Acta.*

Altankhuyag D, **Baatartsogt B**. (2004) Oxygen isotope study of the quartz veins and related Zavkhan terrane. Geology and Geoecology of Mongolia, *Mongolian GeoScientist,* v. **25**.

Dashdavaa S, **Baatartsogt B**, Oyunjargal D. (2002) Genesis of the Ongonkhairhan tungsten deposit. National University of Mongolia. *Problems of geology*. **5**. 144-154.

Baatartsogt B, Dashdavaa S. (1997) Geology and Mineralogy of Ikh-Khairhan tungsten deposit. *Research Paper*, National University of Mongolia, 25-33.

ABSTRACTS

Baatartsogt B, Schwinn G, Wagner T, Taubald H, Markl G. (2005) Fluid inclusion and stable isotope study of the post-Variscan hydrothermal vein deposits in the Schwarzwald district, Germany: origin of the hydrothermal fluid. *DMG (Deutsche Mineralogische Gesellschaft)-2005, Aachen, Germany*. Abstract, *European Journal of Mineralogy*, **17/1**, 9.

Baatartsogt B, Wagner T, Taubald H, Mierdel K, Markl G. (2005) Hydrogen isotope determination of fluid inclusion water from hydrothermal fluorite: The results depend on extraction technique. *ECROFI (European Current Research on Fluid Inclusions) XVIII, Siena-Italy,* 6-9 July, 2005.

Schwinn G, Markl G, **Baldorj B**, Neumann U. (2003): Comparative geochemical study of different hydrothermal vein deposits of the Schwarzwald (Germany) and implications for ore-forming processes. *EGS (European Geophysical Society)-2003, Geophysical Research Abstract,* **5**, 01059.

"Gedruckt mit Unterstützung des Deutschen Akademischen Austauschdienstes"